

THESIS ON NATURAL AND EXACT SCIENCES B201

**SnS Thin Films Deposition by
Chemical Solution Method and Characterization**

MARIA SAFONOVA

TUT
PRESS

TALLINN UNIVERSITY OF TECHNOLOGY
Faculty of Chemical and Materials Technology
Department of Materials Science
Chair of Semiconductor Materials Technology

Dissertation was accepted for the defense of the degree of Doctor of Philosophy in Natural and Exact Sciences on 10 of December.

Supervisors: Dr. Olga Volobujeva, Senior Research Scientist, Department of Materials Science, Tallinn University of Technology, Estonia

Professor Enn Mellikov, Department of Materials Science,
Tallinn University of Technology, Estonia

Consultant: Dr. Karin Kerm, Tallinn University of Technology, Estonia

Opponents: Dr. Smagul Karazhanov, Institute for Energy Technology,
Kjeller, Norway

Dr. Ants Lõhmus, Institute of Physics, University of Tartu,
Estonia

Defense: January 14, 2016, at 13:00.
Lecture hall: U06A-201
Tallinn University of Technology,
Ehitajate tee 5, Tallinn

Declaration:

Hereby I declare that this doctoral thesis, my original investigation and achievement, submitted for the doctoral degree at Tallinn University of Technology has not been submitted for any academic degree.

Maria Safonova



Copyright: Maria Safonova, 2015

ISSN 1406-4723

ISBN 978-9949-23-884-2 (publication)

ISBN 978-9949-23-885-9 (PDF)

LOODUS- JA TÄPPISTEADUSED B201

**SnS õhukeste kilede sadestamine
keemilisest lahusest ja saadud kilede
iseloomustamine**

MARIA SAFONOVA

Contents

LIST OF PUBLICATIONS	7
AUTHOR'S OWN CONTRIBUTION	8
LIST OF ABBREVIATIONS AND SYMBOLS	9
INTRODUCTION	10
1 LITERATURE OVERVIEW	12
1.1 Tin sulphides	12
1.2 Methods of tin sulphide thin film growth.....	13
1.3 Chemical solution deposition method	14
1.4 Mechanisms of chemical deposition	15
1.5 Chemical solution deposition of tin sulphide thin films.....	17
1.6 Literature overview summary and the aim of present work.....	27
2 EXPERIMENTAL DETAILS	28
2.1 Deposition of films	28
2.2 Characterisation of films	30
2.2.1 Morphological studies of films.....	30
2.2.2 Determination of crystal structure and phase composition of films.	31
2.2.3 Optical spectral analysis of films	32
2.2.4 Additional measurements	33
3 RESULTS AND DISCUSSION	34
3.1 Optimization of the chemical solution parameters	34
3.1.1 The influence of concentrations of tin and sulphur in the initial solution on the parameters of chemically deposited films (article II)	34
3.1.2 The influence of ratio of tin to sulphur in solution on the chemical solution deposition of films	39
3.1.3 Influence of pH of the chemical solution on the parameters of deposited films.....	43
3.1.4 Duration of the deposition.....	46
3.1.5 The influence of deposition temperature on the parameters of SnS thin films.....	47
3.2 Photoelectrochemical characterisation of SnS thin films deposited at optimized conditions	49
3.3 Sequential deposition of SnS thin films (article I)	49

3.4 Post-thermal treatment of obtained films (article III).....	56
4. CONCLUSIONS.....	66
ACKNOWLEDGEMENTS.....	68
ABSTRACT	70
KOKKUVÕTE	72
REFERENCES.....	74
APPENDIX A	85
APPENDIX B.....	111

LIST OF PUBLICATIONS

The present doctoral thesis is based on the following papers:

- I. **M. Safonova**, P.K. Nair, E. Mellikov, A.R. Garcia, K. Kerm, N. Revathi, T. Romann, V. Mikli, O. Volobujeva. Chemical bath deposition of SnS thin films on ZnS and CdS substrates, *J Mater Sci: Mater Electron* 25 (2014) 3160-3165.
- II. **M. Safonova**, E. Mellikov, V. Mikli, K. Kerm, N. Revathi, O. Volobujeva. Chemical bath deposition of SnS thin films from the solutions with different concentrations of tin and sulphur, *Advanced Materials Research* 1117 (2015) 183-186.
- III. **M. Safonova**, P.K. Nair, E. Mellikov, R. Aragon, K. Kerm, R. Naidu, V. Mikli, O. Volobujeva. Thermal annealing of sequentially chemically deposited SnS thin films, *Proceedings of the Estonian Academy of Sciences* 64 (4) (2015) 488-494.

In Appendix A copies of the following papers are included.

AUTHOR'S OWN CONTRIBUTION

The contribution of the author to the papers included in the thesis is as follows:

- I. Article I describes sequential deposition of SnS thin films. Deposition experiments were done during studies in National Autonomous University of Mexico: chemical bath deposition of SnS, CdS and ZnS thin films, as well as some characterization of obtained films such as by SEM and EDX, optical and electrical measurements (partly) with a help of local students and supervisor. Additional investigations were done by Raman spectroscopy in TUT Department of Materials Science. The contribution also includes analysis of obtained results and major part of writing.
- II. Chemical bath deposition of SnS thin films was conducted at TUT Department of Materials Science, characterization of obtained films by Raman spectroscopy investigations (partly), analysis of obtained results and major part of writing.
- III. Annealing described in the III article was the next step made with sequentially deposited and described in I article SnS thin films. Thermal annealing of sequentially chemically deposited SnS thin films was done during my studies in National Autonomous University of Mexico as well as preliminary characterization of obtained films by SEM and EDX, optical and electrical measurements (partly), fabrication of solar cell structures and their characterization with a help of local students and supervisor. Raman spectroscopy investigations (partly) were made in TUT Department of Materials Science as well as analysis of obtained results and major part of writing.

LIST OF ABBREVIATIONS AND SYMBOLS

AES	Auger electron spectroscopy
AFM	Atomic force microscope
CBD	Chemical bath deposition
CZT(S/Se)	Copper zinc tin sulphide/selenide
EDX or EDS or EDAX	Energy dispersive X-ray analyser
E_g	Band gap energy
FT-IR	Fourier transform infrared spectroscopy
ITO	Indium tin oxide
I_{sc}	Short circuit current
J_{sc}	Short circuit current density
M_o	Molybdenum
PV	Photovoltaics
r.t.	Room temperature
SEM	Scanning Electron Misroscopy
SnS (OR)	SnS with orthorhombic structure
SnS (ZB)	SnS with zinc-blende structure
<i>TA</i>	Thioacetamide
TEA	Triethanolamine
TO	Tin dioxide
V_{oc}	Open circuit voltage
XPS	X-ray photoelectron spectroscopy
XRD	X-ray diffraction

INTRODUCTION

Solar energy is one among the other renewable energy sources that produces reliable and pollution-free electricity with long term maintenance. The process of conversion of solar energy into electricity is referred as photovoltaics (PV) [1]. The effective wide-spread use of PV technology requires earth abundant, eco-friendly, high efficient and low-cost with long term durable photovoltaic devices [2].

Thin film solar cells are one of the promising approaches in attaining the goal for power production with PV devices in terms of their material usage, cost and stability. Over the decade, thin film growth technology has been intensified for preparing various layers onto distinct substrates (metal, flexible) using different deposition methods [3].

Various inorganic semiconductor materials are widely studied to meet the state-of-the-art of the solar cells technology. $\text{Cu}_2\text{S}/\text{CdS}$ [4] was the first heterojunction device made from thin films that receives significant attention for further development of thin solar cells. Amorphous silicon (a-Si) and micro-crystalline silicon ($\mu\text{-Si}$) are widely used in thin film solar cell technology with cheaper method and less material usage, the reported power conversion efficiencies are 10.1% and 10.8% [5] but degradation in parameters is the major difficulty with this materials.

The two most prominent chalcogenide polycrystalline thin films materials for solar cells preparation are cadmium telluride (CdTe) and copper indium gallium selenide (CIGS) that have direct band gap and high optical absorbance. These devices demonstrated the single-junction conversion efficiencies of 21.5% [6] and 21.7% [7], however, toxic Cd as well as the use of expensive elements such as Te, In and Ga are the major disputes for their large scale production [8].

This lay down the motivation to many researchers to look for substitute materials. Quaternary copper zinc tin sulphide/selenide (CZT(S/Se)) is one emerging material with all its elements are earth abundant. The solar conversion efficiency of around 12.6 % [5] is obtained, although it is difficult to achieve a stable phase of CZT(S/Se) without any other secondary phases. Although numerous semiconductor photoabsorber materials are studied for the solar cell applications, each material has its own merits and demerits towards the final device application. Attempts have been made to overcome all the above problems with cost effective way based on the simple and novel semiconductor materials.

During past decade continuous investigations have been focused on tin monosulphide (SnS) binary material from IV-VI compounds that attain renewed interest as a photoabsorber layer due to its band gap of 1.3 eV, high absorption coefficient of $\sim 10^5 \text{ cm}^{-1}$ and p-type conductivity. It is binary material with abundant constituent's elements Sn and S [9, 10]. SnS -based solar cells are theoretically predicted to achieve efficiency of 32 % and as the minimum

percentage for large-scale usage of solar cells is 20%, it can be considered as very promising material [11, 12]. All these properties make this material a good candidate in low-cost thin film solar cell technology. Some authors proved its potentiality in device applications. Currently the highest laboratory reported power conversion efficiency of SnS-based solar cells is still only 4.4% [13].

Therefore, in this direction the present PhD work was aimed to obtain SnS thin films by chemical solution deposition method as well as annealing of as-grown films in suitable ambient to obtain desired quality. The as-grown and annealed films were systematically characterized to know their elemental and phase composition, crystal structure, surface morphology and optical properties.

The thesis consists of four chapters. First chapter deals with introduction and a brief review on SnS thin films. The experimental techniques used in the PhD work are presented in second chapter. Third chapter gives the results and discussion of the SnS thin films in relation to the deposition conditions. Conclusions drawn from the results will be in the fourth chapter.

This thesis is based on three research articles.

1 LITERATURE OVERVIEW

1.1 Tin sulphides

Different binary forms of tin sulfides exist. Tin (II) sulphide or tin monosulphide is a bluish-black solid with chemical formula SnS, it dissolves in concentrated hydrochloric acid and also in strongly alkaline solutions. Annealing in air converts SnS to SnO₂ [14, 15]. Crystalline structure of tin monosulphide can be orthorhombic or zinc blend (Fig.1) [16].

SnS could be deposited by different chemical and physical methods. Deposition parameters should be controlled well to prevent existence of secondary phases such as SnS₂ or Sn₂S₃ which can be formed very easily. These additional phases affect properties of the SnS thin film for example causing band gap shifting [17].

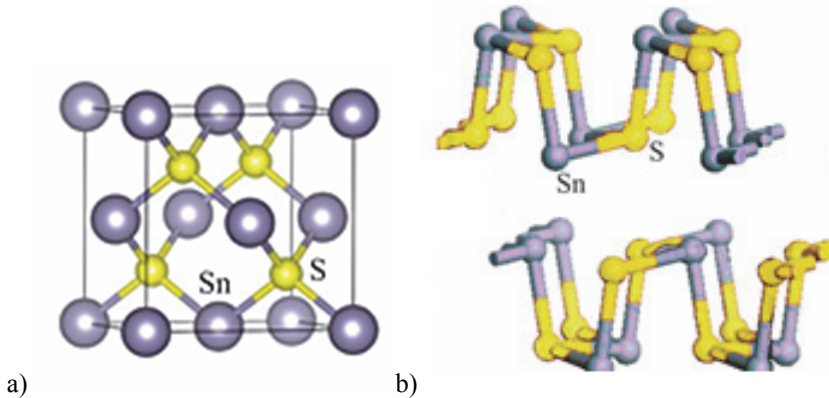


Fig. 1 Crystal structures of SnS: a) zinc blend and b) orthorhombic [18].

Tin (IV) sulphide or tin disulphide (SnS₂) is an n-type semiconductor material with band gap in the range of 2.12-2.44 eV and has yellow color. It has hexagonal cadmium iodide-type (CdI₂) crystal structure, which is composed of sheets of tin atoms sandwiched between two close-packed sheets of sulphur atoms (Fig.2) [19-21].

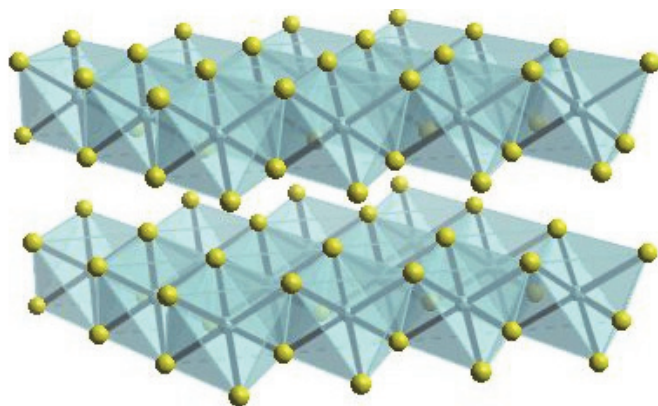


Fig. 2 Crystal structure of SnS_2 [20].

Black tin sesquisulphide - Sn_2S_3 - represents the mixed-valence (II and IV) tin sulphide compound with an ribbon-type structure as shown in Fig. 3 where the trigonal-pyramidal tin(II) locates at the edge and the octahedral tin (IV) at the center of the ribbon [22, 23]. Sn_2S_3 has band gap around 2.0- 2.1 eV [24, 25].

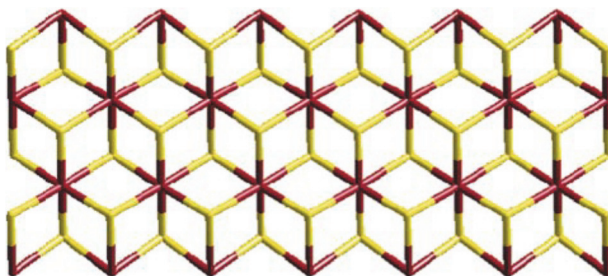


Fig. 3 Ribbon structure of Sn_2S_3 [22].

Following the all above given, tin sulphides of different elemental composition have very different properties and we have to control precisely the composition of formed tin sulphide in our thin film deposition process.

1.2 Methods of tin sulphide thin film growth

Different physical and chemical techniques have been used for deposition of SnS thin films. Physical methods such as physical vapor deposition (thermal vacuum evaporation [26, 27], magnetron sputtering [28, 29] etc.), atomic layer deposition [30, 31] and electron beam deposition [32, 33] along with chemical methods such as chemical vapor deposition [34], sulfurization [35], spray pyrolysis [36-38], electro-chemical deposition

(galvanic) [39] and chemical solution deposition [40] could be applied for SnS thin film preparation.

Among all this methods chemical solution deposition - or also known as chemical bath deposition (CBD) - has a number of benefits [41-43]:

- it is simple technique
- it is inexpensive method due to simple and cheap equipment and starting chemicals, which are also usually inexpensive and available
- the deposition can be held onto the different substrate surfaces, with different shape and sizes
- the method allows depositing films at low temperatures which prevent corrosion or oxidation of substrate material and also gives a possibility to use organic substrates.

1.3 Chemical solution deposition method

Chemical solution deposition means the deposition of a film onto a solid substrate resulting from chemical reactions between dissolved in solution precursors. Solution should be stirred well and then the substrate, which is previously cleaned, places vertically into the solution inside a vessel. The vessel should be closed hermetically to avoid dust or another unwanted particles getting into the solution and prevent escape of the gases phases [44] (Fig. 4).

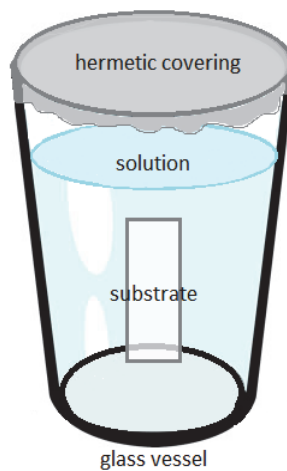


Fig. 4 Schematic of chemical solution deposition of thin films.

Film growth process passes three main stages [45]:

1. During an *induction period (or nucleation or incubation period)* chemical equilibrium is achieved in the solution and on the surface of the substrate forms primary layer of the film.

2. Next follows *growth phase*, when metal and chalcogenide ions of the precursor solution condense on the top of already formed primary film and film growth accelerates.
3. Film ceases to grow at the *terminal phase*.

1.4 Mechanisms of chemical deposition

Chemical solution deposition is extensively applied for making thin films for semiconductor and photo-voltaic devices in laboratories and industrial production, but its definite mechanism is still unclear. Mechanism of the film growth can also change during the deposition [46, 47].

The simplest mechanism which is usually expected to be occurring generally is called *ion-by-ion mechanism*. It has such a name due to ionic reactions taking sequentially place in the solution. This mechanism could be illustrated by the following reaction:



where M^{n+} is metal ion, X^{m-} is chalcogenide ion and M_mX_n is obtained thin film [48].

Thin film has to be formed onto the substrate but not in the solution itself. For this reason formation of complex is essential to preserve the ions of the metal in solution and prevent the formation of precipitating out hydroxide [49]. Complexing agent should not be too weak and be able to block bulk precipitation of hydroxide; on the other hand it has to be not too stable to prevent deposition of the desired film [14]. There are a lot of different complexing agents with distinct complexing strength that could be used. Due to the stable complex the free metal ions release slowly and react with chalcogenide ions forming the desired thin film [50].

Since the solution does not contain particles in it and as the substrate for film presents a degree of heterogeneity, the substrate serves as catalyst and facilitates the nucleation [51], so the deposition of film in the ion-by-ion process happens mainly on surfaces and not as the precipitation in the solution. As it can be seen on the Fig. 4 a, metal and chalcogenide ions diffuse to the surface of the substrate where M_mX_n nuclei will be formed (Fig. 5a and b). Nuclei will grow by absorbing more ions from the solution and at the same time new nuclei start to nucleate (Fig. 5 c). If the nucleation has already started on the surface, film begins to grow faster there because deposition happens quicker on the nucleated than on the clean surface. Formed M_mX_n crystals continue to grow and adhere to each other forming the film (Fig.5 d) [52].

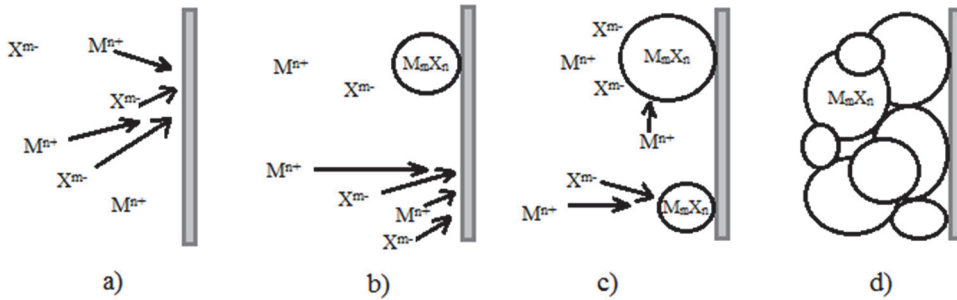
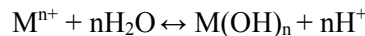


Fig. 5 Scheme of the ion-by-ion mechanism [adapted from 14].

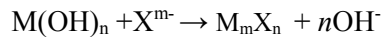
The other mechanism is known as *cluster hydroxide mechanism* [48]. It occurs if formation of metal hydroxide is not avoided completely and metal hydroxide exists as colloid in solution

R.1.2

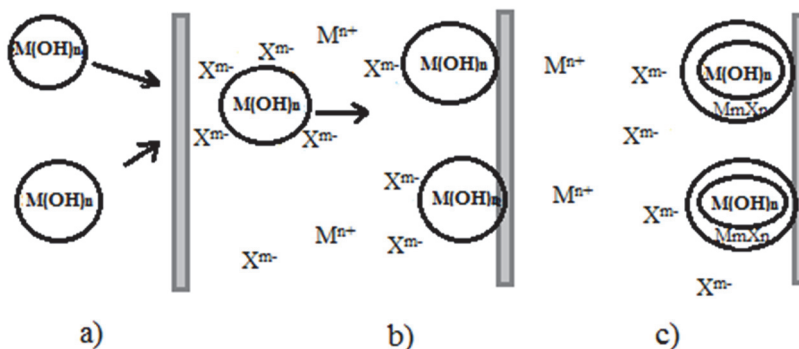


The thin film will be formed by reaction of that cluster with slowly generated chalcogenide ions:

R.1.3



The nucleation in this process happens easier due to the presence of colloidal solid phase of metal hydroxide in the solution [14]. Colloidal particles of hydroxides diffuse to the surface and adhere (Fig.6 a) to the substrate (Fig.5 b). Next metal hydroxides will be converted into $M_m X_n$ by reacting hydroxide with chalcogenide ions at the surface of the colloid and process proceeds inward (Fig.6 c) [52]. Analogical process will go not only on the deposition surfaces but also in the solution (Fig.6 d). Formed $M_m X_n$ crystals will stick to the substrate and to one another (Fig.6 e). Formation of the thin film structure will occur if particles reach the deposition substrate surface before they precipitate out as large aggregates from the solution [53].



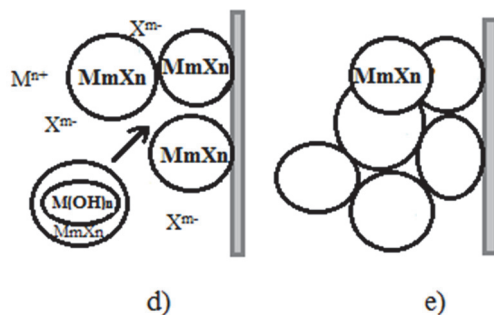


Fig. 6 Scheme of the hydroxide mechanism [adapted from 14].

Another basically distinct from two previous mechanisms is *complex decomposition mechanism* not involving the formation of free chalcogenide ions. This mechanism bases on the formation and decomposition of metal-chalcogenide complexes [54].

Formation of the film involving metal-chalcogenide complex decomposition passes similarly as for the previous two mechanisms. The complex consisting of metal, chalcogenide and ligand decomposes to M_mX_n on the surface of the substrate (Fig. 7 a and b) and also in some amount homogeneously in the solution (Fig. 7 c). M_mX_n nuclei will grow absorbing elements of decomposed complexes until the film of aggregated M_mX_n crystals is formed (Fig. 7 d) [55].

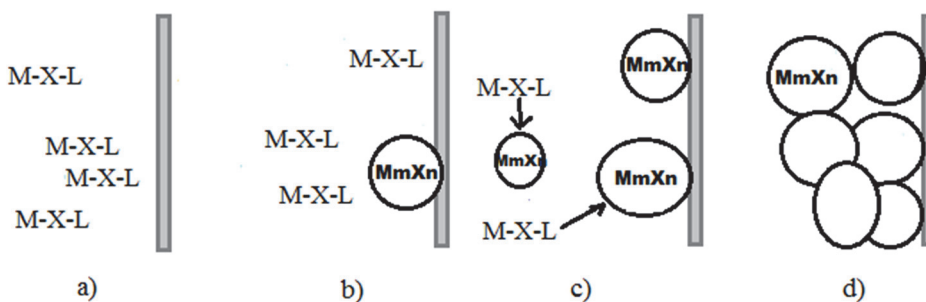


Fig. 7 Scheme of the complex decomposition mechanism [adapted from 14].

1.5 Chemical solution deposition of tin sulphide thin films

The first attempts to deposit tin sulphide thin films by chemical solution deposition had been made by researchers already in early 1870. Deposition was held using boiling solution of tin (II) or tin (IV) chloride. Tartrate was used as a complexing agent and thiosulphate as a source of sulphur [14].

The following table gives overview of recent studies in SnS chemical solution depositions (1991-2015 years).

Chemical solution deposition parameters							
<i>Ref</i>	<i>Precursors</i>	<i>Initial concentration Sn : S</i>	<i>Deposition temperature</i>	<i>Time of deposition</i>	<i>pH of solution</i>	<i>Thickness of film</i>	<i>Annealing temperature and time</i>
[56]	SnCl ₂ *2H ₂ O+ H ₃ CC(S)NH ₂	Sn 0.04M : S 0.08M	a. 75 °C b. 25 °C	5 h 40 h	-	1000 nm	-
[57]	SnCl ₂ + H ₃ CC(S)NH ₂	Sn 0.005M: S 0.08M	40 °C to 75 °C	0,3 -1,5 h	-	40-200 nm	-
[58]	SnCl ₂ *2H ₂ O+ Na ₂ S ₂ O ₃ *5H ₂ O	Sn 0.05M: 0.1M	-	18 h	7	340 nm	250°C 1,8h, 300 °C 1h
[59]	SnCl ₂ *2H ₂ O+ Na ₂ S ₂ O ₃ *5H ₂ O	Sn 0.05M: S 0.05M	r.t.	24 h	7	600 nm	150°C 2 h
[60]	SnCl ₂ *2H ₂ O+ H ₃ CC(S)NH ₂	a. Sn 0.01M: S 0.01M b. Sn 0.005M: S 0.08M	a. r.t. b. 35 °C	a.5 -6 h b. 20 h	-	a. 500 nm b. 500 nm	300 °C and 125-550 °C, different durations
[61]	SnCl ₂ *2H ₂ O+ Na ₂ S ₂ O ₃ *5H ₂ O	Sn 0.045M: S 0.1M	30 °C	24 h	7	290 nm	-
[62]	SnCl ₂ *2H ₂ O+ H ₃ CC(S)NH ₂	-	a. 23 °C b. 40 °C	a. 6 h b. 22 h	-	a. 100 nm b. 500 nm	-
[63]	SnCl ₂ *2H ₂ O+ Na ₂ S ₂ O ₃ *5H ₂ O	Sn 0.045M: S 0.1M	r.t.	24 h	7	1960 nm	-
[64]	SnCl ₂ *2H ₂ O+ H ₃ CC(S)NH ₂	-	r.t.	5 h	-	100-434 nm	-
[47]	SnCl ₂ *2H ₂ O+ H ₃ CC(S)NH ₂	Sn 0.05M: S 0.05M	r.t. (27 °C)	24 h	10,7	-	-
[51]	SnCl ₂ *2H ₂ O+ H ₃ CC(S)NH ₂	Sn 0.05M: S 0.05M	60 °C	2-10 h	9,31	-	Heated to 300°C
[50]	SnCl ₂ + H ₃ CC(S)NH ₂	Sn 0.06M / Sn 0.08M / Sn 0.1M: S 0.1M	r.t., 40 °C – 60 °C	1,5 h	-	270 nm	-
[65]	SnCl ₂ *2H ₂ O+ H ₃ CC(S)NH ₂	Sn 0.005M: S 0.04M	45 °C	-	-	400 nm	-
[55]	SnCl ₂ + Na ₂ S ₂ O ₃ *5H ₂ O	Sn 0.04M: a. S 0.04M b. S 0.08M c. S 0.125M	60 °C, 80 °C	3 h	5	380 nm	-
[66]	SnCl ₂ + Na ₂ S ₂ O ₃ *5H ₂ O	Sn 0.04M: S 0.04M	35 °C	10 h	a. 5 b. 6	-	-

[67]	SnCl ₂ + H ₃ CC(S)NH ₂	-	20 °C – 50 °C	-	-	600 nm	300-600°C 0,5 h
[68]	SnCl ₂ *2H ₂ O+ Na ₂ S	Sn 0.003M: S 0.01M	-	-	7	-	-
[54]	SnCl ₂ *2H ₂ O+ H ₃ CC(S)NH ₂	Sn 0.05M: S 0.05M	27 °C	24 h, 48h, 72 h	9,7	-	-
[69]	a. SnCl ₂ + H ₃ CC(S)NH ₂ b. SnCl ₂ + Na ₂ S ₂ O ₃ *5H ₂ O c. SnCl ₂ + TA	-	a. r.t. b. 90 °C c. r.t.	a. 24 h b. 3 h c. 24 h	-	125 nm	-
[70]	SnCl ₂ *2H ₂ O+ H ₃ CC(S)NH ₂	Sn 0.04M: S 0.08 M	60 °C	6 h	6	-	-
[71]	SnCl ₂ *2H ₂ O+ H ₃ CC(S)NH ₂	Sn 0.04M: S 0.08 M	60 °C	6 h	6	511 nm	-
[72]	SnCl ₂ + H ₃ CC(S)NH ₂	Sn 0.005M: S 0.1M	75 °C	1 h	9	500- 1000 nm	-

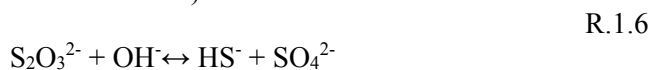
Table 1. Overview of literature results of chemical solution deposited SnS thin films.

In the above-given Table 1 are reported results obtained in the use of different sulphur precursors. In ref [58], [59], [61], [63], [47], [55], [66] and [69] *sodium thiosulphate* pentahydrate (Na₂S₂O₃*5H₂O) was used as a source of sulphur. Mechanism reactions with thiosulphate in the solution are still not clear. Several mechanisms could be found in the literature, but no one had any convincing proof.

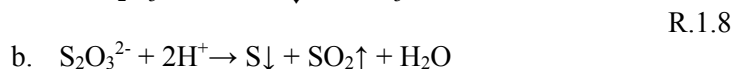
Deposition using thiosulphate (S₂O₃²⁻) is mostly held in a weakly acidic (pH >= 3) solutions. In this case, the possible reactions taking part in solution are assumed to be [14]:



If pH of solution is high (alkaline solution) the reaction could be written as:



In strongly acidic solution thiosulphate decomposes giving elemental sulphur:



In the following results of SnS depositions using thiosulphate as sulphur source, summarized in the Table 1, will be given in more details.

In reference [58] chemically deposited SnS thin films were then thermally treated in argon atmosphere at different temperatures. Thickness of the as-deposited film increased with duration of deposition and maximum value of the thickness of film was obtained after 18 hours of deposition. As-deposited films and films heated in argon atmosphere for one hour had polycrystalline orthorhombic structure and after thermal treatment films became more textured. The value of the optical band gap for as-deposited was 1.38 eV with direct transitions. When as-grown films were heated at 300 °C their photoconductivity increased [58].

Tin sulphide thin films were deposited onto non-conducting glass substrate [59]. Obtained films were without any cracks or pinholes consisting of spherical shaped grains with a compact texture and good adhesion to substrate surface. XRD analysis indicated orthorhombic crystal structure. Crystallinity of the as-deposited films was improved by their annealing. Optical data analysis showed that films exhibited direct allowed transitions with the value of band gap 1.1 eV. Resistivity of films was of the order of $10^6 \Omega\text{cm}$ [59].

Polycrystalline SnS thin films with an orthorhombic-herzenbergite structure were deposited at room temperature onto glass substrates [61]. Obtained films were uniform with good coverage of the deposition surface and of dark brown color. SEM images indicated good morphology in the form of short cylindrical rods of approximately 100 nm in diameter and 500 nm in length. The evaluated lattice parameters were found to be $a = 4.39 \text{ \AA}$, $b = 11.17 \text{ \AA}$, $c = 3.97 \text{ \AA}$. According to EDX analysis atomic ratio of Sn to S was equal to 49.8: 50.2. The band gap was found to be direct with a value of 1.31 eV [61].

Tin sulphide films were deposited onto glass substrates at room temperature and structural and vibrational properties have been investigated in [63]. XRD indicated that films were composed of predominantly orthorhombic phase of SnS with strong preferential orientation of (111) plane and crystallite size of about 67 nm. Additional phases as Sn_2S_3 and SnS_2 are also found in films. The Raman spectrum revealed three peaks at 64, 106 and 239 cm^{-1} attributed to SnS and one peak of 304 cm^{-1} which can be assigned as Sn_2S_3 and/or SnS_2 mode. The FT-IR spectrum indicated vibrations caused by Sn-O, Sn-O₂, S-O and $\text{Sn}(\text{OH})_2$ [63].

SnS layers were deposited onto glass substrates with SnS buffer layers and the influence of deposition temperature and the concentration of ratio of tin and sulphur sources on properties of the film was investigated [55]. Increasing of temperature of the solution led to the increasing of Sn/S molar ratio and to the worse compactness of the films. With increasing of the concentration ratio of $\text{Na}_2\text{S}_2\text{O}_3/\text{SnCl}_2$ in solution increased Sn/S molar ratio and compactness of the deposited films, also changed the shape of the particles from flake to shuttle and size of the particles decreased. Dark and photo conductivities of deposited films increased with the increase of deposition temperature as well as with

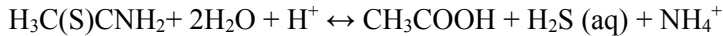
concentration ratio of $\text{Na}_2\text{S}_2\text{O}_3/\text{SnCl}_2$ in deposition solution. The optical band gaps were found to be in the range of 1.01 to 1.26 eV [55].

Difference in the structure of obtained films was determined by pH of the initial solution [66]. At pH=5 films had orthorhombic structure and comprised of short cylindrical rods. Zinc blend structure films were obtained in solutions with pH=6 and films were dense and continuous. Such a difference in the structures was explained to be due to different deposition mechanisms. During the deposition, the solution where pH was 5 remained colorless and the deposition mechanism was supposed to be ion-by-ion. Whereas in the solution with pH=6 precipitation was observed during deposition and mechanism was supposed to be hydroxide cluster. Optical band gaps were found to be 1.75 eV with forbidden direct transitions for zinc blend and 1.12 eV with allowed indirect transitions for orthorhombic SnS [66].

In ref. [56], [57], [60], [62], [64], [47], [51], [50], [65], [67], [54], [69], [70], [71], [72] *thioacetamide or TA* ($\text{H}_3\text{CC}(\text{S})\text{NH}_2$) was used as a source of sulphur. Thioacetamide is a thioamide compound that exists at room temperature as colorless to yellow crystals. It is soluble in water and ethanol [73, 74].

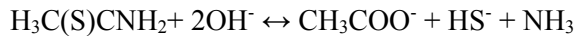
TA has the advantage of working both in acidic and alkaline environment. In strongly acidic solution [14]:

R.1.9



In alkaline solution [14]:

R.1.10



SnS thin films were deposited at different temperatures and during different deposition times [56]. However films were successfully deposited at room temperature it was shown that the increasing of temperature leads to the films faster depositions. Good quality SnS thin films with the thickness of 1000 nm were obtained in 5 hours at 75 °C or in 40 hours at 25 °C. The as-deposited films were p-type, crystalline, with a band gap of 1.3 eV and exhibited high degree of specular reflectance. Dark conductivity showed a marked increase with increase in the film thickness [56].

The influence of temperature and complexing agents as ammonia and triethanolamine (TEA) on the growth of SnS thin films was studied in [57]. Poly-crystalline structure of deposited SnS films was confirmed by XRD studies. SEM results revealed that the surface of the films have islands of nano-clusters formed on the top. Indirect bandgap of obtained films varies from 1.0 eV to 1.4 eV and it increased if concentrations of ammonia and TEA decreased. Temperature of the solution did not affect the band gap value. The resistivity of films was found to be high in range of 60000 Ωcm . Heterojunction thin film solar cells of SnS/CdS had an open circuit voltage (V_{oc}) of around 300 mV and very low short circuit current (I_{sc}) in nA [57].

SnS films were prepared from two solutions with different concentrations of components in [60]. Later the as-grown films were heated in different ambients at various conditions. Films annealed in air converted to SnO₂. Annealing in nitrogen increased the conductivity of the as-grown films. SnS films deposited from different solutions exhibited different band gaps: films from one solution had direct gap of 1.7 eV and from the other solution had indirect band gap of 1.12 eV. Deposited SnS thin films exhibited p-type electrical conductivity. Films were integrated into solar cell structures with different configurations. Best characteristics showed solar cells of the structure: SnO₂:F (conducting glass) – CdS (window layer) – SnS (buffer layer) – Cu₂SnS₃ (additional layer) – silver print after annealing for 15 min in air at 80 °C (V_{oc} = 340 mV and short circuit current density J_{sc} = 6 mA/cm²) [60].

Depending on the deposition solution composition SnS films had different crystalline structures: orthorhombic, SnS (OR), or zinc-blende, SnS (ZB) in [62]. These films had p-type electrical conductivity and band gaps of 1.2 and 1.7 eV respectively. Photovoltaic structures using both OR and ZB SnS were made in superstrate configuration with transparent conducting glass- CdS - SnS (OR) and SnS (ZB) - electrode. Different electrodes as printed Ag paint or evaporated electrodes of In, Sn, Ag were tested. The photovoltaic structure with evaporated Ag-electrode was found to have the best characteristics as V_{oc} of 370 mV, a J_{sc} of 1.23 mA/cm², fill factor of 0.44 and conversion efficiency of 0.2% under 1 kW/m² illumination. The series resistance was found to be different with the different electrode materials. The J_{sc} increased if the thickness of SnS (OR) layer increases [62].

SnS thin films were deposited onto glass substrates from aqueous solutions with multi-deposition runs [64]. Films obtained after one deposition run were amorphous, however their crystallinity improved with more deposition runs. XRD revealed that films were of zinc blend structure. SEM images showed that films have smooth and uniform surface without any pinholes or cracks. Indirect band gap is found to be 1.76 eV [64].

Three different sources of sulphur – sodium thiosulphate, thiourea and TA were used in deposition of SnS films in [47]. In case of using first two reagents precipitation occurred in solution and films were not deposited onto a deposition surface. For this reason TA was chosen as a source of sulphur. XRD results showed that obtained films were of orthorhombic crystal structure, sharp structural peaks indicated good crystallinity of films. The preferential orientation of the SnS film was (110). SEM pictures revealed a needle-shape grain structure surface of films with no any cracks. EDX showed ratio of Sn to S as 54.13: 45.8. The deposited films were of p-type conductivity. Films exhibited allowed direct energy band gap with value of 1.37 eV and allowed indirect energy band gap of 1.05 eV [47].

The effect of deposition time on the structural, electrical and optical properties of SnS thin films by chemical bath deposition onto glass substrates at 60 °C with different deposition times were investigated in [51]. All deposited

films were found to be of orthorhombic structure with preferential orientation of (110) plane. Average grain size increased from 22 nm to 24 nm with deposition time from 2 hours to 6 hours and then decreased to 22 nm for the deposition time of 8 hours. Deposited during 2 hours films were amorphous the same as films deposited at 10 and more hours. Films deposited at 4 hours were crystalline and the best crystallinity of the films was obtained during 6 hours of deposition. With increasing deposition time from 2 hours to 6 hours more homogeneous films were obtained and increasing deposition time to 10 hours led to porous structure of films due to clusters aggregations. EDX analysis was made for films deposited during 6 hours and films were found to be Sn-rich (Sn/S ratio = 1.49). Resistivity of the films decreased from 9.982 Ωcm to 2.156 Ωcm with increasing deposition time from 4 hours to 6 hours and then increased drastically to the value of 12.350 Ωcm . As-grown films were heated at 300 °C to find out the dependence of the electrical conductivity on the temperature. It increased with the increasing temperature. Optical transmittance was found to be the highest for the thinnest films deposited within 2 hours. Optic absorption coefficient was found to be higher than 10^4 cm^{-1} . Hall Effect measurements showed that all films have p-type conductivity. Direct band gap decreased with increase in thickness [51].

The effects of concentration of tin salt, triethanolamine and bath temperature on the growth of tin sulphide films were investigated in [50]. The terminal thickness of the films was obtained after 3 hours of deposition at room temperature and after that thickness started to decrease with deposition time. XRD results revealed that deposited at the concentration of SnCl_2 0.06 M films were found to consist of multiple phases: SnS, Sn_2S_3 , SnS_2 . At concentration of 0.08 M SnCl_2 tin disulphide phase peak disappeared whereas at concentration of 0.1 M only single phase, the formation of polycrystalline SnS with orthorhombic structure was observed. When concentration of SnCl_2 was increased to 0.12 M crystallinity of the films decreased. EDS showed that as the tin salt concentration in the initial solution increased, the atomic percent of tin in the film increased also and films obtained at concentration of SnCl_2 0,1M were found to be Sn-rich. SEM images revealed that at concentration lower than 0,1M SnCl_2 film appeared to be discontinuous. At concentration 0,1 M and higher films were continuous with clusters of grains, where grain size was around 200 nm. Optical transitions were found to be direct allowed with band gap of 1.95 eV for 0.06 M SnCl_2 , 1.75 eV for 0.08 M SnCl_2 and 1.5 eV for 0.1 M SnCl_2 and 0.12 M SnCl_2 . Studying the effect of TEA concentration, the concentration 1.85M is found to be the optimum. At higher concentrations obtained films were amorphous and at lower concentrations film contained Sn_2S_3 phase and had discontinuous nature. Slight decrease in the optical band gap with the increase in the TEA concentration was found. Films were deposited with varying temperature of the solution from 40 °C to 60 °C and with increasing of the deposition temperature thickness of the films was found to increase, however films crystallinity was

found to decrease. No changes in surface morphology and optical band gap were found with changes in deposition temperature [50].

In order to solve the problem of low conductivity of SnS thin films indium chloride was added as a dopant to the deposition solution in [65]. XRD patterns showed that all films exhibited polycrystalline structure. The increase of the InCl_3 content in bath causes the decrease of crystallinity – SnS peaks broadened and decreased. SEM imaged revealed that the morphologies of the films changed nominally with variation of In concentration and the grain size in the doped films decreased slightly comparing with the undoped films. The transmittance of In-doped films is lower than that of undoped films. The band gap value decreased with In-doping probably due to the structural modifications of SnS. The resistivity of In-doped films reduced by approximately two orders in In-doped films [65].

SnS films with consecutive annealing in nitrogen or hydrogen sulphide environment were investigated in [67]. AES and XPS measurements indicated that as-deposited films contained $\text{SnO}_x\text{S}_{1-x}$ and $\text{SnO}_{1+y}\text{S}_{1-y}$ phases on the surface. When films were annealed in hydrogen sulphide (at all temperatures) they converted completely to SnS with a Sn to S ratio of 55(\pm) at%: 45(\pm) at% however the films annealed in nitrogen had yet a lot of oxygen inside. Films were found to be orthorhombic. As-deposited films exhibited band gap of 1.65 eV while annealed films exhibited both indirect allowed transitions at about 1.15 eV and direct allowed transition at about 1.35 eV. Several solar cell devices were made using Mo substrates for SnS films however after annealing in H_2S [67].

The influence of deposition time on the properties of SnS thin films deposited at room temperature was studied in [54]. Films were deposited with TEA as complexing agent. Crystallinity of the films improved with increasing deposition time. XRD analysis showed that films deposited during 24 h were almost amorphous with very poor crystallinity and films deposited during 48 and 74 h were polycrystalline with orthorhombic crystalline structure. The average size of grains also increased from 13 nm to 27 nm with deposition time. SEM images revealed that at longer deposition times the number of crystallites increased resulting in increasing of homogeneity of the films. However, films deposited at 72 h started to peel off from the substrate. EDAX spectrum showed that obtained films were almost in stoichiometric composition, however films deposited at 48 and 72 h were tin-rich (Sn/S atomic ratio equal to 1.19). Authors assume that the presence of Sn excess might be due to the leak of S ions during long deposition time S ions. The optical absorption spectra indicated dominating direct allowed transition type absorption of the films. Band gap was found to be dependent on the duration of deposition and decreased from 2.03 eV to 1.79 eV. No other phases were found in the films so the change in band gap is supposed to be due to increase in thickness with deposition time. The higher value of band gap could be explained by small grain sizes of the SnS films [54].

SnS thin films were prepared using different bath solutions [69]. Precursors in the first solution (solution A) were stannous chloride,

thioacetamide and acetone, second solution (solution B) contained stannous chloride, sodium thiosulphate and tartaric acid and the third solution (solution C) was prepared using stannous chloride, thioacetamide and glacial acetic acid. Films obtained from all solutions were highly adherent to the glass substrate and deep brown in color. XRD showed that the films were polycrystalline and of orthorhombic structure, however films deposited from solutions A and C were more crystalline than that of solution B. SEM images showed that films obtained from solutions A and C were without cracks and pinholes and comprised of nanowires with diameter of 57 nm and 24 nm respectively. Acetone and glacial acetic acid is supposed to play the major role in the formation of nanowires. Films deposited from the solution B comprised of spherical grains of average size 125 nm. EDAX analysis revealed that the films from different solutions showed nearly stoichiometric nature. The transmittance versus wavelength measurement showed transparency of about 80% in the wavelength range 600-1000 nm for the films from the solution A. The films from second and third solution showed transparency of only 50% in the same range. Absorption spectra revealed medium absorption in the visible region and a decreased absorption in higher wavelengths. Films fabricated from these solutions had a direct band gap of 1.9 eV, 1.1 eV and 1.79 eV respectively [69].

Modifications in structural, optical and electrical characteristics of SnS thin films after air and nitrogen plasma treatment at different pressure conditions were studied [70]. XRD results indicate to SnS orthorhombic crystal structure of as-deposited films, however after annealing in air two additional peaks corresponding to Sn₂S₃ phase appeared. Increasing air gas pressure led to transformation of SnS into SnO₂ phase. At the same time treating with nitrogen gas plasma did not lead to any compositional changes. As-deposited samples exhibited direct transitions with band gap of 1 – 1.1 eV. After treating with nitrogen plasma band gap changes were negligible, only at the highest pressure of 4 Torr band gap decreased to 0.85 eV. After treating in air gas plasma films exhibited band gap close to that of as-deposited films however at pressure of 3 Torr the value was 1.6 eV indicating not complete transition of SnS to SnO₂ and existence of different phases with dominant SnO₂ phase. Remarkable increase in conductivity with increasing pressure was noticed for Treated with gas and nitrogen plasma films [70].

Changes in morphological, electrical and optical properties of SnS films were studied in the influence of oxygen plasma treatment in reference in [71]. Surface morphology was changing depending on the time of the treatment. The band gap increased from 1.61 eV to 1.84 eV and electrical resistivity decreased 10⁴ times. “These changes can be attributed to an increase in electron density, percolation effects due to porosity, surface degradation/etching that is an increase in surface roughness, where some structural changes related to crystallinity occurs like a high grain size as revealed by SEM images” [71].

The influence of triethanolamine on SnS growth is studied in [72]. At the lowest concentration of TEA spherically assembled nanoflakes were

obtained in films and at higher concentrations unassembled nanoflakes were formed which were found to be orthorhombic Sn₂S₃. At the highest concentration of TEA solid spheres with unassembled nanoflakes on the top with reduced coverage of the surface were formed which were found to be in composition of orthorhombic Sn₂S₃. Such distinctive phases and their morphologies were explained by different structures of the complexes of TEA with Sn ions which form at different concentration of TEA [72].

Thiourea with different concentrations was used as one type of sulphur source in reference [47], however very rapidly precipitation occurred in a solution and as a result there was no any film formed on the substrate.

Thiourea (SC(NH₂)₂) is the sulphur analogue of urea where oxygen is replaced with sulphur and is commonly used as sulphur precursor [75, 76].

There are several possible decomposition ways for thiourea given in literature. In acidic or neutral conditions, thiourea decomposes to thiocyanate ion:

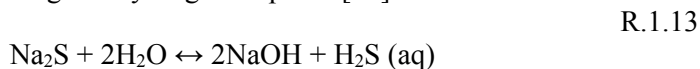


In alkaline conditions the most important decomposition way is:



This reaction is in fact in equilibrium and decomposition can happen only when are presented the cations (metal ions) which are able to create precipitation of insoluble sulphides. These metal ions eliminate sulphide ions and the reaction constantly runs to the right [14].

In reference [68] sodium sulphide (Na₂S) was used as a source of S²⁻ ions. It dissolves in water gives hydrogen sulphide [77]:



Ref [68] reports that SnS nanoflakes obtained using L-tartaric acid as a complexant and ethylene glycol as a solvent. Tin chloride dissolved in L-tartaric acid ethylene glycol solution very easily and obtained solution was clear and transparent. pH of deposition solution was adjusted to neutral before adding Na₂S to prevent formation of colloidal sulphur. XRD pattern showed pure SnS orthorhombic phase in films and no characteristic peaks of other phases were found. TEM images showed nearly rectangular shape of mostly all crystals of 10-20 nm in size [68].

Tin chloride (hydrous or anhydrous) was used commonly as a source of tin. It has colorless or white crystals which form an insoluble basic salt with water, it dissolves in ethanol, acetone, ether, methyl acetate, isobutyl alcohol, alkalies, tartaric acid and methyl ethyl ketone and very soluble in diluted or concentrated hydrochloric acid [78-80].

1.6 Literature overview summary and the aim of present work

The investigations on SnS were done by various researchers because tin monosulphide is a promising novel material for applications as absorber material in low-cost thin film photovoltaic devices. Both Sn and S are low cost, less toxic and SnS is technologically easier compared to ternary and quaternary chalcogenides. SnS is an IV-VI compound semiconductor, with suitable for PV energy band gap and high absorption coefficient of 10^5 cm^{-1} . The supply of tin and sulphur is enough in earth crust to meet our energy need through PV.

Various deposition methods are widely used for preparing SnS thin films. Among them chemical solution method is cheap and simple technique, which can be used to obtain SnS thin film in a cost-effective way.

Although the chemical deposition from solution method consists of very simple experimental technique, the film growth mechanism is generally very complicated as well as controlling of desired properties in depositing film. The key factor is to maintain the rate of the reactions enough slow, so that desired elements can deposit gradually on the substrate and not to compose big particles in solution which will precipitate out as colloidal particles. It can be achieved by slow generation of sulphide ion in the solution.

The results of big number of the studies made until now on chemical solution deposition of SnS thin film are given in Table 1. From the table it can be noticed that thioacetamide has been mostly used as sulphur source for deposition, however our choice in this doctoral dissertation to prepare SnS films by chemical solution deposition technique using sodium thiosulphate is based on its benefits such as good solubility in water, low toxicity and low price and will be mentioned in experimental details. Chemical solution deposition parameters were investigated as well as post-thermal treatment of films was applied in some works to improve the quality of the deposited SnS thin films' characteristics.

However some studies have been done, this relatively novel material needs much more further investigations for dependences of chemical solution parameters on the properties of obtained films.

The aim of the present PhD work was:

To optimize chemical deposition parameters such as pH, concentration of initial Sn and S and their ratios in the solution, duration of deposition, type of a substrate and temperature regimes of deposition and systematically characterize obtained films with different techniques to get information on the quality of the prepared films.

With the intention of obtaining thicker SnS films to employ multiple deposition runs and additionally annealing for deposited SnS films in inert atmosphere to enhance their properties.

2 EXPERIMENTAL DETAILS

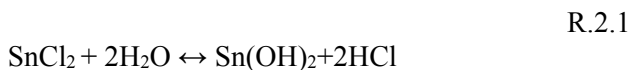
2.1 Deposition of films

This chapter gives description of film preparation conditions and different used analytical techniques. As the films were deposited by chemical solution method in use of solutions with different composition as well as changing of deposition parameters then here will be given only details common for all experiments. The more precise characterization of terms of deposition (solutions composition, duration of deposition, pH of the solution etc.) will be given in results and discussion part.

Deposition of SnS thin films

For SnS thin films different sources of tin and sulphur can be used. In this work as a source of tin (+II) ions was taken reagent stannous (II) chloride while for a source of sulphide (-II) ions sodium thiosulphate pentahydrate was used. Sodium thiosulphate pentahydrate has a number of benefits compared to commonly used thioacetamide as it is non-toxic, well-soluble in water and cheap reagent [81, 82].

When stannous (II) chloride dissolves in water, it forms tin hydroxide:



To avoid this precipitation of $\text{Sn}(\text{OH})_2$, complexing agent was added. The complexant reacts with metal ion and forms complex, reducing the concentration of not-bonded metal ions in the solution and preventing fast bulk precipitation of the colloidal particles of tin sulphide in solution [14].

To prepare solution for depositing SnS films few drops of hydrochloric acid were added to stannous chloride to dissolve it:



Forming complex is stable only in strongly acidic solution however it is not possible to use sodium thiosulphate in such conditions due to its degradation. In water this complex dissociates as:



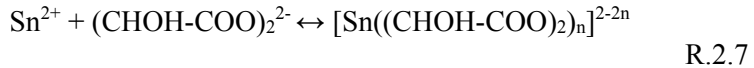
it continues to dissociate:



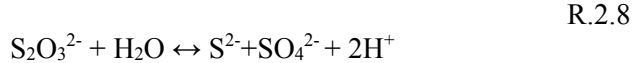
For this reason another more stable complexing agent should be added and tartaric acid $(\text{CHOH})_2(\text{COOH})_2$ was used. It dissociates in water giving tartrate ion:



Tartrate ion makes complex with tin ion which dissociating releases slowly tin ion:



Ammonium hydroxide was added to maintain the pH of solution. Sodium thiosulphate was the last added component. It dissociates in water releasing sulphur-containing anion which joining with tin cation during deposition produces desired SnS film:



Different substrates as indium tin oxide (ITO), tin dioxide (TO), molybdenum (Mo) covered glasses and borosilicate glass were used in our experiments to look for the influence of substrate material on the properties of deposited films. Prior to deposition all substrates were cleaned in ultrasonic bath and sulphuric acid and after were rinsed with distilled water. In addition in several experiments, SnS thin films were deposited onto the glass substrates covered with CdS and ZnS thin films.

Pre-cleaned substrates were placed vertically into glass vessel with conductive side of substrate toward the walls and freshly prepared solution was poured into vessel and then vessel was closed hermetically with paraffin film for film deposition.

Deposition was ordinary held at room temperature during 24 h. Obtained films were rinsed with deionized water and dried.

Deposition of ZnS thin films

ZnS thin films were prepared by chemical solution deposition technique, consecutively stirring zinc sulfate, triethanolamine, ammonium hydroxide, thioacetamide with respective molar concentrations of 0.025M, 0.014M,

concentrated, 0.01M in final solution volume [83]. Deionized water was added to obtain total solution volume of 100 ml. Corning glass substrates, which were previously washed with detergent, were placed vertically in solution. Deposition was carried out at room temperature for 24 hours. Obtained films were cleaned with cotton and rinsed with deionized water and then dried. In following ZnS films were heated in the air for 15 min at 270°C to obtain good adherence of consecutively deposited SnS film.

Deposition of CdS thin films

CdS thin films were prepared by chemical solution deposition, consecutively stirring cadmium nitrate, sodium citrate, ammonium hydroxide and thiourea solutions with respective molar concentrations of 0.025M, 0.15M, concentrated, 0.05M in final solution volume [84]. Deionized water was added to obtain total solution volume of 100 ml. Corning glass substrates, which were previously washed with detergent and then in ultrasonic bath with acetone, were placed vertically in solution. Deposition was held at 80 °C during 1 h and 30 min. Obtained films were cleaned using cotton and rinsed with deionized water and then dried.

2.2 Characterisation of films

The quality of the obtained by chemical solution deposition SnS thin films was characterized by instruments such as SEM-EDX, AFM, XRD and Raman spectroscopy for knowing the morphological, structural and phase composition features along with optical and electrical characterizations were employed.

2.2.1 Morphological studies of films

One of the most common techniques to characterize thin films is *scanning electron spectroscopy (SEM)* equipped with *energy dispersive X-ray analyser (EDX)*. The interaction of focused electron beam with a sample can be monitored in different ways to get information about morphology and composition. Using SEM surface and cross-sectional imaging it is possible to get information about shape and size of samples as well thickness of films.

A variety of different phenomenon occurred as a result of interaction of primary electron beam with sample; secondary and backscattered electrons and X-rays. The low energies of secondary electrons are generated near surface area, due to this secondary electron detector provides the best resolution of fine surface topographical features of the studied materials. Backscattered electrons are produced as a result of elastic collisions with atoms of the sample and the number of backscattered electrons increases with atomic number of the sample increasing [85].

Another type of signals by interaction of the primary electron beam with the sample is the characteristic of X-rays; the excited characteristic X-rays intensities are proportional to the total mass of the respective electrons [86]. The analysis of characteristic X-rays allows providing chemical information about the studied material and it gives useful information about the distribution of the elements in the volume of the materials.

In the present work scanning electron microscopy (Hitachi SUI 510 and HR-SEM Zeiss ULTRA 55) were used to obtain information about SnS thin films surface morphology. The elemental composition and stoichiometry of prepared films was determined by an energy-dispersive X-ray analysis system (Röntec EDX XFlash 3001 detector).

If SEM gives us information about morphology of the samples, *atomic force microscope (AFM)* additionally gives information about their surface roughness and 3D images surface apart from 2D images. It operates using very thin needle which is joined with cantilever beam. The tip of the needle moves over the surface of the sample up and down in accordance to the roughness. The cantilever deflections results in the mapping of the surface images [87]. In the present thesis, “peak force tapping” mode was used for imaging the SnS thin films.

An atomic force microscope (Bruker Multimode) with a Nanoscope V controller was used to determine the surface roughness of the films.

2.2.2 Determination of crystal structure and phase composition of films

X-ray diffraction (XRD) analysis is used to get information on films crystal structure as well as orientation of crystallites in films.

XRD allows us to determine structural properties like average crystallite size as well as lattice parameters, strain and dislocation densities of films, which is based on the interaction of the incident x-rays with the volume of film and is diffracted according to the Bragg's law ($n\lambda = 2d\sin \theta$), where d is the spacing between interatomic planes in the crystalline phase, λ is the wavelength of the x-ray used, θ is diffraction angle and n is order of diffraction [88]. During XRD analysis x-ray diffraction pattern is obtained which is uniquely characteristic to each certain crystalline lattice, it can be compared with “fingerprint” of the lattice [89].

Debye-Scherrer formula was used to find the average size of crystallites D of the film from data of XRD analysis [90]:

$$D = K\lambda / (\beta \cos \theta) \quad \text{Eq.2.1}$$

where D is crystallite size, K is a constant (K= 0.94), λ is the wavelength of the x-ray used, θ is diffraction angle and β is full width at half the maximum of the x-ray diffraction peak .

The crystalline structure of the films was investigated by X-ray diffraction analyses with a Rigaku Ultima IV X-ray diffractometer using Cu K α radiation with 2θ ranging from 10° to 70°.

Raman spectroscopy. Phase composition of deposited films was verified additionally by Raman spectroscopy that provides information about molecular vibrations in films.

In Raman spectroscopy monochromatic source of light is used as excitation that interacts with sample and scattered light is detected and analyzed. Greater part of the scattered light has the same frequency as the laser light however when incident light interplays with the vibrational energy levels of the molecules in sample occurs shifting in energy. Raman spectrum of the film is obtained by plotting the intensity of this "shifted" light versus frequency [91]. When we interpret and compare information about phase composition obtained by Raman and XRD analyses it should be taken into account that these methods give information on phase composition in different thicknesses of film, so from Raman spectroscopy we can obtain information about composition of surface area and from XRD technique phase composition of the volume of the film [89]. Raman spectroscopy measurements were made at room temperature on a high-resolution micro-Raman spectrometer (Horiba JobinYvon HR800) equipped with a multichannel detection system in backscattering configuration. An Nd-YAG laser ($\lambda = 532$ nm) and a He-Ne laser ($\lambda = 633$ nm) with a spot size of 10 μ m in diameter were used for excitation during Raman investigations.

2.2.3 Optical spectral analysis of films

In the present study, the optical transmittance and near-normal specular reflectance of the films were recorded using a scanning spectrophotometer (Shimadzu UV-VIS-NIR) in the wavelength range of 250–2500 nm.

Optical spectral analysis was carried out to determine optical band gap of films. The optical absorption coefficient is calculated from the measured transmittance (T) and specular reflectance (R) spectrum and was mathematically given by the following formula [92]:

$$T = (1-R)^2 e^{-\alpha d} \tag{Eq.2.2}$$

$$\alpha = -1/d \ln (T/(1-R)^2) \tag{Eq.2.3}$$

where α is an absorption coefficient and d is the thickness of the sample.

The optical band gap of films was evaluated from absorption coefficient using the formula [93]:

$$(\alpha h\nu)^n = A(h\nu - E_g) \quad \text{Eq.2.4}$$

where A is a constant, h - Planck's constant, ν - light frequency, E_g – band gap energy and the value of “n” depends on the type of transitions that occur between parabolic bands of the sample, $n=2$ for allowed direct and $n=1/2$ for allowed indirect transitions.

The optical band gap energy was evaluated by extrapolating the linear portion of a plot of $(\alpha h\nu)^n$ versus photon energy ($h\nu$) to x-axis ($h\nu$).

2.2.4 Additional measurements

A profilometer (XP Plus Stylus) was used to determine the thickness of the films.

Electrical characteristics were measured using Keithley 619 electrometer with Keithley 230 programmable voltage source. The photoconductivity of the films were measured under a tungsten halogen lamp providing illumination of 850 W/m^2 . Hot-probe method was used to determine charge-carrier type.

The photoelectrochemical measurements were carried out using Gamry Potentiostat in the standard three-electrode cell with SCE (saturated calomel electrode) as reference. The measurements were performed at room temperature with linear sweep voltammetry in a background electrolyte solution of 0.1M sulfuric acid under the chopped white light with an intensity of 100 mW/cm^2 .

3 RESULTS AND DISCUSSION

3.1 Optimization of the chemical solution parameters

Composition, structure and technical properties of deposited films are influenced by several technological parameters of deposition such as concentration of components in the solution, their ratio, pH and temperature of the solution as well as duration of deposition. To deposit films with tailored parameters we have to understand this influence.

3.1.1 The influence of concentrations of tin and sulphur in the initial solution on the parameters of chemically deposited films (article II)

One of such very important parameters to control during deposition of films is concentration of initial components of tin and sulphur in deposition solution. Goal of the experiments was to determine and understand this influence and to find most suitable concentration of initial tin and sulphur for deposition of SnS film with needed composition, structure and parameters.

Five solutions with different concentrations of tin and sulphur with constant ratio of them (equal to 1: 1) were prepared. The solutions were in compositions of 0.01 M, 0.03M, 0.05 M, 0.07 M and 0.09 M and pH of solution was neutral (equal to 7 in all experiments). Deposition was done at temperature of around 22 ° C using molybdenum (Mo), indium tin oxide (ITO), tin dioxide (TO) and borosilicate glass as substrates.

Incomplete coverage of the surface of the all used substrates by deposited SnS film was typical for the solution 0.01M (Fig. 3.1) and SnS forms on the substrate as separate agglomerated particles or spherical clusters [19, 72] with the sizes of around 300 nm.

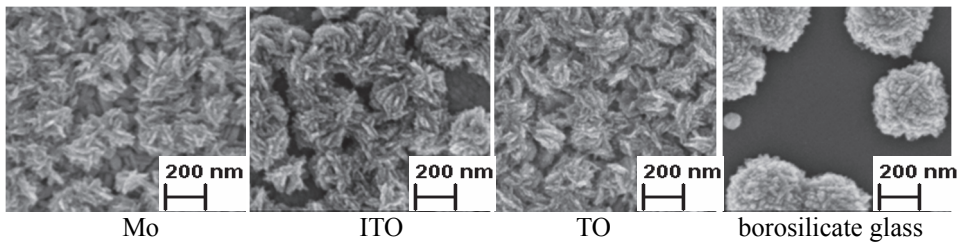


Fig. 3.1 SEM images of the SnS thin films deposited at concentration of 0.01M.

We did not notice the formation of any films structure on borosilicate glass that could be explained by insufficient number of crystallization centres on very smooth borosilicate glass substrate. Similar mode of deposition of separate agglomerated particles was prevailing also in use of ITO substrates; however

agglomerates of tin sulphide were smaller and were with the size of about 150 nm. The deposition onto Mo and TO substrates leads to the denser coverage of the substrate with SnS agglomerates with nearly similar sizes (around 120 and 100 nm, respectively) and to the formation of continuous SnS thin film structure.

The deposited SnS films had uniform and complete coverage of Mo, ITO and TO substrates at concentrations of tin and sulphur in solution 0.03M (Fig. 3.2) and nearly the same average size of films forming SnS agglomerates (190, 200 and 210 nm respectively). This concentration seems to be the optimal for depositing SnS films onto these substrates due to uniform, complete coverage of the substrates by formed SnS films and due to good adhesion of the deposited pin-hole free films to the substrates. At the same time incomplete coverage of substrate by separate agglomerates with average sizes of 240 nm prevails on smooth borosilicate glass substrate.

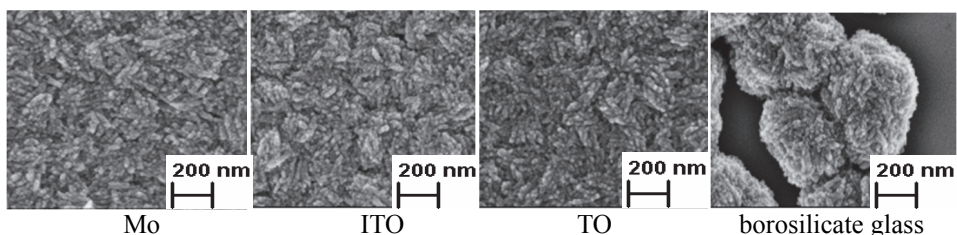


Fig. 3.2 SEM images of the SnS thin films deposited at concentration of 0.03M.

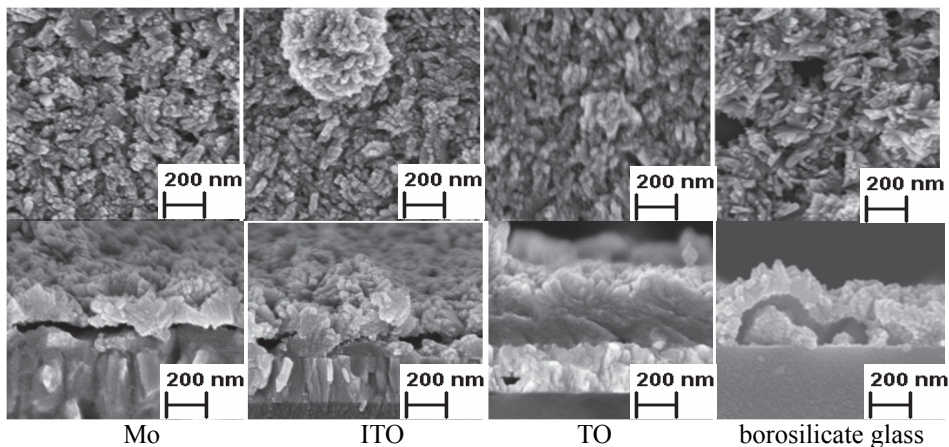


Fig. 3.3 SEM images of the SnS thin films deposited at concentration of 0.05 M.

Starting from deposition solution with concentration of 0.05M (Fig. 3.3) on all substrates, except borosilicate glass substrate, complete and uniform coverage of substrate was typical, but formed SnS films adhered weakly to the deposition substrate and peeled easily off. Here the only exception was TO substrate with strong adhesion of formed SnS films. The use of this solution

composition results in deposited SnS films with maximum thickness: 215 nm, 220 nm and 250 nm respectively on Mo, ITO and TO substrates. Our analysis of the experimental process allows us to conclude that at this concentration of constituents in solution the mechanism of formation of SnS began to change from ion-by-ion mechanism to cluster deposition.

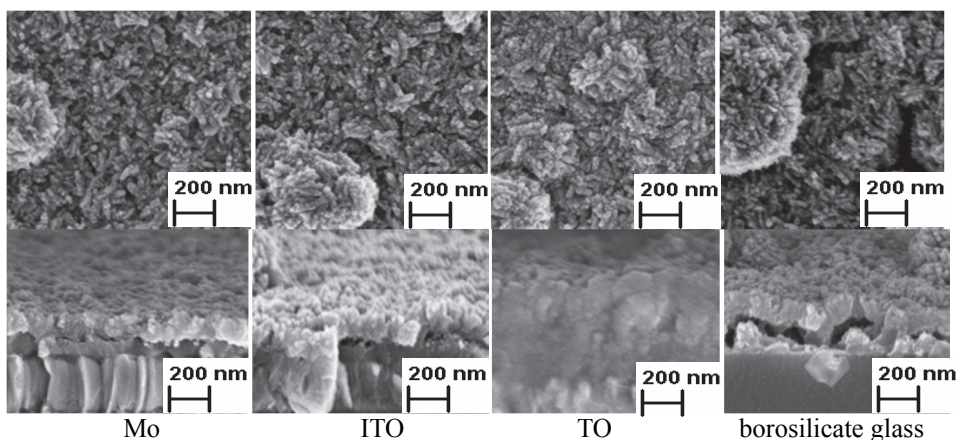


Fig. 3.4 SEM images of the SnS thin films deposited at concentration of 0.07M.

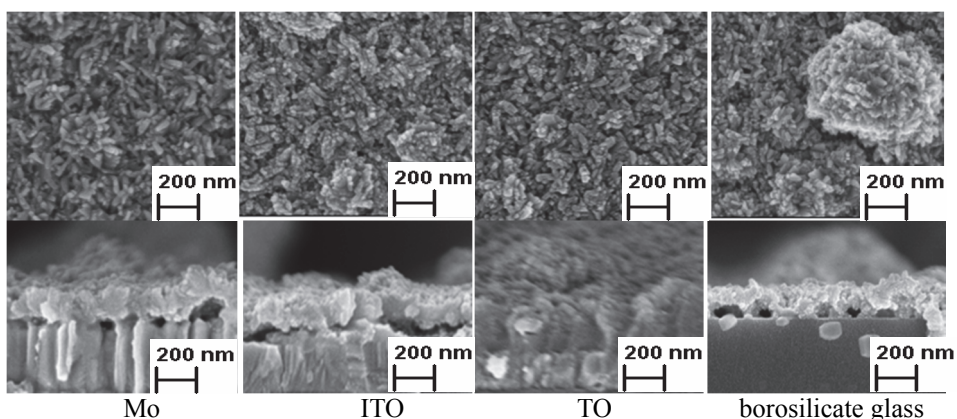


Fig. 3.5 SEM images of the SnS thin films deposited at concentration of 0.09M.

The changes in dominating films formation mechanism leading to big agglomerates formed on the surface of deposited film are well seen at concentration of 0.07 M (Fig. 3.4). This solution results in pinhole-free, uniform and complete coverage of Mo and ITO substrates by formed SnS films and in decreased compared with films deposited in solution with lower concentration of Sn and S (Fig. 3.6) thickness of the deposited SnS films. The formation of SnS big clusters on the surface of substrates with increasing concentration has been also noticed by other researchers [50].

SnS films deposited on all substrates at the highest used concentration of 0.09M (Fig. 3.5) have complete and uniform coverage of substrates, but these films had very weak adhesion with substrate, that results in their easy peeling off from the substrate. Compared with films from lower concentration of solution the thickness of the deposited films decreased.

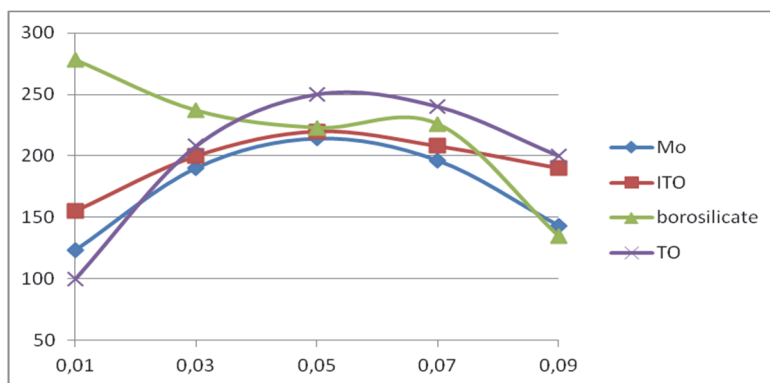


Fig. 3.6 Thickness of SnS films in dependence on deposition solution composition.

EDX analysis (table 3.1) showed that films grown on Mo and ITO substrates at solution concentrations less than 0.05 M have stoichiometric composition. Films deposited on all substrates are in Sn-rich composition at the highest solution concentration (of 0.09 M). EDX did not indicate the presence of chlorine in the films indicating that obtained films does not contain any traces of precursor tin chloride. Sn-rich content of deposited films was also noticed by several other researchers [47, 51, 50, 94] and could be explained by the formation and the existence of different oxygen and tin containing separate phases in deposited films [95].

Concentration of Sn and S	Mo	ITO	borosilicate	TO
	Ratio Sn:S in obtained films			
0.01 M	1.0	1.0	1.2	1.1
0.03M	1.0	1.0	1.2	1.2
0.09M	1.2	1.2	1.1	1.3

Table 3.1. Elemental composition of SnS thin films deposited at different composition of deposition solution.

Raman spectroscopic analysis was made to evaluate phase composition of deposited films. Fig. 3.7 shows Raman graphs for SnS films deposited onto ITO substrates. Raman graphs for films at all solution concentrations were similar and had mainly peaks corresponding to orthorhombic SnS phase: 82 cm^{-1} [96], 95 cm^{-1} , 163 cm^{-1} , 188 cm^{-1} , 227 cm^{-1} , 288 cm^{-1} [97]. Two possible

additional peaks, one at 309 cm^{-1} for films deposited from solution with tin and sulphur concentrations 0.01 M corresponds to Sn_2S_3 phase [98] and weak peak at 333 cm^{-1} in films at all solution concentrations could belong to SnS_2 [99].

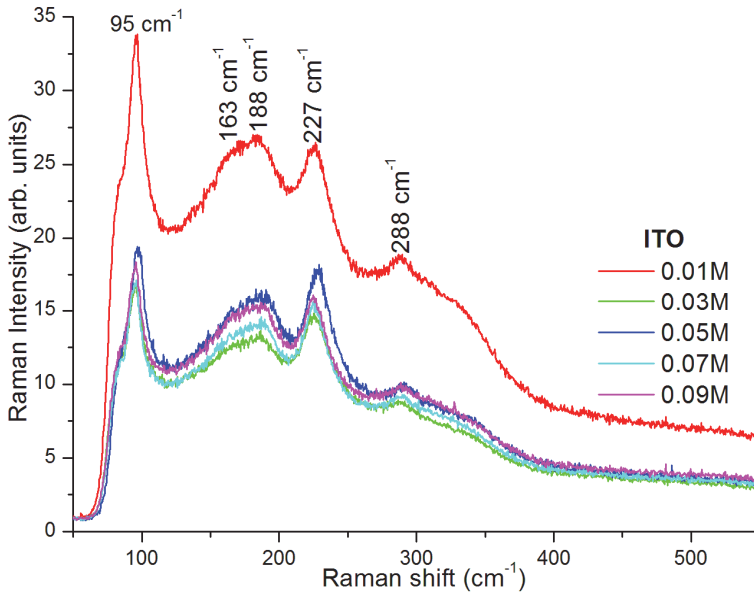


Fig. 3.7 Raman spectras of SnS films deposited on ITO substrates at different concentrations.

Raman spectra of films deposited on Mo, TO and borosilicate glass substrates were similar to films on Raman spectra of films deposited onto ITO substrate. As the only difference we noticed was the formation of Sn_2S_3 phase (peak at 233 cm^{-1}) [98] in films deposited on Mo substrate at concentration of solution equal to 0.01M .

To summarize, the deposition process is strongly influenced by used substrate. The very smooth surface of the borosilicate glass substrate makes difficult for SnS nuclei to adhere and we noticed the formation of SnS films structure on this substrate only at high concentrations. The concentrations of tin and sulphur in solution do not have remarkable influence to the elemental composition of deposited films but at concentration of 0.01M deposited SnS films have incomplete coverage of the substrates. Concentration of 0.03 M was found to be the most suitable to deposit uniform, good-adherent, pin-hole and voids free SnS thin film with complete coverage of a substrate. The deposition of SnS films at higher than 0.05 M solution concentration of tin and sulphur leads to the diminishing of films thickness due to changes in dominating deposition mechanism and weak adhesion of the films to the substrates.

3.1.2 The influence of ratio of tin to sulphur in solution on the chemical solution deposition of films

Evaluation of appropriate ratio of tin to sulphur in solution is important to deposit tin *monosulphide* phase as the excess of one or another component leads to the formation of nonstoichiometric composition of final tin sulphide film or undesired phase composition of the deposited films.

Five solutions were prepared with ratios of initial Sn and S in solution equal to 1:1; 1:1,5; 1:2, 1:2,5 and 1:3 and with concentration of tin fixed to 0.03M in all films using molybdenum (Mo), indium tin oxide (ITO), borosilicate glass and tin dioxide (TO) as substrates. Deposition was held at pH=7 and at temperature of around 22 °C.

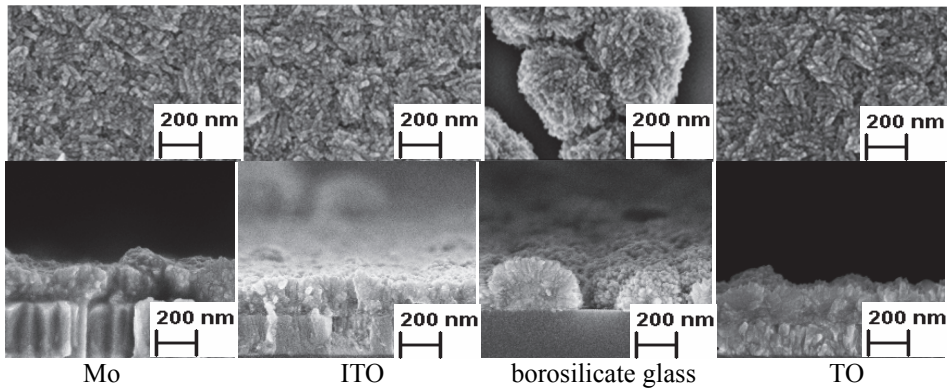


Fig. 3.8 SEM images of the SnS thin films deposited at ratio 1:1.

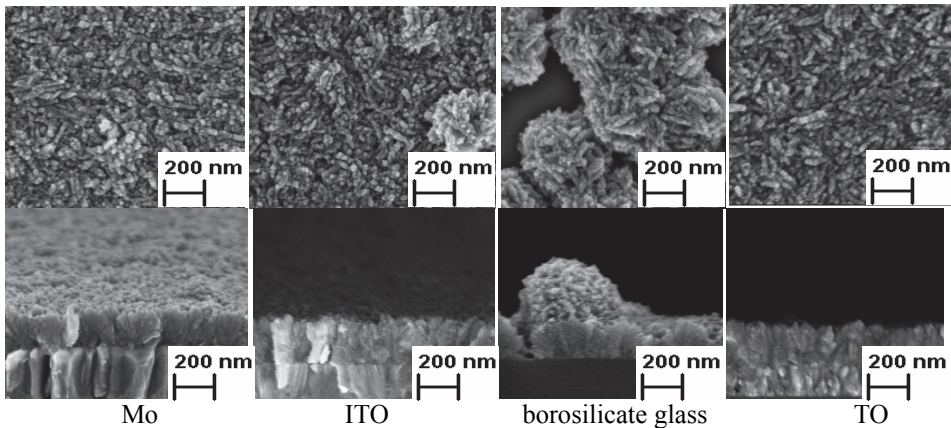


Fig. 3.9 SEM images of the SnS thin films deposited at ratio 1:1.5.

SnS thin films have similar morphology and cover Mo, ITO and TO substrates completely and uniformly and films have good adhesion to the substrates at ratio Sn/S in deposition solution equal to 1:1 (Fig. 3.8) and 1:1.5 (Fig. 3.9). Only deposition onto borosilicate glass substrate leads to deposition of separate agglomerated particles resulting in incomplete coverage of the substrate.

Changes in the shape of particles from rounded shape to ones with sharper edge occur starting from components ratio in solution 1:2 (Fig. 3.10). Thickness of deposited SnS films decreases in solution 1:2 (table 3.2) comparing with thicknesses of films from the solution with S/Sn = 1:1 as well as coverage of the substrates becomes incomplete.

ratio Sn:S in solution	Mo	ITO	borosilicate	TO
	Thickness of obtained films, nm			
1:1	190	200	237	208
1:1,5	205	208	214	214
1:2	190	120	214	179
1:2,5	188	167	197	165
1:3	68	147	167	165

Table 3.2. Films' thickness versus ratio of Sn to S in deposition solution.

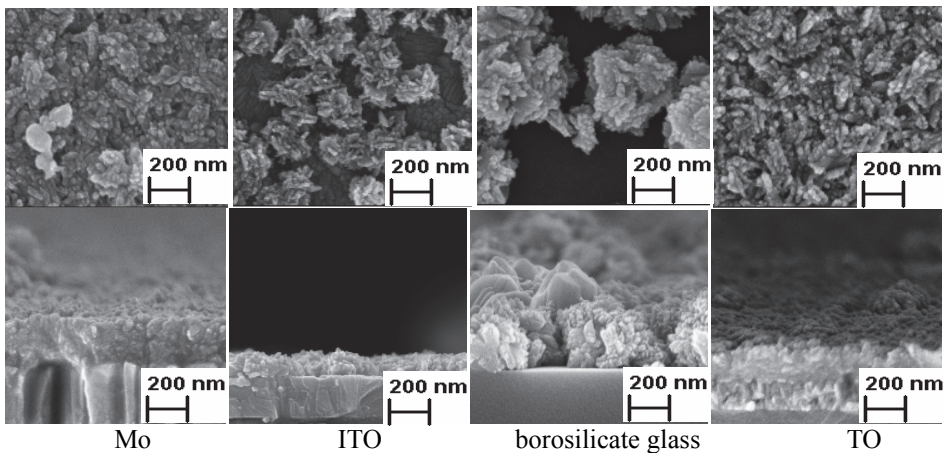


Fig. 3.10 SEM images of the SnS thin films deposited at atomic ratio of components in deposition solution 1:2.

Incomplete coverage of all substrates by SnS film dominates at ratio of film components in solution 1: 2.5 (Fig. 3.11) and the thickness of films continues to decrease. The adhesion of films on substrates was very weak and due to this formed SnS films easily peeled off from the substrates.

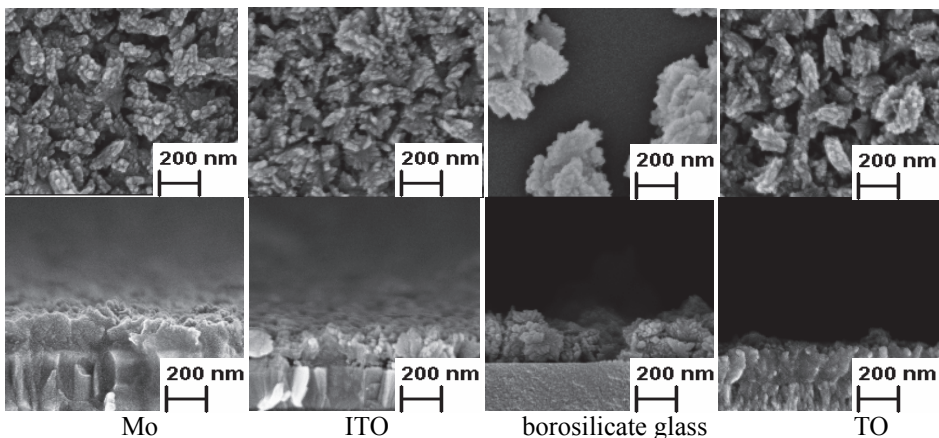


Fig. 3.11 SEM images of the SnS thin films deposited at ratio 1:2.5.

At ratio 1:3 (Fig. 3.12) the deposited SnS films are characterized by huge size non-uniform agglomerated colloidal particles on the surface and with incomplete coverage of substrate and with non-uniform different color of films. The deposited films are thinner in comparison with films from solution with lower tin and sulphur ratios.

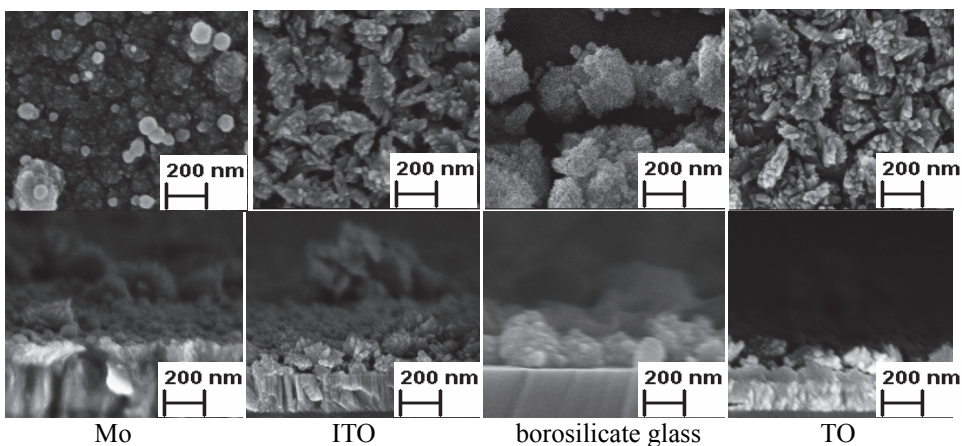


Fig. 3.12 SEM images of the SnS thin films deposited at ratio 1:3.

The reason of these changes could be high velocity of the SnS formation reaction in solution (the solution began to change its color immediately after adding S^{2-} source in) what leads to the rapid formation of SnS colloidal particles in solution and their precipitation to the substrate.

Films are found to be almost in stoichiometric composition of 1:1 (except films deposited on borosilicate glass). It could be seen from the table 3.3 that concentration of sulphur in films starts to increase with increasing ratio of

Sn to S probably due to formation of additional SnS₂ phase in films (existence of SnS₂ phase in films was found by Raman analysis).

	Mo	ITO	borosilicate	TO
ratio Sn:S in solution	ratio Sn:S in obtained films			
1:1	1.0	1.0	1.2	1.2
1:1.5	1.1	1.0	1.1	1.1
1:3	1.0	0.9	1.0	1.0

Table 3.3. Ratio of Sn to S in obtained films versus concentrations in solutions.

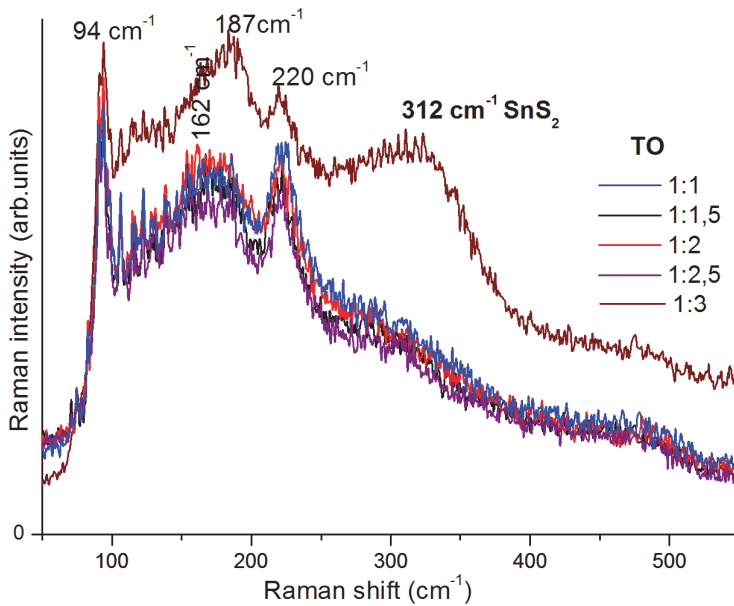


Fig. 3.13 Raman spectras of SnS films deposited on TO substrate at different ratios of components in deposition solution.

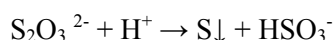
Raman graphs of films deposited on different substrates are similar and contain peaks belonging mainly to tin monosulphide phase: 94 cm⁻¹, 162 cm⁻¹, 187 cm⁻¹, 220 cm⁻¹, 288 cm⁻¹ [100]. However at component ratio 1:3 in solution Raman spectra exhibit additional peak at 312 cm⁻¹ which belongs to the SnS₂ phase [98] as it can be seen on the fig. 3.13 for all substrates.

Obtained results allow us to conclude that the ratio of tin and sulphur in solution has influence to the composition and adhesion of chemical solution deposited films. At ratio 1 to 1 and 1 to 1.5 good adhesion and pin-hole free morphology films have complete coverage of the substrates. Incomplete coverage of the surface and the formation of voids between SnS films and used

substrates are typical for films deposited from solution at ratios of tin to sulphur starting from 1: 2. Raman analysis showed in formed films peaks corresponding only to SnS phase, however at ratio equal to 1: 3 SnS₂ phase forms additionally to SnS.

3.1.3 Influence of pH of the chemical solution on the parameters of deposited films

pH of the solution has to play important role in chemistry of deposition. In spite of chemical solution deposition can be held at different pH values, some reagents are not resistant to strongly acidic or strongly alkaline conditions. This occurs for example in case of sodium thiosulphate, which in this work was used as source of sulphide ion in solution. Sodium thiosulphate degrades at pH equal or lower than 3, releasing elemental sulphur:



For this reason deposition was not held in this study in strongly acidic conditions. Five solutions were prepared using the same recipe as previously with different pH values of the final solution varying from 5 to 10. Ratio of Sn to S was fixed to 1:1 and concentrations of tin and sulphur in solution were fixed to 0.03M. Deposition was held at at temperature of around 22 °C.

Fig. 3.14 shows SEM images of the films deposited at pH = 5. Deposited films cover Mo and TO substrates completely, however contain pin-holes and voids in. Coverage of the ITO substrate was found to be incomplete.

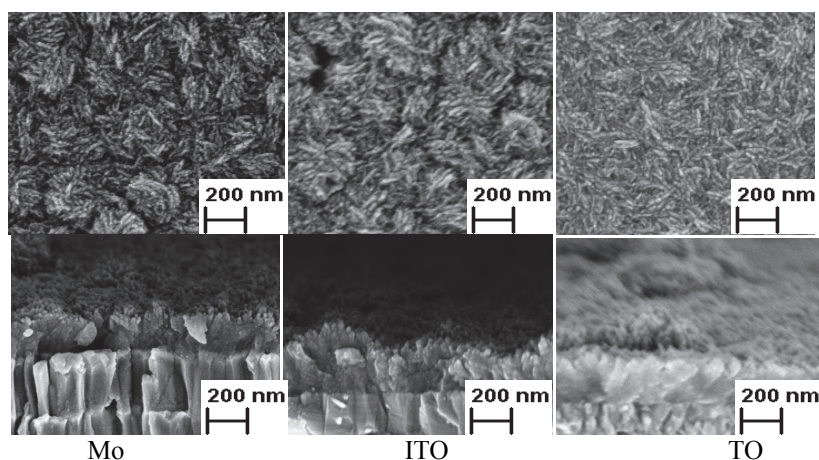


Fig. 3.14 SEM images of the SnS thin films deposited from solution at pH=5. All obtained films were non-uniform in color with spots of greenish-violet color on the surface.

Fig. 3.15 represents films deposited at pH = 6. Films are more uniform compared with films deposited from solution with pH = 5 but contain also voids in. Again incomplete coverage of the ITO substrate by formed film was noticed.

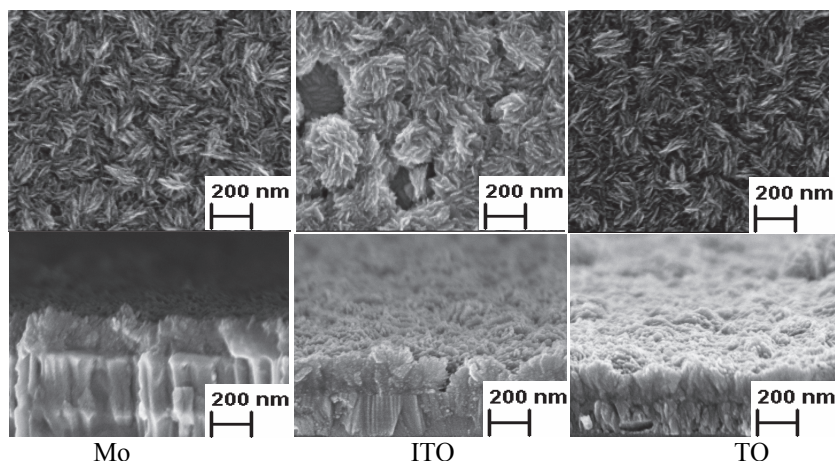


Fig. 3.15 SEM images of the SnS thin films deposited at pH=6.

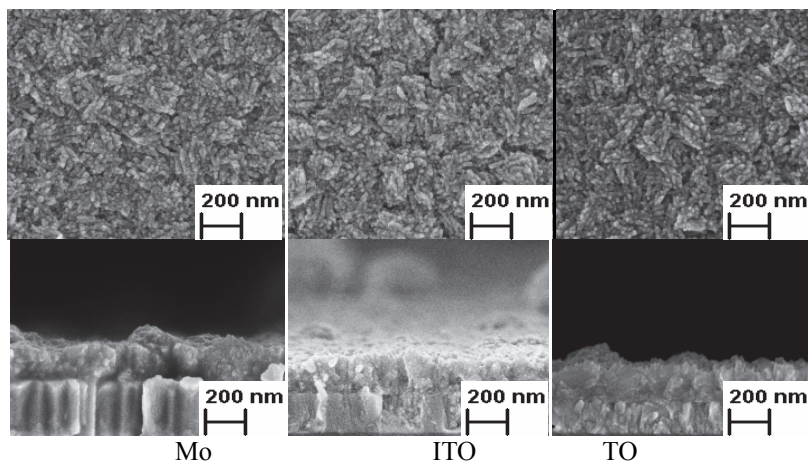


Fig. 3.16 SEM images of the SnS thin films deposited at pH=7.

Deposited films cover all used substrates uniformly and completely at pH = 7 in solution (Fig. 3.16). Further increase in pH led to incomplete coverage of all substrates and formation of big agglomerates on the top of the surface of the films (Fig. 3.18). At pH equal to 10 SnS films did not deposit at all on the substrate.

The pH was found to influence the velocity of the deposition reactions. Increase of pH value led to higher speed of the deposition and film could not

form gradually and uniformly on all of the used substrates. The presence of precipitated out in the solution clusters could also indicate the changes in deposition mechanism from ion-by-ion to cluster mechanism.

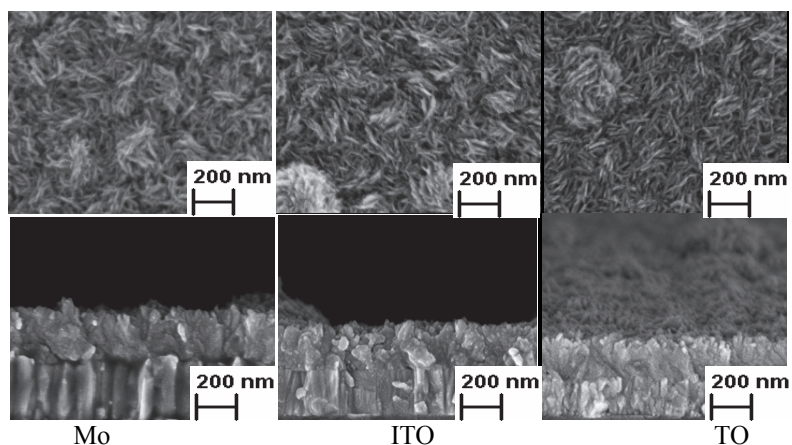


Fig. 3.17 SEM images of the SnS thin films deposited at pH=8.

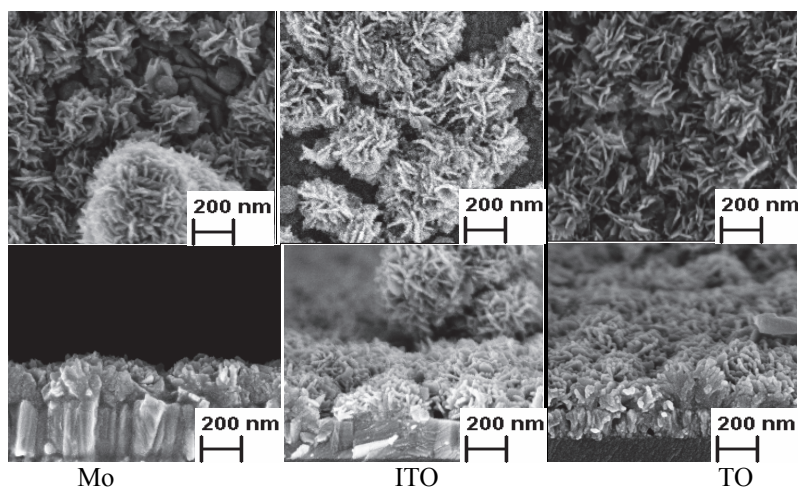


Fig. 3.18 SEM images of the SnS thin films deposited at pH=9.

	Mo	ITO	TO
pH	ratio Sn:S in obtained films		
5	0.9	0.9	1.0
7	1.0	1.0	1.1
9	1.0	1.0	1.0

Table 3.4. Ratio of Sn to S in obtained films versus pH of the solution.

EDX results (table 3.4) showed that films deposited on all substrates are almost of stoichiometric composition.

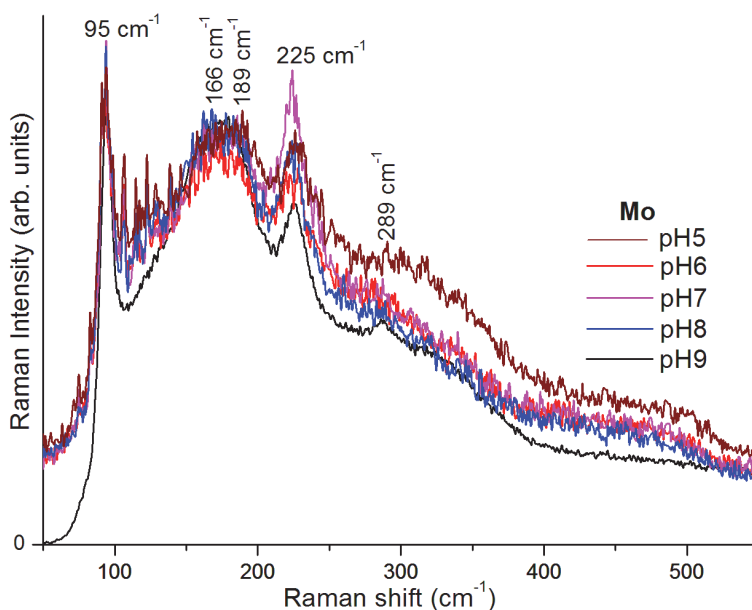


Fig. 3.19 Raman spectras of SnS films on Mo substrates with varying pH.

Raman graphs of films deposited on different substrates are similar indicating that phase composition of films does not depend on material of substrate. All peaks in Raman spectra (fig. 3.19) belong to SnS phase: 95 cm^{-1} , 166 cm^{-1} , 189 cm^{-1} , 225 cm^{-1} , 289 cm^{-1} [100]. At pH=9 peak in the region of 330 cm^{-1} was noticed indicating the presence of SnS₂ phase [99].

Our analyses of obtained results allows us to conclude that in studied deposition solution pH values the optimal pH value for the deposition is neutral (pH = 7). SnS films deposited onto all substrates at pH=7 covered surface completely and uniformly without any voids or pin-holes in. At pH = 9 and at pH values less than 7 we noticed incomplete coverage of substrates by the formed SnS films and formation of voids between substrate and film as well as presence of secondary phase in films.

3.1.4 Duration of the deposition

During chemical processes occurring in solution, sulphide and metal (Sn) ions react with each other, producing SnS which deposits on the substrate. If all existing ions in solution already have reacted, the reaction stops and films

growth ends. In this series of experiments we have tried to determine the optimal duration of deposition that is indicated by the ending of film's growth.

Chemical solutions were prepared with ratios of initial Sn and S sources equal to 1:1 and concentrations of 0.03 M in the total solution. Deposition was done at pH=7 in glass vessels at 22 °C. Substrates were removed from the vessels after 3, 5, 10, 15, 17, 19, 21, 23 and 36 hours to evaluate growing process of SnS thin film.

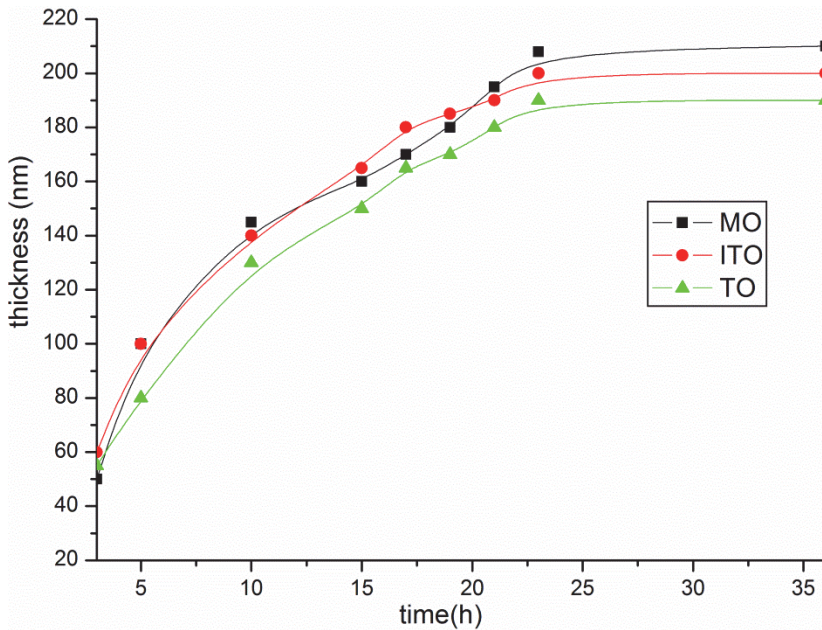


Fig. 3.20 Dependence of films thickness on deposition time.

It could be noticed (fig.3.20) that in the beginning growth process is rapid and it becomes slower with time. The thickness of the films deposited on all used substrates does not change after around 24 hours of deposition indicating the use of all reacting ions and the end of growing process of the films. Taking this into account the duration of deposition of around 24 hours is sufficient for deposition of SnS thin films with the maximal use of SnS films components from solution.

3.1.5 The influence of deposition temperature on the parameters of SnS thin films

Temperature is a factor which influences drastically the velocity of the reactions taking place in the solution. With increasing temperature mass transport accelerates and reactants can reach each other and substrate faster. As

the stability of complexes is lower at higher temperatures, then tin ions will release faster and concentration of free tin ions in the solution will be higher. Release of chalcogenide ions becomes also faster. All this leads to two opposite effects: to the faster growth of the film and on the other hand it result in bigger number of collisions between particles in volume and intense precipitation of aggregates in solution. For this reason it is difficult to predict whether increasing of the temperature will benefit growth of thick and uniform films or not. At this work films were mainly deposited at room temperature (around 22 °C), but in several experiments we deposited at higher temperatures.

Three similar deposition solutions were prepared. Deposition temperatures were 35 °C, 45 °C and 55 °C. The deposition was held on ITO, TO and Mo-covered glass from solution with concentrations of initial Sn and S sources equal to 0.03M with ratios of Sn to S equal to 1:1. SnS films growth ended after 3 hours of deposition at 55 °C. At lower temperatures (45 °C and 35 °C) films growth ended after 4 and 6 hours respectively.

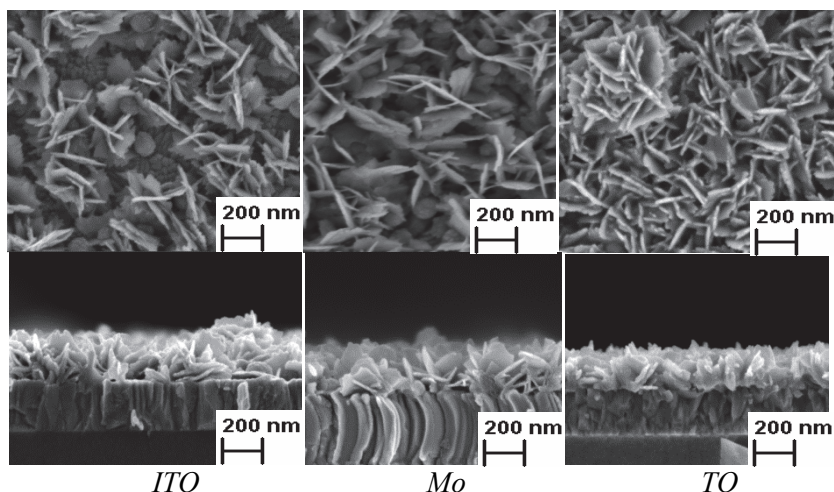


Fig. 3.21 SEM images of the SnS thin films deposited at 55 °C.

Raman analyses of obtained films revealed that films do not contain any secondary phases and all peaks belong to SnS phase. However, films exhibited very non-uniform structure and did not cover all used substrates uniformly. On Fig. 3.21 are shown SEM images of SnS thin films deposited at 55 °C, deposited at 35 and 45 °C films have similar morphology. The reason is that SnS formation proceeded too quickly and SnS precipitation occurred already in the solution and not only on the substrates.

Our experiments confirmed that increase of deposition temperature leads to rapid precipitation and do not let gradual films formation. All deposited at higher than room temperature films were non-uniform and did not cover substrate completely .

3.2 Photoelectrochemical characterisation of SnS thin films deposited at optimized conditions

The type of electroconductivity of SnS films deposited onto different substrates in use of our optimized deposition parameters was determined by photoelectrochemical measurements under pulsed white light irradiation.

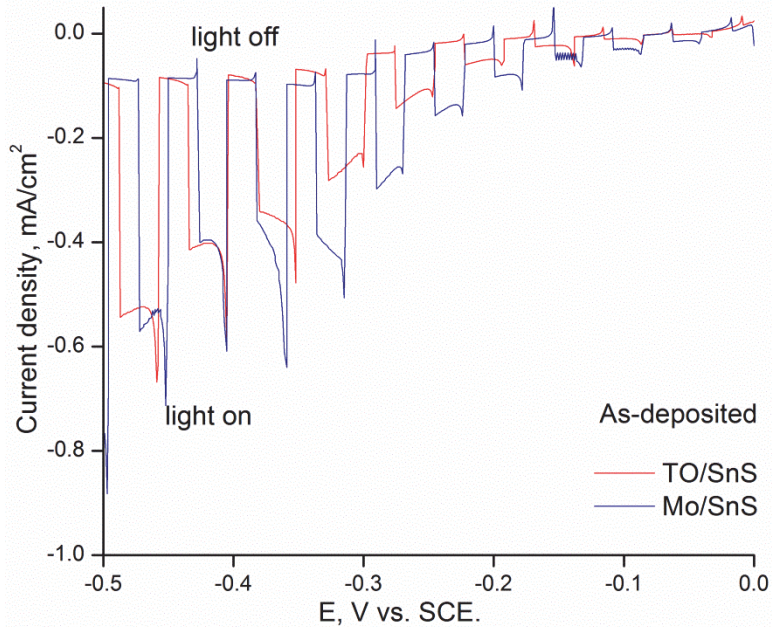


Fig. 3.22 Photocurrent response of SnS thin films.

Noticed increase in photocurrent toward negative potential region indicates that all as-deposited SnS films exhibit p-type conductivity [115] (Fig.3.22). On the figure 3.22 results of photocurrent measurements of as-deposited SnS thin films deposited on TO and Mo substrates are given, however all deposited films show similar high photoresponse, that did not depend on used deposition substrate (TO, Mo, ITO).

3.3 Sequential deposition of SnS thin films (article I)

As it was mentioned in the theoretical part, one of the most important applications of SnS thin films could be using them in photovoltaic devices as absorber layer. For such application thickness of the deposited film should be more than 200 nm [13, 101]. That thickness of SnS films cannot be achieved by one deposition run and multiple sequential depositions are needed.

Films were deposited on ZnS and CdS substrates because by literature they suit as buffer layers for solar cells with SnS absorber layer. SnS thin films

were prepared with molar concentration of stannous chloride in total volume of 0,03 M and ratio Sn/S= 1:1 and the pH of solution equal to 7. Corning glass substrates with previously deposited CdS or ZnS thin films were placed vertically in solution. Deposition was held at temperature of around 22 ° C during 24 hours. Obtained films were washed and rinsed with deionized water and then dried. Consecutive depositions of two and three times were made additionally to obtain thicker films.

series	Number of deposition counts	Sn:S ratio
ZnS/SnS	1	1.0
	2	1.1
	3	1.2
CdS/SnS	1	1.0
	2	1.0
	3	1.0

Table 3.5. Atomic ratios of tin and sulphur in films of series ZnS/SnS and CdS/SnS.

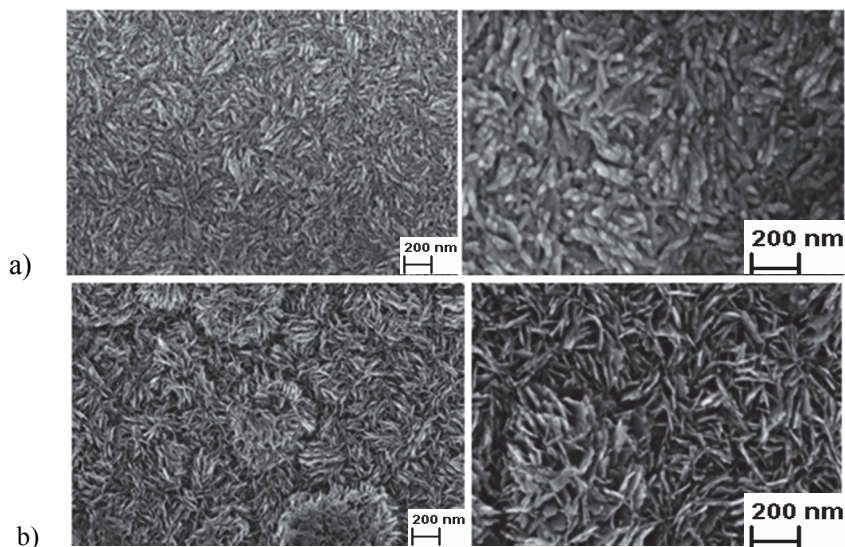


Fig. 3.23 SEM images at different magnifications of two times deposited SnS films of series a) ZnS/SnS and b) CdS/SnS.

Film thickness increased approximately in two times with each deposition cycle. For series CdS/SnS it was found increase from 220 nm for one-time deposition to 570 nm for three-time deposition. Around the same thickness

was observed for ZnS/SnS series and at two-deposition cycle it exhibited the thickness of 440 nm.

Table 3.5 shows changes in composition of SnS thin films of series ZnS/SnS and series CdS/SnS in multiple deposition process. In series CdS/SnS in multiple deposition process the ratio of tin to sulphur was 1:1, which means, that these films were in composition of a nearly stoichiometric stannous monosulphide. The films deposited on ZnS substrate were nearly stoichiometric only after single deposition run, but slightly tin-rich in multiple deposition series, with a continuous increase of concentration of tin in films. The similar increase of Sn concentration in SnS films by sequential deposition process was reported by T.H. Patel [54]. At the same time, Raman investigations did not indicate the existence of any additional to SnS phases in multiple deposited films on ZnS substrate. However, as it was suggested previously, it may have tin and oxygen containing phases which cannot be clearly seen from the Raman graphs as their peaks are too weak or coincide with those of SnS.

Fig. 3.23 show SEM images of SnS films of the CdS/SnS and ZnS/SnS series. Images indicate uniform pin-hole free surface of the SnS thin films on both substrates. The films of similar thickness on CdS and ZnS substrates demonstrate slightly different morphology, but in general they consist of vertically stacked flake structures, of about 100-150 nm laterally and of thickness of around 20 nm. The film morphology reported here is similar to those obtained by Yu Wang [102]. Films deposited on CdS substrate have bigger number of aggregates or clusters with larger crystals on their surface compared to SnS films deposited on ZnS substrate. The big number of precipitates on the surface of films indicates that the dominating films growth mechanism during sequential deposition of SnS films on CdS substrate is the cluster mechanism. At the same time no precipitations were observed on the surface of films during the deposition of the SnS films on ZnS substrate, indicating indirectly that the dominating deposition mechanism of the films on ZnS substrate has to be ion-by-ion mechanism [53, 55], resulting in smoother surface of the films. The surface illustrated here appears smooth at optical wavelengths, with optical transmittance and reflectance summing up to 100%, as will be discussed later on.

Atomic force microscopy images (Fig. 3.24) show the roughness of two-times deposited SnS films of series ZnS/SnS and CdS/SnS. The images show complete and uniform coverage over the substrate surface. Average roughness (Ra) of the films of series ZnS/SnS is 10.8 nm and for series CdS/SnS is 14.2 nm and root mean square roughness (Rq) is 13.4 nm and 18.00 nm respectively. Based on the above the films deposited on CdS substrate show higher profile of the grains. The observed difference in the surface morphology of the deposited SnS thin films on different substrates could result from the difference in surface energies for different substrates and their distinct morphology.

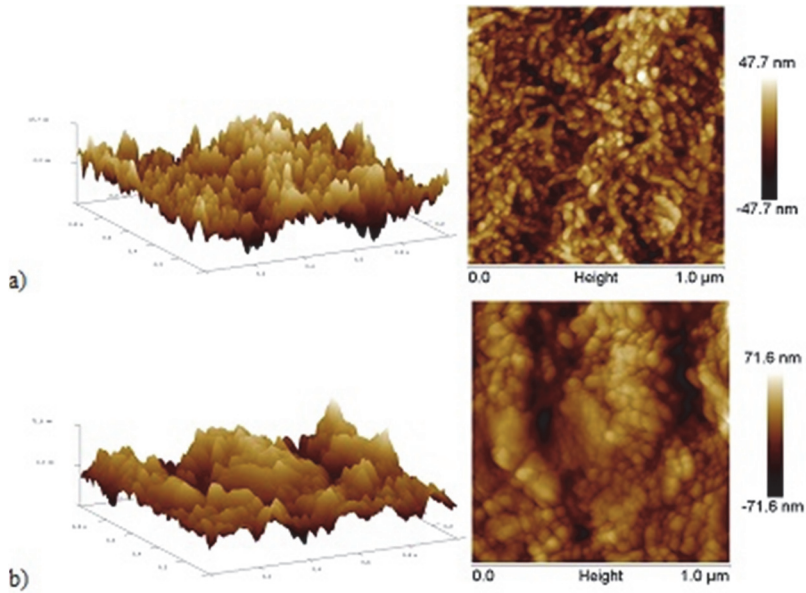


Fig. 3.24 AFM images of two-times deposited SnS films on a) ZnS substrate and b) CdS substrate.

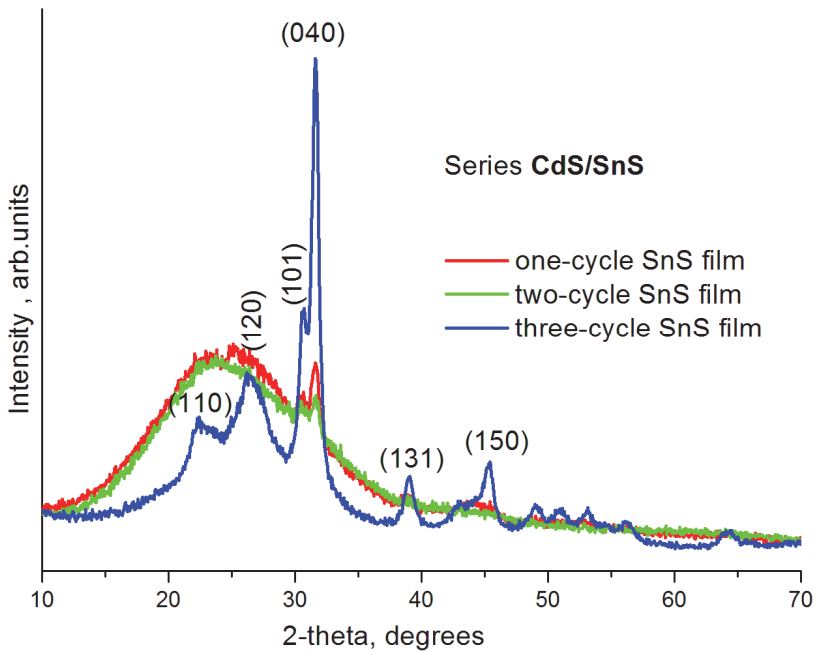


Fig. 3.25 XRD patterns of CdS/SnS thin films of one, two and three-cycles deposited SnS films of series CdS/SnS.

The x-ray diffraction patterns of thin films of one, two and three-times deposited films of the series CdS/SnS are shown in Fig. 3.25. Similar dependence of XRD pattern on the film thickness was noticed for series ZnS/SnS as well, the only difference was that peaks in series CdS/SnS were stronger and sharper than peaks for films from series ZnS/SnS. The peaks of SnS are not very clearly seen in one and two times deposited thin films due to not good crystallinity of these films. However, triple deposited films have good crystallinity, which can be seen from the high and sharp peak at $2\theta = 31.60^\circ$ corresponding to (040) plane, from the peak at $2\theta = 26.5^\circ$ corresponding to plane (120), peak at $2\theta = 22.6^\circ$ corresponding to (110) plane, peaks at $2\theta = 38.9^\circ$ corresponding to (131) plane and peak at $2\theta = 45.3^\circ$ corresponding to (150) plane of the orthorhombic phase of herzenbergite SnS. Small peaks at 49.3° , 51.1° , 52.96° , 64.3° correspond to planes (230), (151), (160), (251) of orthorhombic SnS, respectively. All the major peaks in the pdf card [103] for SnS match those of the XRD pattern of the thicker films. Improvement of crystallinity with the thickness was observed also by other researchers [64]. XRD pattern may contain also some peaks of CdS structure at $2\theta = 26.5^\circ$, 30.6° , 51.1° , 53.1° and 64.1° , but this peaks coincide with SnS peaks. There is no indication of other possible additional phases in the films.

All the films exhibit (040) plane as preferred and peak of this plane was used for crystallite size calculations. Crystallite size slightly grows with thickness in both series: from 112 Å to 130 Å for series ZnS/SnS and from 130 Å to 161 Å for series CdS/SnS.

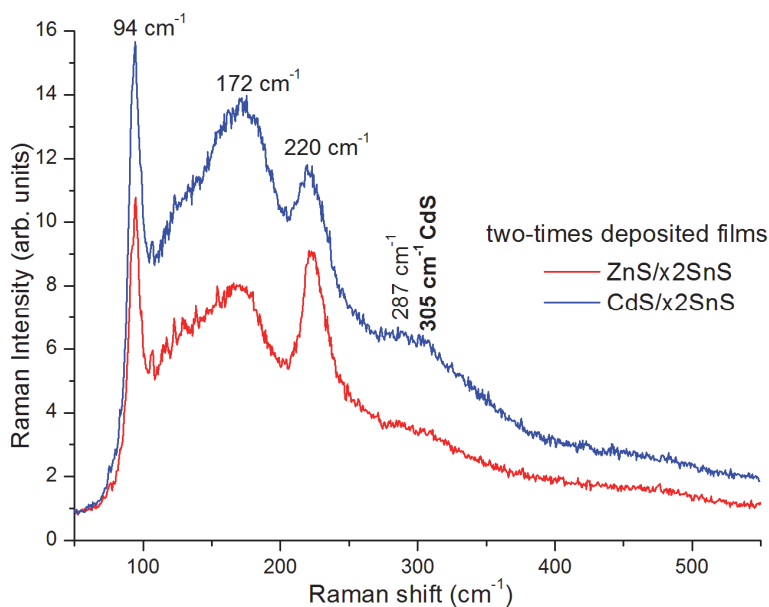


Fig. 3.26 Raman spectra of SnS thin films two-times deposited on ZnS and CdS substrates.

Fig. 3.27 shows the room temperature optical transmittance (T) and specular reflectance (R) curves of one and three-times deposited SnS films of series ZnS/SnS and CdS/SnS recorded at the wavelength range of 200 – 2500 nm. The specular nature of the films is illustrated by $T+R$ of $> 90\%$ in general for all the films for large wavelengths, > 2000 nm.

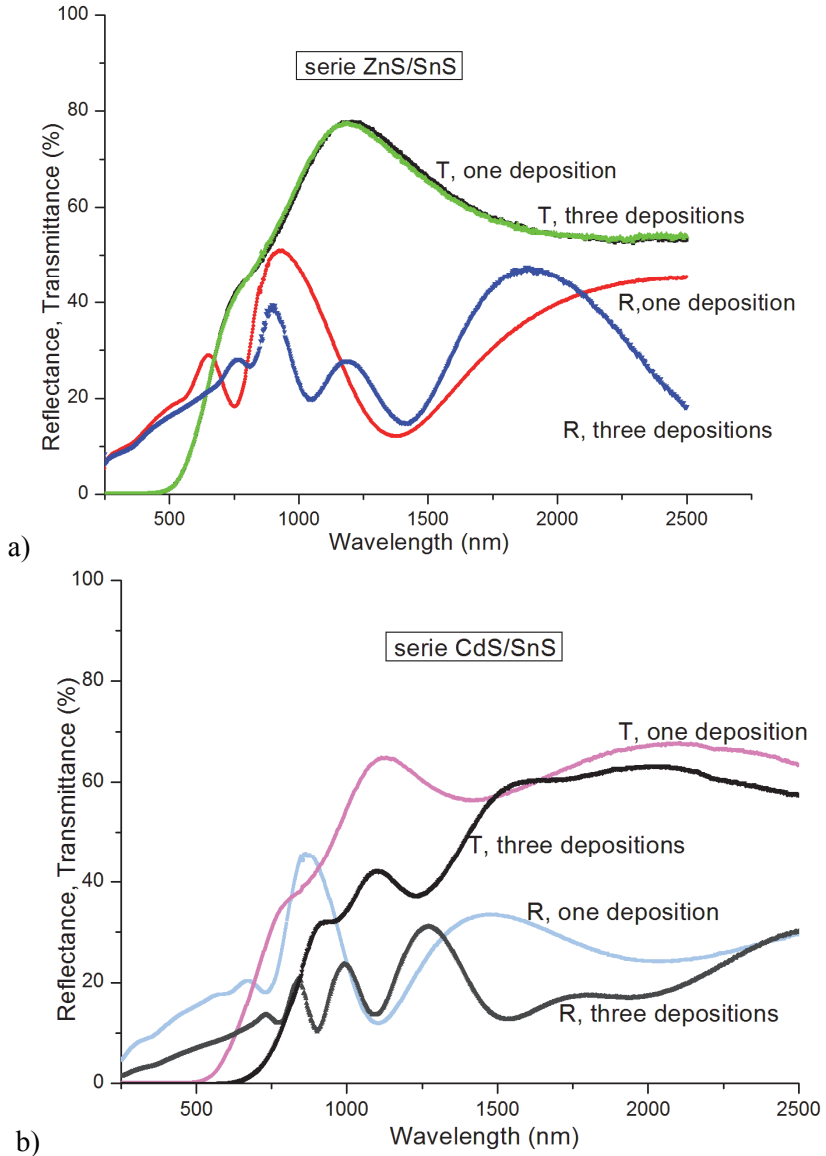


Fig. 3.27 Transmittance and reflectance spectra of one and three-times deposited SnS films of series a) ZnS/SnS and b) CdS/SnS.

The absorption edge in the transmittance curves fall in the region of 700-900 nm without any bending, which indicates once more the absence of additional phases presented in material. It can be observed from the Fig. 3.27 that the absorption edge shifts toward the higher wavelength as the thickness increases with number of depositions in series CdS/SnS.

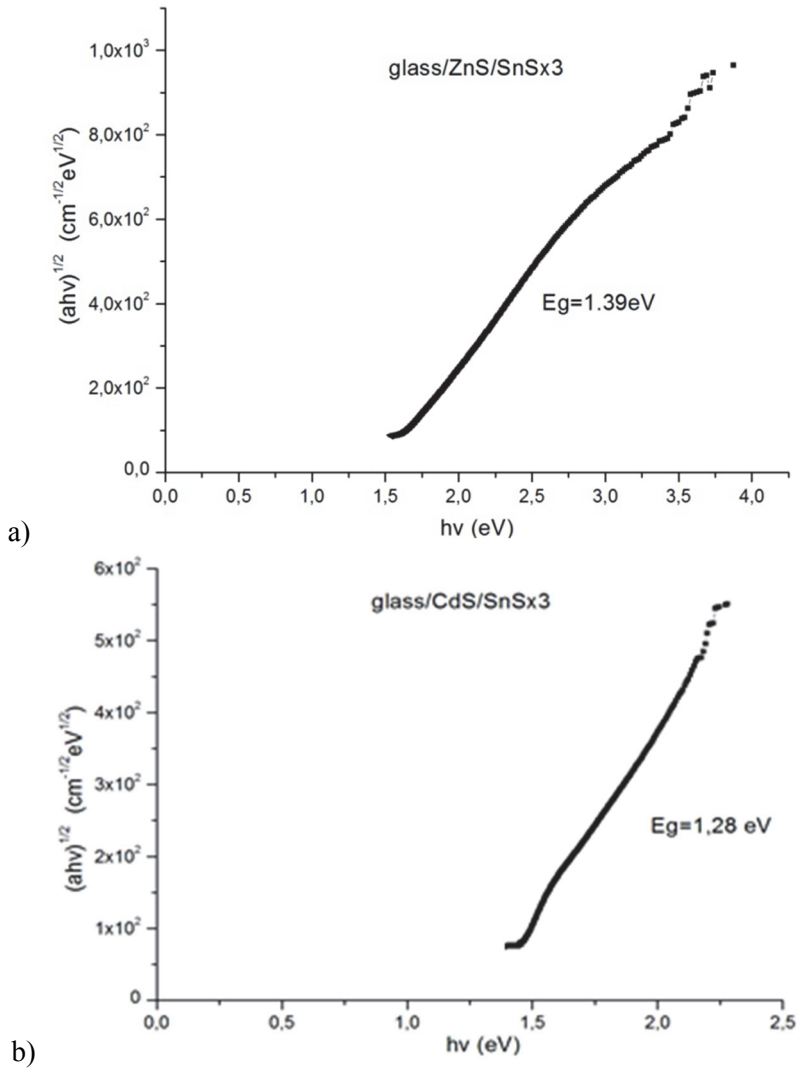


Fig. 3.28 Band gap of three-time deposited SnS films on a) ZnS and b) CdS substrates.

The optical energy band gap of the as-grown SnS layers was calculated. In the present study, the nature of the transitions is indirect allowed and the energy band gap can be determined by extrapolating the straight line portion of the curve $(\alpha h\nu)^{1/2}$ versus $h\nu$ onto the energy axis (Fig. 3.28). Band gap values decreased with number of depositions from 1.49 eV to 1.39 eV for films

deposited on ZnS substrate and from 1.5 eV to 1.28 eV for films deposited on CdS substrate. Such tendency was also observed by B. Ghosh [108]. This decrease could be attributed to the grain size dependency of band gap [14, 54] and transitions from amorphous to polycrystalline state [106, 107].

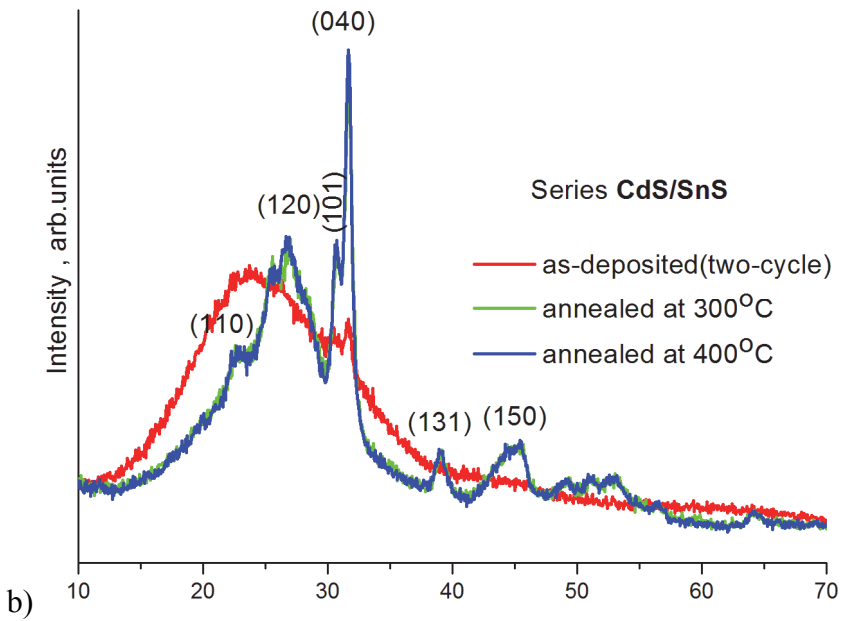
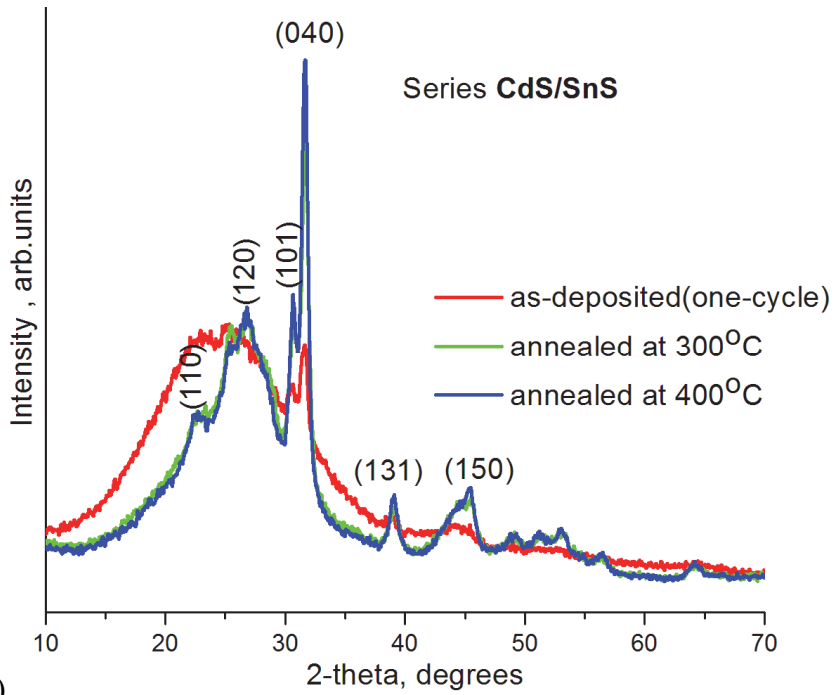
Hot-probe method was used to determine type of conductivity of the SnS films and all the layers showed p-type conductivity. Films of both series have very high resistivity: 120 M Ω cm for three-times deposited films of series CdS/SnS and 130 M Ω cm for three-time deposited films of series ZnS/SnS. Resistivity decreases with increasing films thickness. High resistivity of the films could be due to defects presented in films and they decrease with thickness and due to bad crystallinity which also improves with the thickness. Formation of other tin and oxygen containing additional phases could be the reason of high resistivity.

Summing up results of the sequential deposition it can be concluded, that crystallinity of the as-deposited films improves in multiple deposition process and three-time deposited films have well-determined crystalline structure of orthorombic herzenbergite tin monosulphide. Different surface morphology of grown SnS thin films results from distinct morphology of CdS and ZnS substrates. One, two and three times sequentially deposited films have nearly stoichiometric composition and good pin-hole free surface morphology of rod (for ZnS substrate) or flake (for CdS substrate) shape of the particles. All the major peaks of XRD and Raman graphs belong to SnS monophase without indicating any additional phases over detection limit in the films. Grain sizes slightly grow in multiple deposition process of films. Band gap decreases during multiple depositions. Films on both substrates have very high electro resistivity which decreases with deposition counts.

3.4 Post-thermal treatment of obtained films (article III)

Films obtained during chemical solution deposition have often amorphous structure and their post-treatment is essential to improve of the crystalline structure of films. Deposited SnS thin films were annealed in inert atmosphere (argon) at pressure of 10 Torr at different temperatures (300 °C, 400 °C or 460 °C) for 30 min to evaluate influence of heat-treatment on the properties of as-deposited SnS thin films. Samples were covered with aluminum foil, placed in a Petri dish and covered again with aluminum foil. Covered samples were placed in the oven and then the chamber was evacuated to about 30 mTorr. Argon was introduced into the chamber to give a pressure of 10 Torr, and the furnace was heated up.

The thicknesses of both series of films (CdS/SnS and ZnS/SnS) decreased slightly following thermal annealing; indicating that annealing caused the densification of films. It indirectly confirms our conclusion in XRD measurement part, that multiple depositions improve crystallinity of films and make them denser.



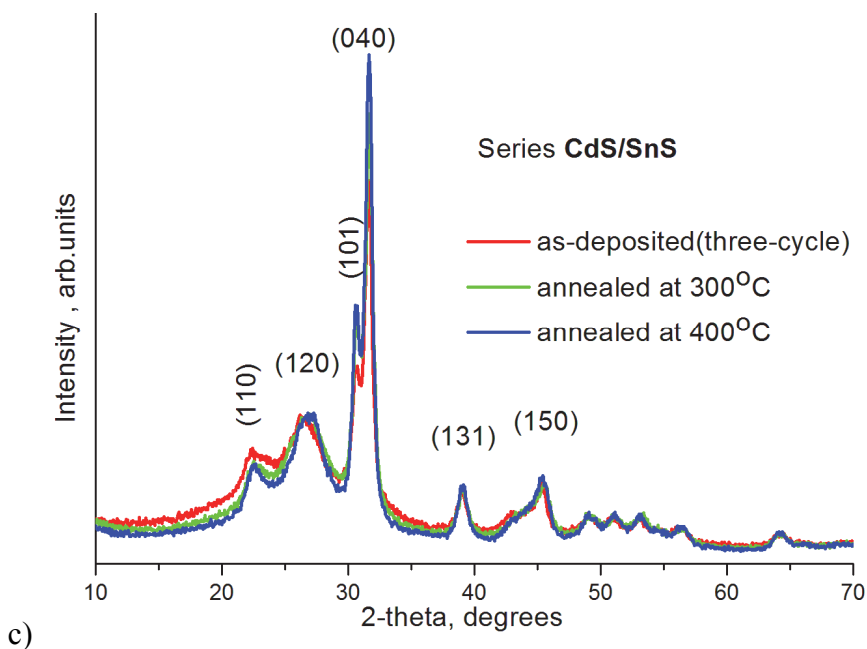


Fig. 3.29 XRD patterns of CdS/SnS thin films as-deposited and annealed at 300 °C and 400 °C for 30 min in inert atmosphere a) one-, b) two- and c) three-cycles deposited.

Fig. 3.29 shows the influence of heat treatment on the crystalline structure of the SnS films deposited on CdS substrates, films deposited on ZnS substrate have the same tendency. Thermal annealing improves the crystallinity of the deposited SnS thin films and these changes are more noticeable for one- and two-deposition-cycle films.

The absence of peaks of orthorhombic herzenbergite structure of as-deposited SnS films in the XRD patterns of the one- and two-deposition-cycle films indicates that these films are amorphous. The broad peak situated at a small diffraction angles is specific to the amorphous network. However, as the annealing temperature increases, the crystallinity of the films improves; the peaks related to SnS become narrower and more intense. This infers that annealing improves the quality of films.

All annealed films clearly show peaks at 31.60°, 30.46°, 26.5°, 22.6°, 38.9° and 45.3° corresponding to the (040), (101), (120), (110), (131) and (150) planes of the orthorhombic phase of herzenbergite SnS structure, respectively [103].

The existence of CdS with peaks at 26.5°, 30.7°, 51.2°, 53.1° and 64.1° [109, 110] in the XRD patterns of the films containing a CdS under layer could not be determined precisely because these peaks are very close to those of dominating SnS. There is no indication of other possible Sn-containing phases in the XRD patterns of the annealed films.

XRD patterns of one-, two- and three-deposition-cycle SnS films deposited on CdS and annealed at 460 °C are shown in Fig. 3.30. Compared to SnS films deposited on ZnS substrate, the SnS films deposited on CdS substrate and annealed at 460 °C have sharper and higher peaks, indicating that they are more crystalline. All of the films exhibit a preferred (040) plane. The peak associated with this plane was used by us later to calculate crystallite size in films. We can observe additional peaks at angles 25° and at 44° which correspond to (100) [111] and (220) [112] CdS planes, respectively, and are not found on the graphs of ZnS/SnS films.

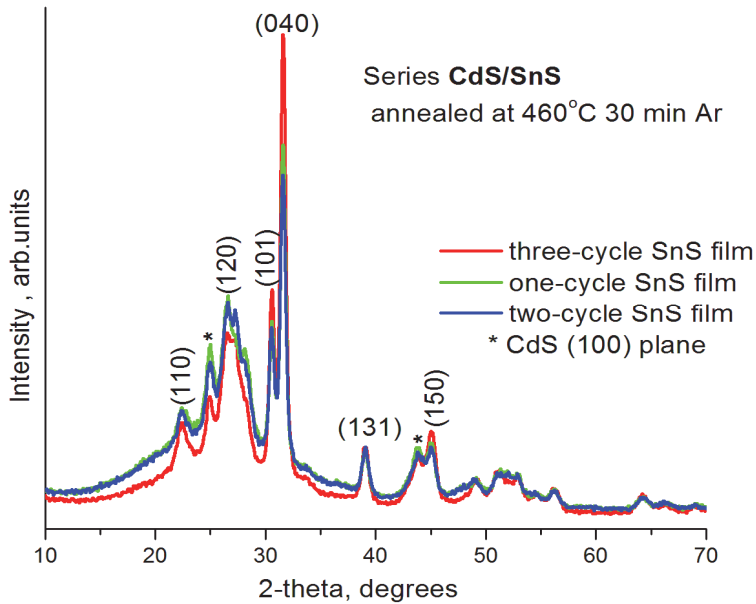
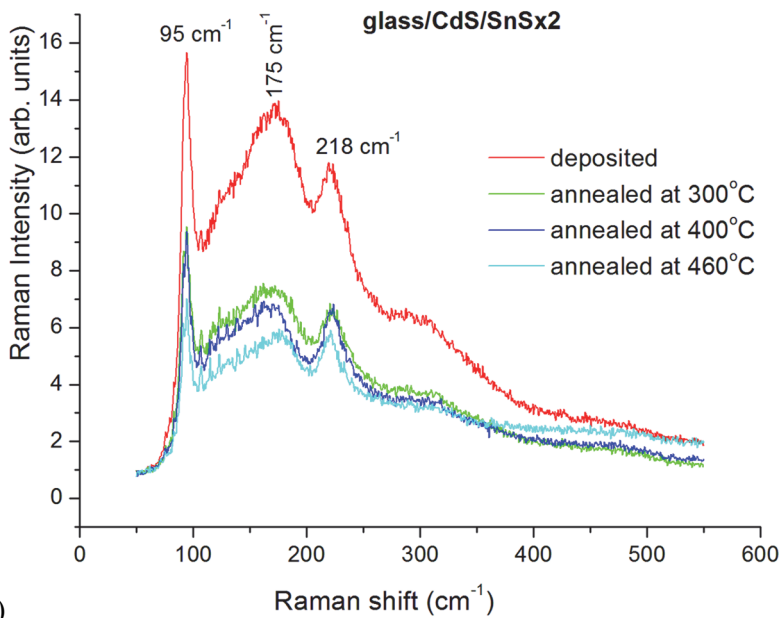


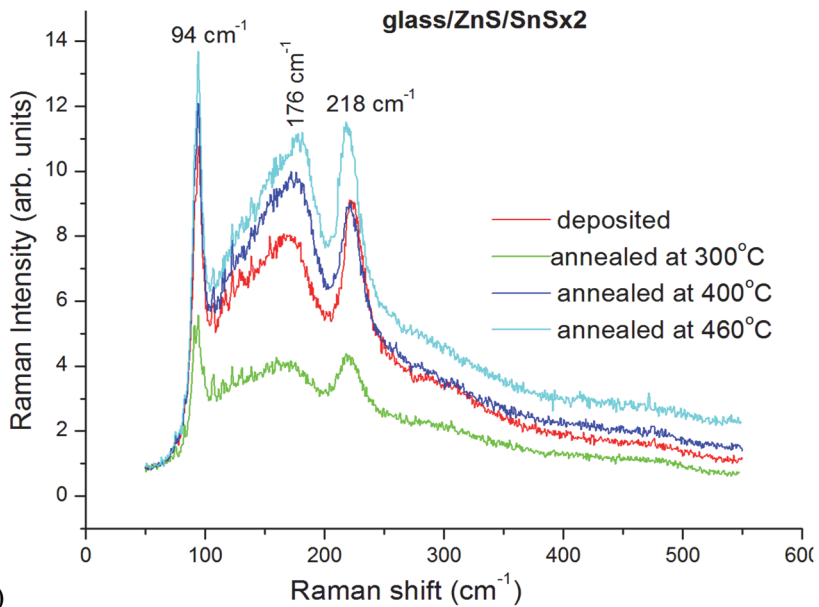
Fig. 3.30 XRD patterns of CdS/SnS films annealed at 460 °C for 30 min in inert atmosphere.

Crystallite size with annealing increases more in films deposited by one-deposition-cycle than by multiple-depositions, for the series annealed at 460 °C from 130 to 160 Å for the one-deposition-cycle CdS/SnS films and from 130 to 143 Å for the three-deposition-cycle ZnS/SnS films.

Results of Raman analyses of the films are presented at Fig. 3.31. Raman graphs of as-deposited and annealed films are similar and only show peaks corresponding to the SnS phase: 94/95 cm⁻¹, 218 cm⁻¹ [98], 175/176 cm⁻¹ [23]. In the Raman spectrum of the films deposited on CdS substrate a weak peak at 306 cm⁻¹ was detected that was attributed to CdS (305 cm⁻¹) [113]. This peak could also be attributed to Sn₂S₃ (307 cm⁻¹) [98]; however XRD analysis did not indicate the presence of any additional SnS phases. The absence of this peak from the spectra of the ZnS/SnS films (Fig. 3.31 b) indirectly supports our assumption that this peak originates from the CdS substrate.



a)



b)

Fig. 3.31 Raman analyses of two-deposition-cycle films of a) CdS/SnS and b) ZnS/SnS annealed at various temperatures.

Figures 3.32 and 3.33 show SEM images of the as-deposited and annealed at 300 °C, 400 °C and 460 °C CdS/SnS and ZnS/SnS thin films.

Uniform pinhole-free surfaces were observed for both the deposited and thermally annealed films. Consistent with the calculations from XRD data, particle size remained nearly the same regardless of annealing temperature and increased a little with the number of deposition cycles. Films deposited on ZnS substrates have rod-shaped particles, whereas CdS/SnS films contain flake-shaped particles. Annealing at 460°C changes the surface structure of the CdS/SnS films and results in films with rod-shaped particles.

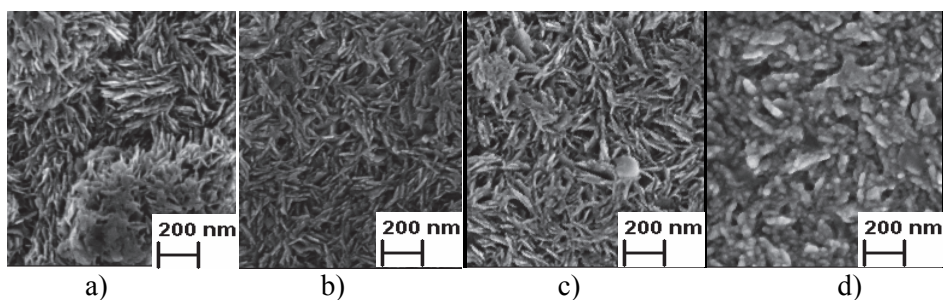


Fig. 3.32 SEM images of two times a) as-deposited films of serie CdS/SnS and annealed at b) 300°C, c) 400°C and d) 460°C in inert atmosphere for 30 min.

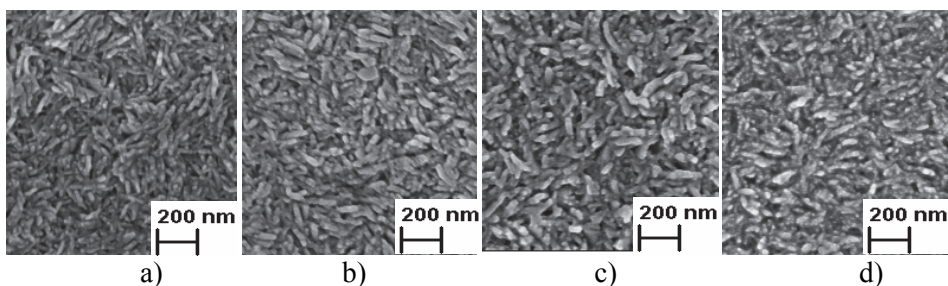


Fig. 3.33 SEM images of two times a) as-deposited films of serie ZnS/SnS and annealed at b) 300°C, c) 400°C and d) 460°C in inert atmosphere for 30 min.

series	Sn:S ratio	
	As-deposited	Annealed at 460 °C
CdS/SnS x1	1.0	1.0
x2	1.0	1.0
x3	1.0	1.1
ZnS/SnS x1	1.0	1.2
x2	1.1	1.2
x3	1.2	1.2

Table 3.6 Atomic ratio of tin and sulphur in the series CdS/SnS and ZnS/SnS films from EDX.

Table 3.6 shows the atomic ratios of Sn to S in deposited and thermally annealed CdS/SnS and ZnS/SnS films. EDX revealed ratios of Sn to S of almost 1:1 in the deposited and annealed at 300°C and 400°C films formed on CdS substrates, so annealing did not lead to remarkable changes in the composition of the films and the annealed CdS/SnS films maintain their initial stoichiometric composition of tin monosulphide. Films deposited on ZnS substrates were slightly tin-rich and sulfur-poor following deposition and their composition did not change after thermal annealing. Annealing at 460 °C caused the tin composition of films to increase slightly probably because more sulphur is lost from films during annealing at high temperatures.

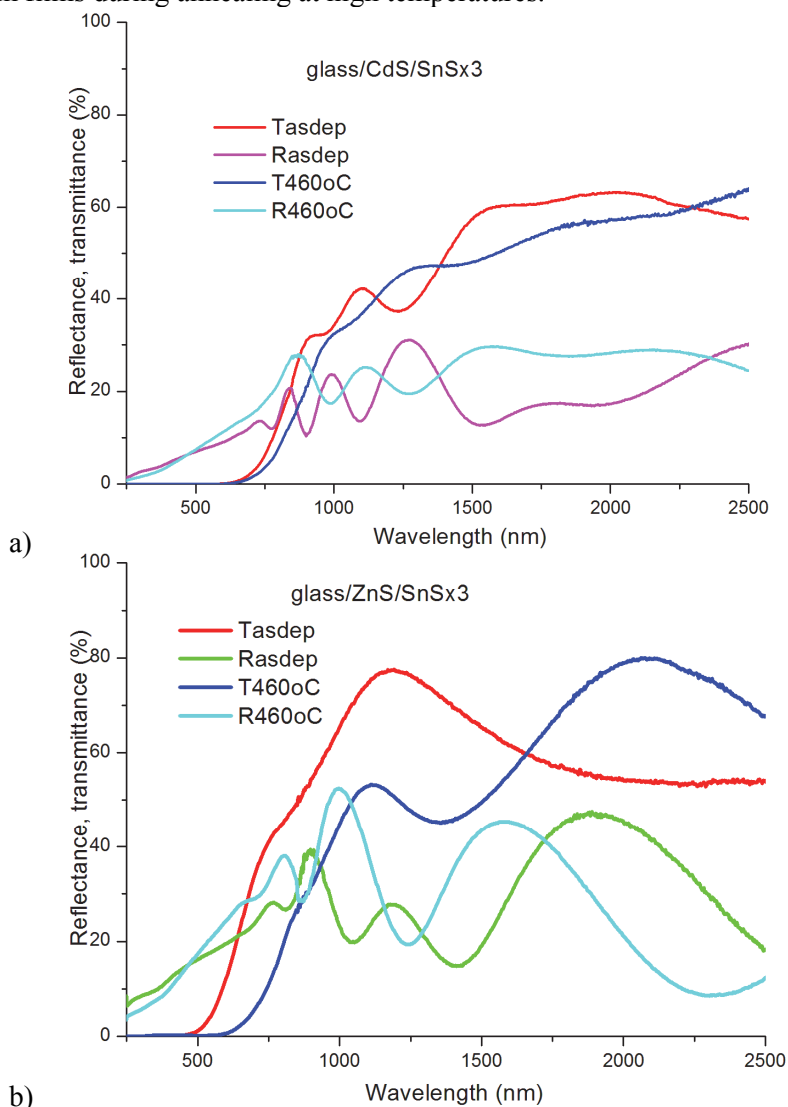


Fig. 3.34 Transmittance and reflectance spectra of a) CdS/SnS and b) ZnS/SnS.

Fig 3.34 shows the comparison of optical transmittance and reflectance spectra of the CdS/SnS and ZnS/SnS thin films as-deposited and annealed at 460°C. The absorption edge of the films shifts to longer wavelength with increasing annealing temperature for both series.

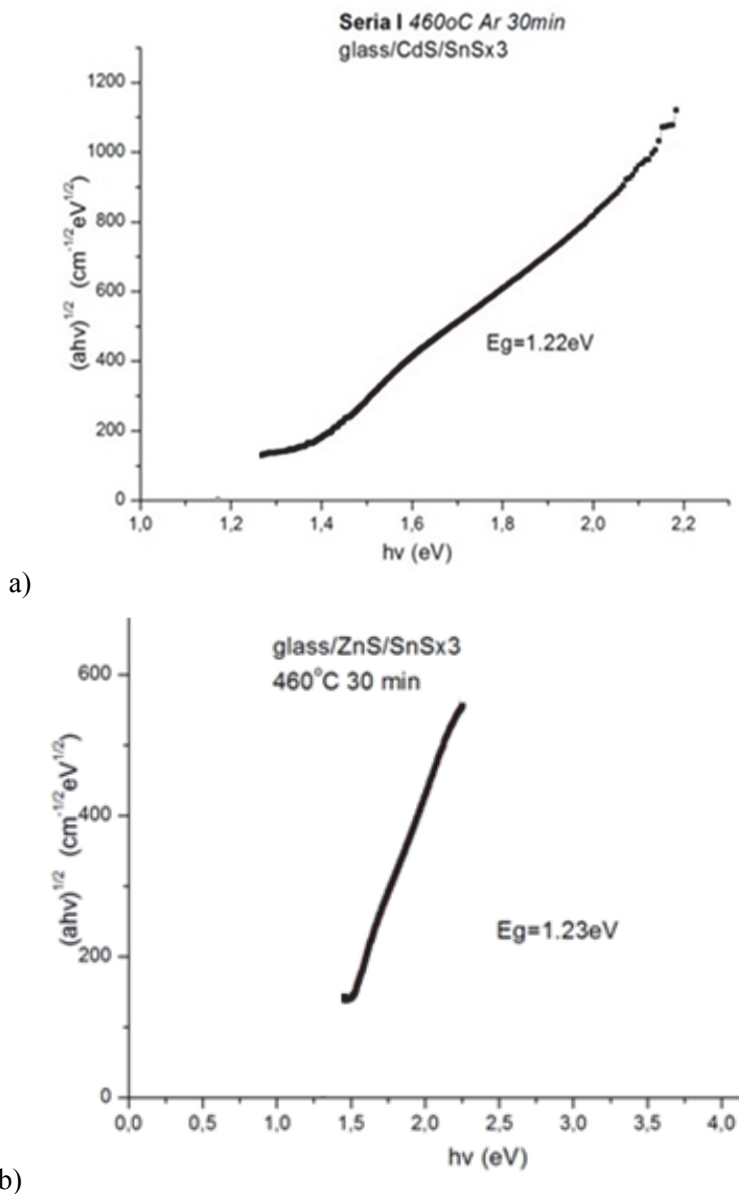


Fig. 3.35 Band gap of three-times deposited and annealed at 460°C SnS films of series a) CdS/SnS and b) ZnS/SnS.

The energy band gap (E_g) of the films was determined from plots of $(\alpha h\nu)^{1/2}$ against photon energy $h\nu$ (Fig. 3.35). The calculated optical band gaps for the CdS/SnS thin films varied from 1.28 eV for the film formed after three deposition cycles to 1.22 eV after annealing at 460 °C for 30 min under an inert atmosphere. For the ZnS/SnS films, the band gap of the three-deposition-cycle film was 1.39 eV and decreased to 1.23 eV as the annealing temperature was increased to 460 °C. Reduction in E_g with annealing temperature was also noticed by other researchers [114]. This decrease could be attributed to the grain size dependency of band gap [14, 54, 106, 107] and disappearing of oxygen from the material what is in agreement with XPS results.

The hot-probe method was used to determine the type of conductivity of the films. All deposited and annealed SnS films showed p-type conductivity. All films of both series showed photosensitivity. Photoresponse increased with annealing temperature (Fig. 3.36).

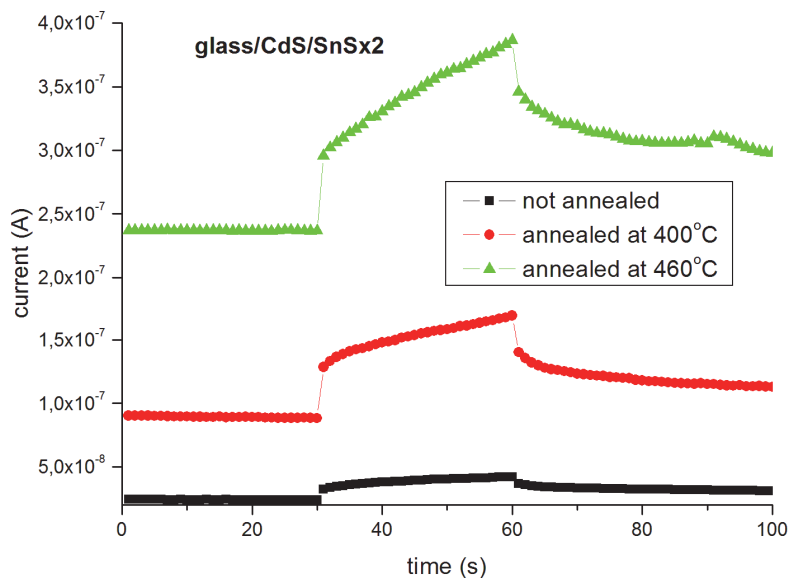


Fig. 3.36 Photo-current response of two-cycle SnS thin films on CdS as-deposited and annealed at 400°C and 460°C.

Resistivity of the films decreased with annealing and with deposition counts from 130 M Ω cm of three-times as-deposited films of series CdS/SnS until 56 M Ω cm for annealed at 460°C and from 120 M Ω cm of three-times as-deposited films of series ZnS/SnS until 12 M Ω cm for annealed at 460°C.

To sum up, our results show, that heat treatment in argon atmosphere makes one-run deposited amorphous SnS films crystalline, however, does not indicate remarkable changes in the crystallinity of multiply deposited SnS films.

Crystallite size in SnS films increases with annealing temperature. Deposited on ZnS substrate films have rod-shape structure and films deposited on CdS substrate have flake-like structure. However, after annealing at 460 °C CdS/SnS films have similar to ZnS/SnS structure. All annealed films clearly show peaks corresponding to orthorhombic phase of herzenbergite SnS structure and there are no peaks of other additional Sn-containing phases in the films, this also was confirmed by the results of Raman analyse, indicating that annealing until 460 °C do not lead to conversion of SnS to other phases. From EDX results it can be seen, that CdS/SnS films are keeping their initial stoichiometric composition of tin monosulphide after annealing. Deposited on ZnS substrates films were tin-rich and sulfur-poor from the deposition and kept its composition during thermal annealing. SEM images show uniform pinhole-free surface of both for the deposited and thermally annealed films.

The optical transmittance and reflectance spectra of CdS/SnS and ZnS/SnS thin films show that for series CdS/SnS there were only marginal changes in the optical transmittance and reflectance spectra after annealing, while for series ZnS/SnS significant changes are marked. When annealing temperature increased, the absorption edge for ZnS/SnS films shifted towards the higher wavelength side. The evaluated optical band gap was found to be indirect and it decreased for CdS/SnS three-runs thin films from 1.28 eV for deposited to 1.22 eV after annealing at 460 °C. ZnS/SnS films show the similar change: for un-annealed films band gap was 1.39 eV that decreased to 1.23 eV after annealing. Absorption coefficient was found to increase to one order of magnitude from 10^4 cm^{-1} for as-deposited to 10^5 cm^{-1} for annealed films. The evaluated absorption coefficient did not change after annealing and its value remained $\sim 10^5 \text{ cm}^{-1}$. All deposited and annealed SnS films showed p-type conductivity and their photoresponse increased with annealing temperature.

4. CONCLUSIONS

In agreement with the aim of the work different chemical deposition parameters were studied and optimal conditions for obtaining of uniform, good-adherent and completely covering the substrate, voids and pin-hole free tin monosulphide films from the solution containing stannous (II) chloride as tin source and sodium thiosulphate pentahydrate as a sulphur source and tartaric acid as a complexing agent were found to be: stannous (II) chloride concentration equal to 0.03 M, stannous (II) chloride / sodium thiosulphate pentahydrate ratio equal to less than 1:2, pH of the solution equal to 7, deposition temperature equal to 22 °C and duration of around 24 hours. The optimization is based on following regularities of deposition:

- At concentration of tin and sulphur 0.01 M in deposition solution incomplete coverage of all used substrates is dominating and films deposited at concentrations higher than 0.03 M peeled easily off from the substrates.
- At ratios Sn:S in deposition solution starting from 1:2 deposited thin films exhibited incomplete coverage of substrates and at ratio equal to 1:3 additional SnS₂ phase was detected.
- SnS thin films deposited from acidic solutions (pH equal to 5 and 6) contained voids and pin-holes. Increase in pH (8 and 9) accelerated velocity of the reactions in the solution and changed the deposition mechanism from “ion-by-ion” to “cluster”.
- Deposition at higher temperatures (35 °C, 45 °C and 55 °C) leads to rapid precipitation of SnS agglomerated particles in solution and as a result to non-uniform films.
- Material of deposition substrate influences the deposition process by its smoothness. The difficulty of adhering for nuclei to the smooth surface does not allow the formation of continuous SnS film's structure.
- Multiple depositions improved crystallinity of films, but had no influence to the elemental composition of SnS thin films. Optical band gap of deposited films decreases with deposition counts what was attributed to the grain size dependency of band gap.
- The additional annealing of one-cycle and multiply-deposited films in inert atmosphere at 300 °C, 400 °C and 460 °C increased crystallinity of deposited SnS films.
- The additional annealing led to the purification of films from oxygen containing compounds leading to the decrease of resistivity of the films.

- Deposited as well as annealed SnS thin films showed p-type conductivity and their photosensitivity increased with increase of annealing temperature.
- Based on our experiments chemically deposited SnS thin films could be applied in the production of solar cells as an absorber layer.

ACKNOWLEDGEMENTS

I would like to express my gratitude first of all to Karin Kerm, who helped me more than others in conduction of deposition experiments and in understanding of chemistry of all processes involved. Her knowledge is very wide in chemistry and enormous and she shared it really generously.

My special thanks to Professor Andres Öpik who was a Dean of the Faculty of Chemical and Materials Technology at TUT during my studies and for many fruitful discussions and advices about my thesis that he gave. I am very deeply appreciated to the present Dean and Leading Research Scientist Malle Krunks for permitting to have an opportunity to conduct and present my work for a defense. I wish to thank Head of the Department of Material science Dr. Marit Kauk-Kuusik for giving opportunity to use research facilities in the Department.

My warmest feelings and affection belong to my supervisors Professor Enn Mellikov and Senior Research Scientist Dr. Olga Volobujeva for their kind attitude to me, for their belief in my abilities, encouraging, having all the time positive view on me and creating very warm atmosphere on a workplace that is so essential for me for motivating and working in any field. Thank you so much, that I always felt free to come to you anytime for an advice, help and support during all these years. Thank you for the way you gave advices, coordinated work and had ability to see the best way of acting. Thank you for knowledge you shared with me, you are the best supervisors I have ever had!

I am very thankful for Dr. Smagul Karazhanov from Institute for Energy Technology of Norway and Dr. Ants Lõhmus from University of Tartu for accepting to be opponents on my PhD defense, for their valuable time and comments.

I also want to thank deeply Dr. Revathi Naidu for support and co-operation in our team, for big help in explaining questions connected to my work, readiness and kind offering of time for helping me in practical and theoretical parts of my work. I am also very appreciated to Dr. Sergei Bereznev for his valuable discussions. PhD students Jelena Gurevits and Mihkel Loorits for sharing her working tools and experience and for offering help in resolving equipment problems, to Master student Hrachya Kocharyan for helping with photocurrent response measurements.

I am grateful to Dr. Mare Altosaar for her useful and on-time advices, to Dr. Jaan Raudoja for making extremely useful experimental tools and helping with samples' annealing; to Dr. Tiit Varema, Dr. Kristi Timmo and PhD student Maris Pilvet for their help in different films' deposition, PhD student Mati Danilson for XPS, Dr. Valdek Mikli for analyzing my samples by SEM and EDX; Professor Jüri Krustok, Dr. Maarja Grossberg and Dr. Taavi Raadik for valuable help in understanding material's aspects as well as in Raman measurements; and the rest of the lab for their friendly treatment and scientific

spirit: Dr. Jaan Hiie, Dr. Natalia Maticiuc, PhD student Inga Klavina, PhD student Nickolae Spalatu for resolving equipment problems, Dr. Julia Kois, Dr. Andri Jagomägi.

My acknowledges to professor P.K. Nair and his PhD students Ana-Rosa Garcia and Rebeca Aragon from UNAM university of Mexico for a big help in practical and theoretical result and knowledge I obtained working with them.

The work was financially supported by Estonian Ministry of Education and Research IUT 19-28 and SF0140099s08, Estonian Science Foundation grant G-8147, Estonia Centre of Excellence in Research High-Technology Materials for Sustainable Development (TK117), Estonian National program in new energy technologies and material sciences (projects AR 12128, AR 10128, AR 12150).

My mother and grandparents are those to whom I owe all my biggest acknowledges for everything I have and for their true love!

Maria Safonova

ABSTRACT

Current work was concentrated on the preparation and characterization of tin sulphide (SnS) thin film grown by chemical solution deposition method. The inquiry for thin films for devices which convert solar energy has arisen in recent years. Among several perspective metal chalcogenides SnS attracted appreciable attention as potential contender as absorber material in production of low-cost solar cells due to suitable properties of this material such as high absorption coefficient, band gap near to the optimum value, theoretically high conversion efficiency and its suitability from the aspects of toxicity, price and availability.

SnS thin film could be deposited by different deposition techniques. Comparing with another methods, several benefits of chemical solution deposition can be highlighted: it is relatively simple and cheap method, which can be applied for deposition of the thin film on the substrates of different sizes, shapes and morphologies at low temperatures.

In spite of simpleness of the technique of chemical solution deposition, the process reactions are drastically influenced by the solution composition and deposition process parameters and should be controlled well. This method has been widely and successfully employed for deposition of CdS, however the deposition of SnS thin films is not very well developed and investigated. Thus, the goal of present work was to study regularities of the formation of SnS thin films by chemical solution deposition process and optimisation of solution parameters for good quality layers.

Obtained by chemical solution deposition films were analyzed and characterized by different techniques to evaluate quality of the grown SnS thin films. SEM, EDX and AFM techniques were used to get data about morphology, elemental composition and surface roughness; XRD and Raman analyses were applied to determine crystal structure and to know different phases presented in the material; optical spectral analysis was conducted to evaluate changes in optical band gap; electrical characteristics and photocurrent response of the SnS thin films structures were also measured. Different substrates such as borosilicate glass, indium tin oxide, tin dioxide, molybdenum and CdS as well as ZnS thin films were used in the present work as substrates to deposit SnS thin films onto. Such investigations are useful in the view of very few reports given in literature about the influence of substrate materials on the parameters and deposition process of SnS thin film by chemical solution deposition method.

Although thioacetamide is widely used by other researchers as a sulphur source, in this work sodium thiosulphate was chosen, because it is non-toxic, well-soluble and cheap reagent and good-quality SnS thin film was obtained.

The influence of concentration of precursor components and their ratio on the composition, structure and properties of the SnS thin films was investigated and optimized with the aim to obtain single phase tin monosulphide composition. Deposition was held at different temperature regimes to select

optimal temperature of the deposition, because it a priori affects the rate of the reactions taking place in the chemical solution. Increase in temperature accelerates reactions in solution as a result leads to faster deposition but on the other hand higher temperature favors rapid precipitation of the SnS already in the volume of solution. pH value of the solution was also found to influence the reactions in deposition solution for SnS thin growth. Evaluation of optimal duration of deposition process was essential to obtain film with highest thickness and maximal use of film-composing components. As a result pinhole-free, uniform and good-adherent tin monosulphide thin films were obtained.

After determining all parameters of the chemical deposition, sequential deposition of the SnS film layers was applied to increase thickness of the SnS thin films as obtained by single deposition run SnS films are thinner than needed for absorber layer in solar cells. It was noticed that multiple deposition improves crystallinity of films, decreases films resistivity and band gap values comparing with single step SnS films. Different annealing temperatures (300 °C, 400 °C and 460 °C) were used to treat thermally deposited SnS thin films in argon ambient. Experiments revealed that annealing converted films to more crystalline. Increase in annealing temperature led to decrease in band gap value and resistivity of the SnS thin films and increase in photosensitivity.

The aim of the work was achieved: optimal parameters for chemical solution deposition of SnS thin films were found.

KOKKUVÕTE

Käesolev uurimistöö on pühendatud õhukeste SnS kilede saamistehnoloogiale keemilise sadestamise meetodil. Töö on motiveeritud viimaste aastate jooksul kasvanud vajadusest välja töötada odav tehnoloogia päikesepatareides kasutatavate SnS absorberkihtide valmistamiseks. SnS on *p-tüüpi* pooljuhtühend, millel on kõrge valguskiirguse absorptsioonivõime ja sobiv keelutsooni laius päikesekiirguse muutmiseks elektrienergiaks foto-volt päikesepatareides. SnS on tõusnud huviorbiiti oma odava hinna, vähese toksilisuse ning koostiselementide laia leviku tõttu maakoos. SnS päikeseenergia muundamise teoreetiline efektiivsus ületab 20%.

Õhukeste SnS kilede sadestamiseks on erinevaid tehnoloogiaid, kuid keemilise sadestamise meetod paistab silma oma suhtelise lihtsuse ning odavusega. Seetõttu on see meetod saanud kõrgendatud tähelepanu osaliseks, kuna ta võimaldab sadestada pidevaid kihte erineva suuruse, kuju ja morfoloogiaga materjalidele madalatel, toatemperatuuri lähedastel temperatuuridel.

Vaatamata keemilise sadestamise meetodi näilisele lihtsusele on protsess ise äärmiselt tundlik sadestuslahuse keemilise koostise ja teiste protsessi parameetrite suhtes. Meetodit on edukalt kasutatud CdS kilede sadestamisel, kuid SnS kilede keemilise sadestamise seaduspärasusi pole veel piisavalt uuritud. Seetõttu on antud töö ülesanne uurida SnS kilede element- ja faasikoostist ja struktuuri sõltuvana erinevatest sadestamise tingimustest ning vastavalt saadud tulemustele optimeerida sadestusprotsessi parameetreid.

Sadestatud kilede morfoloogilisteks uuringuteks ja elementkoostise määramiseks kasutati SEM, EDS ja AFM meetodeid. Kilede faasikoostist ja struktuuri uuriti Raman-spektroskoopia ja röntgendifraktsiooni abil. Sadestatud SnS kilede optilisi omadusi ja nende muutusi termiliste töötluste käigus uuriti spektrofotomeetristel meetoditel. SnS sadenemise seaduspärasusi erinevatele materjalidele uuriti kasutades sadestusalustena boorsilikaat klaasi, ITO (tinaga legeritud indiumoksiid), Mo ja SnO₂ kattega juhtivaid klaasaluseid, samuti ZnS ja CdS õhukeste kiledega kaetud klaasaluseid. Erinevate klaasaluste kasutamine võimaldas jälgida seaduspärasusi sadestusaluse pinnastruktuuri, keemilise loomuse ja sadestatud SnS kilede element- ja faasikoostise vahel.

Antud töös kasutati väävlit allikana naatriumtiosulfaati tavaliselt sulfiidsete kilede sadestamiseks kasutatava tioatsetamiidi asemel. Selline valik on põhjendatud naatriumtiosulfaadi parema lahustuvuse, väiksema mürgisuse ja odavama hinnaga. Töös näidati, et naatriumtiosulfaadi kasutamisel on võimalik saada kõrge kvaliteediga SnS kilesid.

Ühefaasiliste õhukeste kilede saamisviisi leidmiseks muudeti SnS lähtelahuste kontsentratsioone ning nende vahelkorda sadestuslahuses, sadestamised viidi läbi erinevatel temperatuuridel ja erinevate pH väärtuste juures. Näidati, et temperatuuri tõstmisel toimuv kiire SnS kolloidosakeste väljasadenemine lahusesse ja mitte klaasalustele ei võimalda kontrollida

sadestusprotsessi kiirust ja teeb võimatuks ka kilelise struktuuri tekke. Tõestati, et optimaalse sadenemiskiiruse saavutamine ning õige komponentide vahekord lahuses on määrava tähtsusega sobiva paksusega ja struktuuriga kilede kasvatamiseks.

Kuna ühekordsel sadestamisel ei olnud võimalik saada vajaliku paksusega kilesid, siis kasutati kilede järjestikulist korduvsadestust üksteise peale. Võrreldes ühekordsel sadestamisel saadud kiledega paranes korduvsadestatud kilede struktuur, vähenes nende elektriline takistus ning ka keelutsooni laius. Kilede termiline järeltöötlus erinevatel temperatuuridel (300°C, 400°C and 460°C) argooni keskkonnas andis tulemuseks ühe- ja kahekordselt sadestatud kilede parema kristallstruktuuri. Temperatuuri tõusuga järeltöötlustes kaasnes keelutsooni laiuse vähenemine ja elektrijuhtivuse tõus ning suurenenud fototundlikkus.

Töö eesmärgid on täidetud: on leitud SnS õhukeste kilede keemilise sadestamise seaduspärasused erinevate aluspindadele ja leitud optimaalsed sadestamise parameetrid.

REFERENCES

- [1] Photovoltaic technology basics, Office of energy efficiency and renewable energy (2013) [Online]. Available: <http://energy.gov/eere/energybasics/articles/photovoltaic-technology-basics>
- [2] P. Sinsermsuksakul, K. Hartman, S.B. Kim, J. Heo, L.Sun, Enhancing the efficiency of SnS solar cells via band-offset engineering with a zinc oxysulfide buffer layer, *Appl. Phys. Lett.* 102 (2013) 053901.
- [3] K. L. Chopra, P. D. Paulson and V. Dutta, Thin Film Solar cells: An overview, *Progress in Photovoltaics* 12 (2004) 69.
- [4] D.C. Reynolds, G. Leies, L. L. Antes and R. E. Marburger, Photovoltaic effect in cadmium sulfide, *Phys. Rev.* 96 (1954) 533.
- [5] M. A. Green, K. Emery, Y. Hishikawa, W. Warta, and E. D. Dunlop, Solar cell efficiency tables (version 43), *Progress in Photovoltaics* 22 (2014) 1–9.
- [6] First solar achieves efficiency, Durability milestones (2015) [Online]. Available: <http://investor.firstsolar.com/releasedetail.cfm?ReleaseID=895118>.
- [7] P. Jackson, D. Hariskos, R. Wuerz, O.Kiowski, A. Bauer, Properties of Cu(In,Ga)Se₂ solar cells with new record efficiencies up to 21,7 %, *Physica status solidi* 9(1) (2015) 28-31.
- [8] L.A. Burton and A. Walsh, Band alignment in SnS thin-film solar cells: Possible origin of the low conversion efficiency, *Appl. Phys. Lett* 102 (2013)132111.
- [9] Sam Zhang, Organic Nanostructured Thin Film Devices and Coatings for Clean Energy, Taylor & Francis (2010).
- [10] M. Leacha, K.T. Ramakrishna Reddy, Tin sulphide thin films synthesised using a Two Step Process, *Energy Procedia* 15 (2012) 371–378.
- [11] Richard H. Bube, Photovoltaic Materials, Imperial college press (1998).
- [12] W. Shockley and H. J. Queisser, Detailed Balance Limit of Efficiency of P-N Junction Solar Cells, *Journal of Applied Physics* 32 (1961) 510-519.
- [13] P. Sinsermsuksakul, L. Sun, S. W. Lee, H. H. Park, S. B. Kim, C. Yang, R. G. Gordon, Overcoming Efficiency Limitations of SnS-Based Solar Cells, *Advanced Energy Materials* 4 (15) (2014) 1-7.

- [14] G. Hodes, Chemical solution deposition of semiconductor films, Marcel Dekker, New York (2002).
- [15] Краткая химическая энциклопедия, III, Москва (1964).
- [16] Ch. Gao, H. Shen, L. Sun, Preparation and properties of zinc blende and orthorhombic SnS films by chemical bath deposition, *Applied Surface Science* 257 (2011) 6750–6755.
- [17] T. Raadik, Application of modulation spectroscopy methods in photovoltaic materials research, PhD thesis (2015).
- [18] L.A. Burton and A. Walsh, Phase stability of the earth-abundant tin sulphides SnS, SnS₂ and Sn₂S₃, *J. Phys. Chem. C* 116 (45) (2012) 24262–24267.
- [19] Ya-Ting Lin, Jen-Bin Shi, Yu-Cheng Chen, Chih-Jung Chen and Po-Feng Wu, Synthesis and characterization of tin disulfide (SnS₂) nanowires, *Nanoscale Res Lett.* 4(7) (2009) 694–698.
- [20] Web Elements, Tin disulphide [Online]. Available: http://www.webelements.com/compounds/tin/tin_disulphide.html
- [21] B. Thangaraju, P. Kaliannan, Spray pyrolytic deposition and characterization of SnS and SnS₂ thin films, *J. Phys. D: Appl. Phys.* 33 (2000) 1054–1059.
- [22] Tong Jiang and Geo Very, A. Ozin, New directions in tin sulfide materials chemistry, *J. Mater. Chem.* 8(5) (1998) 1099–1108.
- [23] R.Kneip, D.Mooz, U.Severin and H.Wunderlich, Structure of tin (II) tin (IV) trisulphide, a redetermination, *Acta Cryst. B* 38 (1982) 2022–2023.
- [24] Emine Güneri, Fatma Göde, Behiye Boyarbay, Cebrail Gümüş, Structural and optical studies of chemically deposited Sn₂S₃ thin films, *Materials Research Bulletin* 47 (2012) 3738–3742.
- [25] M. Khadraoui, N. Benramdane, C. Mathieu, A. Bouzidi, R. Miloua, Z. Kebbab, K. Sahraoui, R. Desfeux, Optical and electrical properties of Sn₂S₃ thin films grown by spray pyrolysis, *Solid State Communications* 150 (2010) 297–300.
- [26] B. Ghosh, M. Das, P. Banerjee, S. Das, Fabrication of vacuum-evaporated SnS/CdS heterojunction for PV applications, *Solar Energy Mater and Solar*

Cells 92(9) (2008) 1099-1104.

[27] Hongnan Li, Shuying Cheng, Jie Zhang, Weihui Huang, Haifang Zhou, Hongjie Jia, Fabrication of CdS/SnS Heterojunction for Photovoltaic Application, *World Journal of Condensed Matter Physics* 5 (2015) 10-17.

[28] M. Patel and A. Ray, Magnetron sputtered Cu doped SnS thin films for improved photoelectrochemical and heterojunction solar cells, *RSC Advances* 4 (2014) 39343-39350.

[29] R.E. Banai, H.Lee, M. A. Motyka, R. Chandrasekharan, Optical properties of sputtered SnS thin films for photovoltaics absorbers, *IEEE Journal* 3 (2013) 1084-1089.

[30] J. Y. Kim and S. M. George, Tin monosulfide thin films grown by atomic layer deposition using tin 2,4-pentanedionate and hydrogen sulfide, *J. Phys. Chem. C* 114 (2010) 17597–17603.

[31] R. Jaramillo, V. Steinmann, Ch. Yang, K. Hartman, R. Chakraborty, J. R. Poindexter, M. L. Castillo, R. Gordon, T. Buonassi, Making record-efficiency SnS solar cells by thermal evaporation and atomic layer deposition, *J. Vis. Exp.* 99 (2015) 52705.

[32] A. Tanuševski, D. Poelman, Optical and photoconductive properties of SnS thin films prepared by electron beam evaporation, *Solar Energy Materials and Solar Cells* 80(3) (2003) 297–30.

[33] H. Johnson, K. Mohanraj, S. Kannan, Structural and optical properties of SnS nanoparticles and electron-beam-evaporated SnS thin films, *J. Exp. Nanoscience* 10 (2) (2015) 76-84.

[34] A. Ortiz, J. C. Alonso, M. Garcia and J. Toriz, Tin sulphide films deposited by plasma-enhanced chemical vapour deposition, *Semicond. Sci. Technol.* 11 (2) (1996) 243.

[35] M. Sugiyama, K. Miyauchi, T. Minemura, K. Ohtsuka, K. Noguchi and H. Nakanishi, Preparation of SnS Films by Sulfurization of Sn Sheet, *Japanese Journal of Applied Physics* 47 (2008).

[36] K.T.R. Reddy, P.P. Reddy, R.W. Miles, P.K. Datta, Investigations on SnS films deposited by spray pyrolysis, *Optic Mater.* 17 (1–2) (2001) 295-298.

[37] S. Polivtseva, I. Oja Acik, A. Katerski, A. Mere, V. Mikli and M. Krunk, Tin sulfide films by spray pyrolysis technique using L-cysteine as a novel sulfur

source , *Phys. Status Solidi C* (2015) 1– 6.

[38] M. Krunk, E. Mellikov, Metal sulfide thin films by chemical spray pyrolysis, *Proceedings of SPIE* 4415 (2001) 60-65.

[39] R. Mariappan, M. Ragavendar, V. Ponnuswamy, Structural and optical characterization of SnS thin films by electrodeposition technique, *Optica Applicata* XLI (4) (2011) 988-997.

[40] M. Ristov, G. Sinadinovski, M.Mitreski, M.Ristova, Photovoltaic cells based on chemically deposited p-type SnS, *Solar Energy Mat.&Solar Cells* 69 (2001) 17-24.

[41] A. Bayer, D. S. Boyle , P.O'Brien, In situ kinetic studies of the chemical bath deposition of zinc sulfide from acidic solutions, *J. Mater. Chem.* 12 (2002) 2940.

[42] R.S. Mane, C.D. Lokhande, Chemical deposition method for metal chalcogenide thin films, *Materials Chemistry and Physics* 65(1) (2000) 1–31.

[43] A. M. A. Haleem and M. Ichimura, Experimental determination of band offsets at the SnS/CdS and SnS/InS_xO_y heterojunctions, *J. of Appl. Phys.* 107 (2010) 034507.

[44] B. A. Ezekoye, P.O. Ofor, V. A. Ezekoye, F. I. Ezema, Chemical bath deposition technique of thin films: a review, *International Journal of Scientific Research* 2(8) (2013) 2277-8179.

[45] P.K Nair , P Parmananda , M.T.S Nair, Mathematical model simulating the growth of compound semiconductor thin films via chemical bath deposition, *Journal of Crystal Growth* 206 (1–2) (1999) 68–74.

[46] Mark Wolverton, U.S. department of energy, Argonne national laboratory, Revealing the Secrets of Chemical Bath Deposition (2010) [Online]. Available: http://www.aps.anl.gov/Science/Highlights/Content/APS_SCIENCE_20101123.php

[47] E. Guneri, F. Gode, C. Ulutas, F. Kirmizigul, G. Altindemir, C. Gumus, Properties of p-type SnS thin films prepared by chemical bath deposition, *Chalcogenide Letters* 7(12) (2010) 685-694.

[48] S.M. Pawar , B.S. Pawar , J.H. Kim, Oh-Shim Joo, C.D. Lokhande, Recent status of chemical bath deposited metal chalcogenide and metal oxide thin films, *Current Applied Physics* 11 (2011) 117-161.

- [49] A. Carrillo-Castillo, R.C. Mbroso Lazaro, A. Jimenez-Perez, C.A. Martinez Perez, E.C de la Cruz Terrazas, Role of complexing agents in chemical bath deposition of lead sulfide thin films, *Mater. Lett.* 121 (2014) 19-21.
- [50] Y. Jayasree, U. Chalapathi, P. Uday Bhaskar, V. Sundara Raja, Effect of precursor concentration and bath temperature on the growth of chemical bath deposited tin sulphide thin films, *Applied Surface Science* 258 (2012) 2732–2740.
- [51] E. Guneri, C. Ulutas, F. Kirmizigul, G. Altindemir, F. Gode, C. Gumus, Effect of deposition time on structural, electrical, and optical properties of SnS thin films deposited by chemical bath deposition, *Applied Surface Science* 257 (2010) 1189–1195.
- [52] Rodrigo Sáez Araoz, Chemical bath deposition of Zn(S,O) buffer layers and application in Cd-free chalcopyrite-based thin-film solar cells and modules, PhD thesis (2009).
- [53] Rodrigo Sáez Araoz, Chemical bath deposition of Zn(S,O) buffer layers and application in Cd-free chalcopyrite-based thin-film solar cells and modules, PhD thesis (2009).
- [54] T.H. Patel, Influence of Deposition Time on Structural and Optical Properties of Chemically Deposited SnS Thin Films, *The Open Surface Science Journal* 4 (2012) 6-13.
- [55] Ch. Gao, H. Shen, Influence of the deposition parameters on the properties of orthorhombic SnS films by chemical bath deposition, *Thin solid films* 520 (2012) 3523-3527.
- [56] M.T.S. Nair and P.K.Nair, Simplified chemical deposition technique for good quality SnS thin films, *Semicond. Sci. Technol.* 6 (1991) 132-134.
- [57] T. Zi, Y. B. K. Reddy and G. Hao, Investigation on quickly deposited SnS thin films by chemical bath deposition. [Online]. Available: <http://www.nus.edu.sg/nurop/2009/FoE/U057684A.PDF>
- [58] A. Tanuševski, Optical and photoelectric properties of SnS thin films prepared by chemical bath deposition, *Semicond. Sci. Technol.* 18 (2003) 501–505.
- [59] P.P. Hankare, A.V. Jadhav, P.A. Chate, K.C. Rathod, P.A. Chavan, S.A. Ingole, Synthesis and characterization of tin sulphide thin films grown by

chemical bath deposition technique, *Journal of Alloys and Compounds* 463 (2008) 581–584 .

[60] D. Avellaneda, G. Delgado, M.T.S. Nair, P.K. Nair, Structural and chemical transformations in SnS thin films used in chemically deposited photovoltaic cells, *Thin Solid Films* 515 (2007) 5771–5776.

[61] E. Turan, M. Kul, A. S. Aybek and M. Zor, Structural and optical properties of SnS semiconductor films produced by chemical bath deposition, *J. Phys. D: Appl. Phys.* 42 (2009) 245408-245414.

[62] D, Avellaneda, M.T.S. Nair, P.K. Nair, Photovoltaic structures using chemically deposited tin sulfide thin films, *Thin Solid Films* 517 (2009) 2500–2502.

[63] S. Aksay, T. Ozer, and M. Zor, Vibrational and X-ray diffraction spectra of SnS film deposited by chemical bath deposition method, *Eur. Phys. J. Appl. Phys.* 47 (2009) 30502.

[64] A. Akkari, C. Guasch, N. Kamoun-Turki, Chemically deposited tin sulphide, *Journal of Alloys and Compounds* 490 (2010) 180–183.

[65] Ge Yan-hui, Guo Yu-ying, Shi Wei-min, Qiu Yong-hua, Wei Guang-pu, Influence of In-doping on resistivity of chemical bath deposited SnS films, *Journal of Shanghai University (English Edition)* 11(4) (2007) 403–406.

[66] Ch. Gao, H. Shen, L.Sun, Z. Shen, Chemical bath deposition of SnS films with different crystal structures, *Materials Letters* 65 (2011) 1413–1415.

[67] S. M. Herron, A. Wangperawong, S.F. Bent, Chemical bath deposition and microstructuring of tin (II) sulfide films for photovoltaics, *Photovoltaic Specialists Conference* 37 (2011) 000368 – 000371.

[68] Y.J. Yang, B.J. Xiang, A simple synthesis of SnS nanoflakes at ambient conditions, *Appl. Phys. A* 83 (2006) 461-463.

[69] A. J. Ragina, K. C. Preetha, K. V. Murali, K. Deepa and T. L. Remadevi, Wet chemical synthesis and characterization of tin sulphide thin films from different host solutions, *Advances in Applied Science Research* 2 (3) (2011) 438-444.

[70] H.Martinez, D.Avellaneda, Modifications in SnS thin films by plasma treatments, *Nuclear instruments and methods in physics research B* 272 (2012) 351-356.

- [71] A. Gómez, H. Martínez, M. Calixto-Rodríguez, D. Avellaneda, P.G. Reyes, O. Flores, Modification of optical and electrical properties of chemical bath deposited SnS using O₂ plasma treatments, *Applied Surface Science* 275 (2013) 273–277.
- [72] Ming Du, Xuesong Yin, Hao Gong, Effects of triethanolamine on the morphology and phase of chemically deposited tin sulfide, *Materials Letters* 152 (2015) 40–44.
- [73] Chemical Book, Data Base List, Thioacetamide [Online]. Available: http://www.chemicalbook.com/ChemicalProductProperty_EN_CB7755552.htm
- [74] Report on cancerogene, 13-th edition, Thioacetamide [Online]. Available: <http://ntp.niehs.nih.gov/ntp/roc/content/profiles/thioacetamide.pdf>
- [75] Encyclopedia Britannica, Thiourea Chemical compound (2013) [Online]. Available: <http://www.britannica.com/EBchecked/topic/592308/thiourea>
- [76] Thiourea, Concise International Chemical Assessment Document 49, World Health Organization, Geneva, (2003) [Online]. Available: <http://www.who.int/ipcs/publications/cicad/en/cicad49.pdf>
- [77] Margaret-Ann Armour, Hazardous Laboratory Chemicals Disposal Guide, Third Edition, Lewis publishers, CRC Press (2003).
- [78] Stannous chloride, Heavy metals and arsenic specifications revised at the 61st JECFA (2003), [Online]. Available: <http://www.fao.org/ag/agn/jecfa-additives/specs/Monograph1/additive-438-m1.pdf>
- [79] Tin(II) chloride, Material Safety Data Sheet (2008) [Online]. Available: <http://www.ch.ntu.edu.tw/~genchem99/msds/exp10/SnCl2.pdf>
- [80] J.M. Spero, B. DeVito, L. Theodore, Regulatory Chemicals Handbook, CRC Press (2000).
- [81] Open chemistry database, sodium thiosulphate (2015) [Online]. Available: http://pubchem.ncbi.nlm.nih.gov/compound/Sodium_thiosulphate#section=Use-and-manufacturing
- [82] Safety data sheet, sodium thiosulphate. [Online]. Available: <http://www.jmloveridge.com/cosh/Sodium%20Thiosulphate.pdf>

- [83] O. L. Arenas, M. T. S. Nair and P. K. Nair, Chemical bath deposition of ZnS thin films and modification by air annealing, *Semicond. Sci. Technol.* 12 (1997) 1323.
- [84] M. T. S. Nair, P. K. Nair, R. A. Zingaro and E. A. Meyers, Conversion of chemically deposited photosensitive CdS thin films to n-type by air annealing and ion exchange reaction, *J. Appl. Phys.* 75(3) (1994) 1557-1564.
- [85] Scanning Electron Microscopy coupled with Energy Dispersive X-ray (SEM/EDX) Spectroscopy, Surface Science Western (2014) [Online]. Available: <http://www.surfacesciencewestern.com/analytical-services/scanning-electron-microscopy-coupled-with-energy-dispersive-x-ray-semedx-spectroscopy/>
- [86] J. Goldstein, D. Newbury, D. Joy, Ch. Lyman, P. Echlin, Scanning electron microscopy and X-ray microanalysis, III edition, Kluwer academic/Plenum publishers, New York (2003).
- [87] N. A. Geisse, AFM and combined optical techniques, *Materials today* 12 (2009) 40-45.
- [88] B. Howorth, Detecting ZnS thin films on Si substrates using X-ray diffraction, PhD thesis (2013).
- [89] X-Ray diffraction – XRD, *Particle analytical* (2015) [Online]. Available: <http://particle.dk/methods-analytical-laboratory/xrd-analysis/>
- [90] L. Alexander, H. P. Klug, Determination of crystallite size with the x-ray spectrometer, *J. Applied Phys.* 21 (1950) 137- 142.
- [91] What is Raman spectroscopy? (2015) [Online]. Available: <http://www.inphotonics.com/raman.htm>
- [92] G. Benno, K. Joachim, Optical properties of thin semiconductor films (2003) [Online]. Available: http://home.fnal.gov/~jkopp/tum/pdf/F/hl_spekt.pdf
- [93] R. Mariappan, M. Ragavendar, V. Ponnuswamy. Structural and optical characterization of SnS thin films by electrodeposition technique, *Optica Applicata XLI* 4 (2011) 989-997.
- [94] Anis Akkari, Meriem Reghima, Cathy Guasch. Effect of copper doping on physical properties of nanocrystallized SnS zinc blend thin films grown by chemical bath deposition, *J. Mater. Sci.* 47 (2012) 1365-1371.
- [95] A. Garcia, M.T.S. Nair, P.K.Nair, Evolution of crystalline structure in SnS

thin films prepared by chemical deposition, *Solid State Sci.* 30 (2014) 26-53.

[96] H. R. Chandrasekhar, R.G. Humphreys, U.Zwick, M.Cadona, Infrared and Raman spectra of the IV-VI compounds SnS and Sn, *Sem Phys Rev B* 15 (1977) 2177-2183.

[97] P. Sinsermsuksakul, J.Heo, W.Noh, A.S. Hock, R.G. Gordon, Atomic layer deposition of tin monosulfide thin films, *Adv. En. Mat.* 1 (2014) 1116-1125.

[98] L.S. Price, I.P. Parkin, A.M.E. Hardy , R.J.H. Clark, T.G. Hibbert, K.C. Molloy, Atmospheric Pressure Chemical Vapour Deposition of Tin Sulfides (SnS,Sn₂S₃, SnS₂) on glass, *Chem Mater* 11 (1999) 1792-1799 .

[99] T. H. Sajeesh, K. P, Dr.Vijayakumar, Spray Pyrolysed Tin Chalcogenide Thin Films: Optimization of optoelectronic properties of SnS for possible photovoltaic application as an absorber layer, PhD thesis (2012).

[100] H.R. Chandrasekhar, R.G. Humphreys, U.Zwick, M. Cardona, Infrared and Raman spectra of the IV-VI compounds SnS and SnSe, *Phys Review B* 15 2177-2183.

[101] R. Miles, SNS PV CELLS Report Summary, Community research and development information service (2014) [Online]. Available: http://cordis.europa.eu/result/rcn/56258_en.html

[102] Yu Wang, Y. Bharath Kumar Reddy, Hao Gong, Large-surface-area nanowall SnS films prepared by chemical bath deposition, *J. Electrochem. Soc.* 156(3) (2009) 157-160.

[103] The standard XRD database card 01-072-8499.

[104] Subba Ramaiah Kodigala, Thin film solar cells from earth abundant materials: growth and characterization of Cu₂(ZnSn)(SSe)₄ thin films and their solar cells, Elsevier Inc. (2014).

[105] K.K. Nanda, S.N. Sarangi, S.N. Sahu, S.K. Deb, S.N. Behera, Raman spectroscopy of CdS nanocrystalline semiconductors, *Physica B: Condensed Matter* 262 (1999) 31-39.

[106] C.V. Ramana, R.J.Smith and O.M. Hussain, Grain size effects on the optical characteristics of pulsed-laser deposited vanadium oxide thin films, *Phys. Stat. Sol.* 199 (2003) 4-6.

[107] S. T. Tan, B. J. Chen, X. W. Sun, W. J. Fan, H. S. Kwok, X. H. Zhang, and

S. J. Chua, Blueshift of optical band gap in ZnO thin films grown by metal-organic chemical-vapor deposition, *J.of Appl. Phys* 98 (2005) 013505.

[108] B. Ghosh, R. Bhattacharjee, P. Banerjee, Structural and optoelectrical properties of vacuum evaporated SnS thin films annealed in argon ambient, S. Das, *Appl. Surface Sci.* 257 (2011) 3670-3676.

[109] The standard XRD database card 04-008-2190.

[110] The standard XRD database card 04-008-2191.

[111] P. Nandakumar, C. Vijayan, K. Dhanalakshmi, G. Sundararajan, Synthesis and characterization of CdS nanocrystals in a perfluorinated ionomer (Nafion), *Mater. Sci. and Engineer. B* 83 (2001) 61-65.

[112] A. M. A. Al-Hussam, S.A-J. Jassim. Synthesis, structure, and optical properties of CdS thin films nanoparticles prepared by chemical bath technique, *J. of the Association of Arab Universities for Basic and Appl. Sci* 11(2012) 27-31.

[113] R.C.C. Leite, S.P.S Porto, Enhancement of Raman cross section in CdS due to resonant absorption, *Phys. Rev. Lett* 17(1966) 10.

[114] D. Avellaneda, B. Krishnan, A.C. Rodriguez, T.K. Das Roy, S. Shaji, Heat treatment in chemically deposited SnS thin films and their influence in CdS/SnS photovoltaic structures, *J Mater Sci : Mater Electron* 26 (2015) 5585-5592.

[115] N. Sato, M. Ichimura, E. Arai and Y. Yamazaki, Characterization of electrical properties of SnS thin films prepared by the electrochemical deposition method, 3rd World Conference on Photovoltaic Energy Conversion (2003) 38-41.

APPENDIX A

Article I

M. Safonova, P.K. Nair, E. Mellikov, A.R. Garcia, K. Kerm, N. Revathi, T. Romann, V. Mikli, O. Volobujeva. Chemical bath deposition of SnS thin films on ZnS and CdS substrates, *J Mater Sci: Mater Electron* 25 (2014) 3160-3165.

Chemical bath deposition of SnS thin films on ZnS and CdS substrates

M. Safonova · P. K. Nair · E. Mellikov ·
A. R. Garcia · K. Kerm · N. Revathi ·
T. Romann · V. Mikli · O. Volobujeva

Received: 6 March 2014 / Accepted: 8 May 2014 / Published online: 15 May 2014
© Springer Science+Business Media New York 2014

Abstract We illustrate that Tin sulfide (SnS) thin films of 110–500 nm in thickness may be deposited on ZnS and CdS substrates to simulate the requirement in developing window-buffer/SnS solar cells in the superstrate configuration. In the chemical bath deposition reported here, tin chloride and thiosulfate are the major constituents and the deposition is made at 25 °C. In a single deposition, film thickness of 110–170 nm is achieved and in two more successive depositions, the film thickness is 450–500 nm. The thicker films are composed of vertically stacked flakes, 100 nm across and 10–20 nm in thickness. The Sn/S elemental ratio is ~ 1 for the films 110–170 nm in thickness, but it slightly increases for thicker films. The crystalline structure is orthorhombic, similar to the mineral herzenbergite, and with crystallite diameters 13 nm (110–170 films) and 16 nm (450–500 nm films). The Raman bands at 94, 172 and 218 cm^{-1} further confirm the SnS composition of the films. The optical band gap of SnS is 1.4–1.5 eV for the thinner films, but is 1.28–1.39 eV for the thicker films, the decrease being ascribed to the increase in the crystallite diameter. Uniform pin-hole free SnS thin films were

successfully grown on two different substrates and can be applied in solar cell structures.

1 Introduction

Tin sulfide (SnS) is one of the most promising materials for low-cost thin film solar cells, since its band gap (1.3–1.4 eV) is near to the optimum value of 1.3–1.5 eV for solar cell and its absorption coefficient is appreciably high in the visible region ($>10^4 \text{ cm}^{-1}$). In addition, the elemental constituents of this material are nontoxic and abundant in nature [1].

For the deposition of thin films of SnS various methods like thermal evaporation, pulse electrodeposition, spray pyrolysis, SILAR, electron beam evaporation, chemical bath deposition (CBD) have been employed [2]. Among these methods CBD is relatively simple, and inexpensive method suitable for deposition at low temperature on large substrates irrespective of the shape and morphology of substrates [3]. However, CBD is a complicated process. There are many parameters which influence the deposition of SnS films, such as atmosphere medium, ion concentration, defect chemistry, aqueous medium of the bath solution, temperature [4] and substrate nature.

Recently, a record efficiency SnS solar cell of 1.95 % (active area) was fabricated from p–n homojunction nanowires using boron and phosphorus as dopants. In addition, SnS-based solar cells have been reported using different n-type partners such as ZnO, CdS, $\text{Cd}_{1-x}\text{Zn}_x\text{S}$. So far, the best SnS planar heterojunction device was fabricated with SnS/CdS, achieving power conversion efficiency (η) of 1.3 % [5]. However, there are some concerns that CdS can have harmful effects on the kidneys and bone.

M. Safonova (✉) · E. Mellikov · K. Kerm · N. Revathi ·
V. Mikli · O. Volobujeva
Department of Materials Science, Tallinn Technical University,
Ehitajate tee 5, 19086 Tallinn, Estonia
e-mail: marija.safonova@gmail.com

P. K. Nair · A. R. Garcia
Department of Solar Energy Materials, Instituto de Investigación
en Energía, Universidad Nacional Autónoma de México,
62580 Temixco, Morelos, Mexico

T. Romann
Institute of Chemistry, University of Tartu, Ülikooli 18,
50090 Tartu, Estonia

On the other hand, ZnS is very suitable for a window layer of heterojunction solar cells [6].

The aim of this work was to investigate properties of SnS films depending on the substrate materials and number (1–3) of sequential deposition. Films were deposited on ZnS and CdS substrates, because they suit well as buffer layers for solar cells with SnS absorber layer. One, two and three times deposited SnS films were prepared. The structural, morphological, optical and electrical properties of these films were investigated.

2 Experimental

2.1 Deposition of ZnS films

ZnS thin films were prepared by CBD technique, consecutively stirring zinc sulfate, triethanolamine, ammonium hydroxide, thioacetamide with respective molar concentrations of 0.025, 0.014 M, concentrated, 0.01 M in total volume [7]. Deionized water was added to obtain total solution volume of 100 ml. Corning glass substrates, which were previously washed with detergent, were placed vertically in solution. Deposition was held at room temperature for 24 h. Obtained films were washed with cotton and rinsed with deionized water, then dried. Films were heated in the air for 15 min at 270 °C to obtain good adherence of consecutively deposited SnS film.

2.2 Deposition of CdS films

CdS thin films were prepared by CBD, consecutively stirring cadmium nitrate, sodium citrate, ammonium hydroxide and thiourea solutions with respective molar concentrations of 0.025, 0.15 M, concentrated, 0.05 M in total volume [8]. Deionized water was added to obtain total solution volume of 100 ml. Corning glass substrates, which were previously washed with detergent and then in ultrasonic bath with acetone, were placed vertically in solution. Deposition was held at 80 °C during 1 h and 30 min. Obtained films were washed using cotton and rinsed with deionized water, then dried.

2.3 Deposition of SnS films

SnS thin films were prepared by CBD. Few drops of hydrochloric acid were added to stannous chloride to dissolve it, molar concentration of stannous chloride in total volume is 0.03 M. Next, tartaric acid was added with molar concentration in total volume of 0.44 M. Deionized water

was added and then ammonium hydroxide to obtain the pH of solution equal to 7. The last component added was sodium thiosulphate with molar concentration in total volume of 100 ml 0.03 M [9]. Corning glass substrates with previously deposited CdS or ZnS thin films were placed vertically in solution. Deposition was held at room temperature during 24 h. Obtained films were washed and rinsed with deionized water, then dried. Consecutive depositions of two and three times were made additionally to obtain thicker films. Deposition made directly on glass substrates lacks the good quality obtainable on CdS or ZnS substrate layers.

2.4 Characterization of films

XP Plus Stylus Profilometer was used to determine thickness of the films. X-ray diffraction analysis was made to evaluate crystalline structure of films, using Rigaku Ultima IV X-ray diffractometer using Cu-K α radiation with 2 θ ranging from 10° to 70°. Scanning electron microscope (SEM) Hitachi SUI 510 and HR-SEM Zeiss ULTRA 55 images were taken to obtain information on films surface morphology and attached EDAX Oxford x-act analyser to determine the elemental composition of the films. The optical transmittance and near-normal specular reflectance of the films were recorded using a Shimadzu UV–VIS–NIR scanning spectrophotometer in the wavelength range of 250–2,500 nm. Electrical characteristics were measured using Keithley 619 electrometer with Keithley 230 programmable voltage source. Hall-effect measurements were done at room temperature using an MMR Technologies H-50 unit, allowing for the determination of charge-carrier type. Raman spectral measurements were made at room temperature on a high resolution micro-Raman spectrometer (Horiba JobinYvon HR800) equipped with a multi-channel CCD detection system in the backscattering configuration. An Nd-YAG laser ($\lambda = 532$ nm) with a spot size of 10 μm in diameter was used for excitation. Bruker Multimode 8 Atomic Force Microscope (AFM) with nanoscope V controller was used to determine roughness of the films surface.

3 Results and discussion

3.1 Thickness

Film thickness in series CdS/SnS found to be slightly higher (173 nm for one-time and 505 nm for three-times deposition) than that in the ZnS/SnS series (114 nm for one-time and 455 nm for three-times deposition). Whether this is due to dissolution of the ZnS substrate layer is not clear.

Table 1 Changes in composition of SnS thin films of series ZnS/SnS and series CdS/SnS in multiple deposition process

Series	Sn atomic %	S atomic %
ZnS/SnS		
X1	50.95	48.04
X2	53.44	46.56
X3	56.09	43.60
CdS/SnS		
X1	50.18	49.82
X2	50.20	49.80
X3	50.69	49.31

3.2 Elemental analyses and surface morphology

Table 1 shows atomic ratios of tin and sulphur in as-deposited films of series ZnS/SnS and CdS/SnS. In series CdS/SnS in multiple deposition process the ratio of tin to sulphur is almost 1:1, which means, that these films were in a nearly stoichiometric composition of stannous monosulphide. The films deposited on ZnS substrate were stoichiometric only after single CBD, but tin-rich in multiple deposition series, with a continuous increase of concentration of tin in films. The similar increase of Sn concentration in SnS films by CBD deposition process was reported by Patel [10]. At the same time, Raman investigations did not indicate the existence of any additional to SnS phases in CBD films on ZnS substrate.

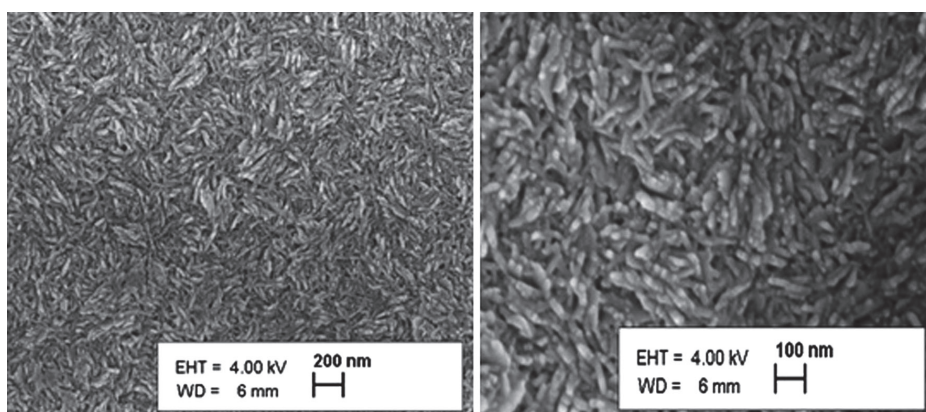
Figures 1 and 2 show SEM images of SnS films of the CdS/SnS and ZnS/SnS series. Images indicate uniform pin-hole free surface of the SnS thin films on both substrates. The images also show complete, continuous and uniform coverage of material over the surface of the films. The

films of similar thickness on CdS and ZnS substrates demonstrate slightly different morphology, but in general they consist of vertically stacked flake structures, of about 100–150 nm laterally and of thickness of around 20 nm. The film morphology reported here is similar to those obtained by Wang et al. [11]. The absence of particulate precipitate in both cases indicates that the dominating deposition mechanism of the films on ZnS substrate may be ion-by-ion mechanism [3]. The surface illustrated here appears smooth at optical wavelengths, with optical transmittance and reflectance summing up to 100 %, as discussed later on.

Atomic force microscopy (AFM) images (Fig. 3) show the roughness of two-times deposited SnS films of series ZnS/SnS and CdS/SnS. Average roughness (R_a) of the films of series ZnS/SnS is 10.8 nm and for series CdS/SnS is 14.2 nm and root mean square roughness (R_q) is 13.4 and 18.00 nm respectively. Maximum height of the profile (R_t) is 95.4 nm for series ZnS/SnS and 143.2 nm for series CdS/SnS. The observed difference in the surface morphologies of the films on different substrates could result from the difference in the deposition mechanisms of the films on different substrates. The roughness at the film surface is smaller than the optical wavelengths, and the films would behave specular in optical reflectance.

3.3 Structural properties

The X-ray diffraction (XRD) patterns of thin films of one, two and three-times deposited films of the series CdS/SnS are shown in Fig. 4. Similar dependence of XRD pattern on the film thickness was noticed for series ZnS/SnS as well. All the major peaks in the PDF card 01-072-8499 for SnS match those of the XRD pattern of the thicker film. The

**Fig. 1** SEM images of SnS films of series ZnS/SnS

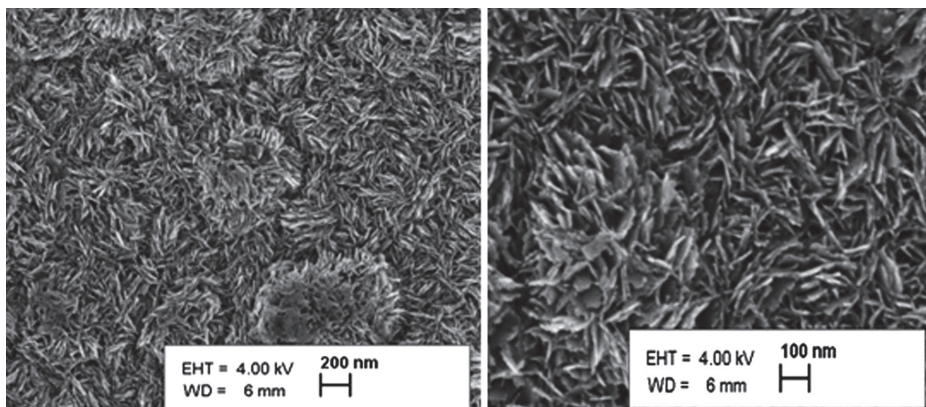
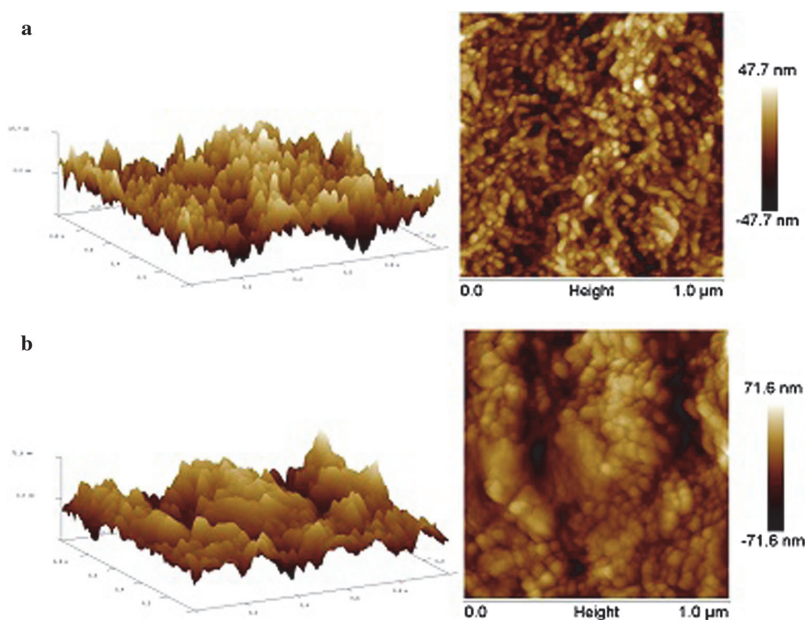


Fig. 2 SEM images of SnS films of series CdS/SnS

Fig. 3 AFM images of two-times deposited SnS films on **a** ZnS substrate and **b** CdS substrate



peak at $2\theta = 31.60^\circ$ corresponding to (040) planes; at 26.5° of (120); at 22.6° of (110); at 38.9° of (131); and at 45.3° corresponding to (150) planes of the orthorhombic phase of herzenbergite SnS are all noted. Improvement of crystallinity with the thickness was observed also by other researchers [12]. XRD pattern may contain also some peaks of CdS structure at $2\theta = 26.5^\circ, 30.6^\circ, 51.1^\circ, 53.1^\circ$ and 64.1° , but this peaks coincide with SnS peaks. There is no indication of other possible additional phases in the films. All the films exhibit (040) plane as preferred and

peak of this plane was used for crystallite size calculations. Crystallite size slightly grows with thickness in both series: from 112 to 130 Å for series ZnS/SnS and from 130 to 161 Å for series CdS/SnS.

Raman analyse was also made to determine more precisely phase composition of films on different substrates. Results of Raman analyse (Fig. 5) were analogical to our XRD results and didn't show the existence of any additional phases in the films, all the peaks in Raman spectra correspond to tin monosulphide phase [13, 14]. On the plot

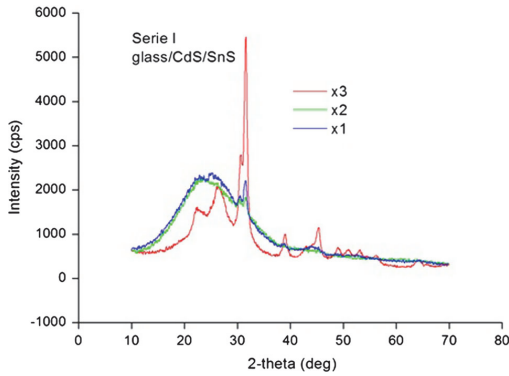


Fig. 4 XRD patterns of CdS/SnS thin films of one and three-times deposited SnS films of series CdS/SnS

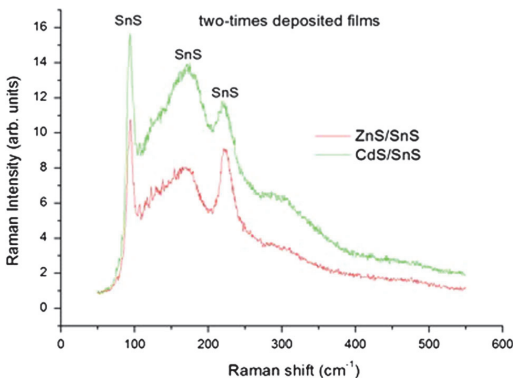


Fig. 5 Raman spectra of SnS thin films deposited on ZnS and CdS substrates

of CdS/SnS serie can be seen small peak at 306 cm^{-1} , which can be attributed to CdS peak (305 cm^{-1}). At the same time there is no peak at the same place on the graph of serie ZnS/SnS.

3.4 Optical properties

Figure 6 shows the room temperature optical transmittance (T) and specular reflectance (R) curves of one and three-times deposited SnS films of series (a) ZnS/SnS and (b) CdS/SnS recorded at the wavelength range of 200–2,500 nm. The specular nature of the films is illustrated by $T + R > 90\%$ in general for all the films for large wavelengths, $>2,000\text{ nm}$.

The absorption edge in the transmittance curves fall in the region of 700–900 nm without any bending, which indicates once more to the absence of additional phases

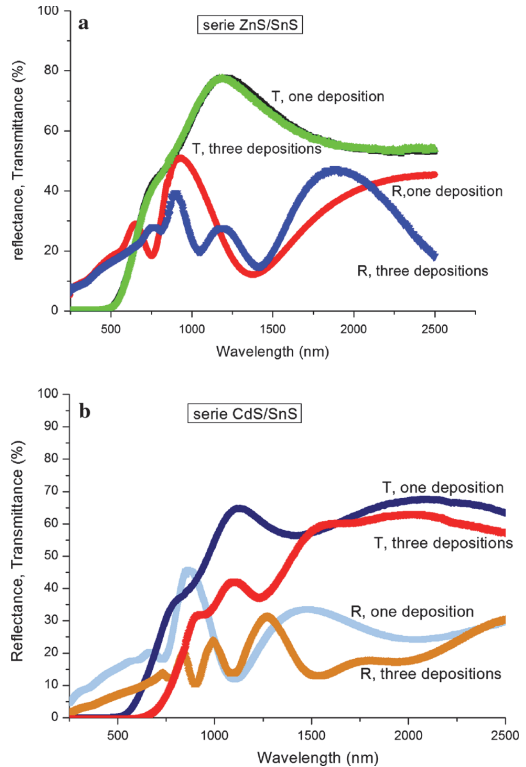


Fig. 6 Transmittance and reflectance spectra of one and three-times deposited SnS films of series **a** ZnS/SnS and **b** CdS/SnS

presented in material. It can be observed from the Fig. 6 that the absorption edge shifts toward the higher wavelength as the thickness increases with number of depositions in series CdS/SnS. Such tendency was also observed in other works [16].

The optical energy band gap (E_g) of the as-grown SnS layers was calculated using the relation, $(\alpha h\nu) = A(h\nu - E_g)^n$. Where α is the absorption coefficient, A is a constant, $h\nu$ is the energy of the incident light and n is the nature of transition between the bands in the material.

In the present study, the nature of the transition followed is indirect allowed ($n = 2$) and the energy band gap can be determined by extrapolating the straight line portion of the curve $(\alpha h\nu)^{1/2}$ versus $h\nu$ on the energy axis. Band gap values decrease with number of deposition from 1.49 to 1.39 eV for films deposited on ZnS substrate and from 1.5 to 1.28 eV for films deposited on CdS substrate. This decrease could be attributed to the grain size dependency of band gap [10]. Such tendency was also observed by Ghosh et al. [15].

The E_g of the CdS/SnS thin film (1.28 eV) is close to that of orthorhombic SnS (1.3 eV) as determined from photoreflection measurements.

Hot-probe method was used to determine type of conductivity of the SnS films and all the layers showed p-type conductivity. Films of both series have very high resistivity: 120 M Ω for three-times deposited films of series CdS/SnS and 130 M Ω for three-time deposited films of series ZnS/SnS. Resistivity increases with decreasing films thickness. Further experiments are needed to decrease it.

4 Conclusions

Films have the structure of orthorhombic herzenbergite tin monosulphide with stoichiometric composition and good pin-hole free surface morphology of rod (ZnS substrate) or flake (CdS substrate) shape of the particles. XRD, Raman and EDX analyses didn't show any additional phases in the films. Crystallinity of the as-deposited films improves in multiple deposition process and three times deposited films have well-determined crystalline structure. Grain sizes slightly grow in multiple deposition process of films. Band gap decreases with the thickness of the films and for three-times deposited it is equal to 1.28 eV. Films on both substrates have very high electro resistivity which should be improved with further chemical and thermal treatments.

Acknowledgments The authors are grateful to Patricia Altuzar for the XRD measurements, Jose Campos for the SEM-compositional analyses and photoconductivity response measurement, Oscar Gomez Daza for the optical measurements, all of them at the *Instituto de Energias Renovables—UNAM*. We acknowledge the use of experimental facility of CONACYT-Mexico project 123122-LIFYCS. Estonian Centre of Excellence in Research Project TK117T “High-technology Materials for Sustainable Development”, Estonian Energy

Technology program (project AR 10128), Estonian Ministry of Higher Education and Science (targeted project T099) and Estonian Science Foundation (MJD213, G8147) are acknowledged for the financing of the research.

References

1. G.E. Yan-hui, G.U.O. Yu-ying, S.H.I. Wei-min, Q.I.U. Yong-hua, W.E.I. Guang-pu, J. Shanghai Univ. (Engl. Ed.) **11**(4), 403–406 (2007)
2. E. Guneri, F. Gode, C. Ulutas, F. Kirmizigul, G. Altindemir, C. Gumus, Chalcogenide Lett. **7**(12), 685–694 (2010)
3. G. Hodes, *Chemical Solution Deposition of Semiconductor Films* (Marcel Dekker Inc., New York, 2002)
4. S. Aksaya, T. Ozer, M. Zor, J. Appl. Phys. **47**, 30502 (2009)
5. P. Sinsermsuksakul, K. Hartman, S.B. Kim, J. Heo, L. Sun, H.H. Park, R. Chakraborty, T. Buonassisi, R.G. Gordon, Appl. Phys. Lett. **102**, 053901 (2013)
6. W. Wu, W. Shi, Z. Hu, S. Liu, W. Yang, G. Wei, in *Proceedings of SPIE 7995, Seventh International Conference on Thin Film Physics and Applications*, (February 17, 2011), 79952D
7. O.L. Arenas, M.T.S. Nair, P.K. Nair, Semicond. Sci. Technol. **12**, 1323 (1997)
8. M.T.S. Nair, J. Appl. Phys. **75**(3), 1557–1564 (1994)
9. P.P. Hankare, A.V. Jadhav, P.A. Chate, K.C. Rathod, P.A. Chavan, S.A. Ingole, J. Alloys Compd. **463**, 581–584 (2008)
10. T.H. Patel, Open Surf. Sci. J. **4**, 6–13 (2012)
11. Y. Wang, Y. BharathKumar Reddy, H. Gong, J. Electrochem. Soc. **156**(3), H157–H160 (2009)
12. A. Akkari, C. Guasch, N. Kamoun-Turki, J. Alloys Compd. **490**, 180–183 (2010)
13. L.S. Price, I.P. Parkin, A.M.E. Hardy, R.J.H. Clark, Chem. Mater. **11**, 1792–1799 (1999)
14. S. Kodigala, *Thin Film Solar Cells From Earth Abundant Materials: Growth and Characterization of Cu₂(ZnSn)(SSe)₄ Thin Films and Their Solar Cells* (Elsevier Inc., London, 2014), p. 26
15. B. Ghosh, R. Bhattacharjee, P. Banerjee, S. Das, Appl. Surf. Sci. **257**, 3670 (2011)
16. A.-H.K. Elttayef, H.M. Ajeel, A.I. Khudiar, J. Mater. Res. Technol. **2**, 182–187 (2013)

APPENDIX A

Article II

M. Safonova, E. Mellikov, V. Mikli, K. Kerm, N. Revathi, O. Volobujeva.
Chemical bath deposition of SnS thin films from the solutions with different concentrations of tin and sulphur, *Advanced Materials Research* 1117 (2015) 183-186.

Chemical bath deposition of SnS thin films from the solutions with different concentrations of tin and sulphur

M. Safonova^{1, a *}, E. Mellikov^{1, b}, V. Mikli^{1, c}, K. Kerm^{1, d}, N. Revathi^{1, e},
O. Volobujeva^{1, f}

¹ Department of Materials Science, Tallinn Technical University, Ehitajate tee 5, Tallinn 19086, Estonia

^amarija.safonova@gmail.com, ^benn.mellikov@ttu.ee, ^cvaldek.mikli@ttu.ee, ^dkarin.kerm@mail.ee, ^erevathi.naidu@ttu.ee, ^fv.olga@staff.ttu.ee

Keywords: SnS thin films, chemical bath deposition, SEM, EDX, Raman analysis

Abstract. The aim of the current research was to study regularities of chemical bath deposition (CBD) of tin sulphide thin films as function of tin and sulphur concentrations in the solutions. SnS thin films were deposited onto Mo-, ITO- and TO-coated glass and onto borosilicate glass substrates at room temperature for 24 hours. The concentrations of sulphur and tin (ratio 1:1) in the deposition solution were varied from 0.01 M to 0.09 M. Films were characterized by SEM and Raman spectroscopy. The structurally best tin mono-sulphide films with good adhesion to the substrate were deposited at concentration of constituents in solution 0.03M. The films deposited at concentration of 0.01M had non-uniform and incomplete coverage of the surface on all used substrates whereas at tin and sulphur concentrations of 0.05M and higher films were peeling off of the substrate.

Introduction

New materials consisting of nontoxic and widely abundant elements are required for wide use in solar energetic [1]. Among them very attractive binary semiconductor of IV-VI group is SnS [2] due to its energy band gap of 1.35 eV that is close to the optimum for solar cells value of 1.5 eV and for high absorption of solar radiation. This compound has also high chemical and environmental stability and involves earth abundant elements [3]. Chemical bath deposition can be used to deposit SnS films. This technique is one of the simplest and cheapest methods because it does not require expensive equipment and can be done at room temperature and allows large scale manufacturing [4].

The aim of work was to investigate peculiarities of deposition of the SnS thin films from the solutions with different concentrations of tin and sulphur on different substrates.

Experimental

Preparation of the films. Five baths were prepared with molar concentrations of initial Sn and S sources equal to 0.01 M, 0.03M, 0.05 M, 0.07 M and 0.09 M in the total solution with ratios of Sn to S equal to 1:1. Tartaric acid was added as a complexing agent. Stannous (II) chloride was used as a source of Sn²⁺ ions and sodium thiosulphate pentahydrate as a source of S²⁻ ions. Indium tin oxide (ITO), tin dioxide (TO), molybdenum (Mo) covered glass and borosilicate glass were used as substrates. Deposition was held onto vertically placed substrates at room temperature of about 22 degrees centigrade during 24 hours at pH=7 in glass vessels.

Characterization of the films. Scanning electron microscope (SEM) HR-SEM Zeiss ULTRA 55 was used to study surface morphology of the deposited films and for elemental analysis was attached energy dispersive X-ray (EDX). Raman spectral measurements were made at room temperature using a high resolution micro-Raman spectrometer (Horiba Jobin Yvon HR800) equipped with a multichannel CCD detection system in the backscattering configuration. A HeNe

laser ($\lambda = 633 \text{ nm}$) with a spot size of $10 \mu\text{m}$ in diameter was used for excitation during Raman investigations.

Results and discussion

SEM. Films deposited at concentration of constituents in solution 0.01 M had incomplete coverage of formed SnS of the surface on all used substrates. We did not notice the formation of continuous film on borosilicate glass, the surface was covered with separate agglomerated SnS particles with the height of around 300 nm . Noticed incomplete coverage could be explained by insufficient number of crystallization centres on the surface of borosilicate glass. SnS formation of similar mode was prevailing on ITO substrates; however agglomerates are smaller with the height of about 155 nm . Tin sulphide films deposited on Mo and TO substrates have more dense coverage of the substrates with agglomerates with nearly similar size (around 120 and 100 nm , respectively).

At concentration of constituents 0.03 M deposited films have uniform and complete coverage of the substrate (Mo, ITO and TO) with size of tense and continuous film forming agglomerates of 190 , 200 and 210 nm , respectively. Visually films have uniform and homogeneous dark brownish-grey colour over the entire surface. This concentration seems to be the most appropriate for depositing SnS films onto Mo, TO and ITO substrates due to the good adhesion of the obtained pinhole free films with substrates and uniform, complete coverage of the substrates by films. Incomplete coverage of surface by agglomerates with the size of 240 nm prevails in films on borosilicate glass substrate.

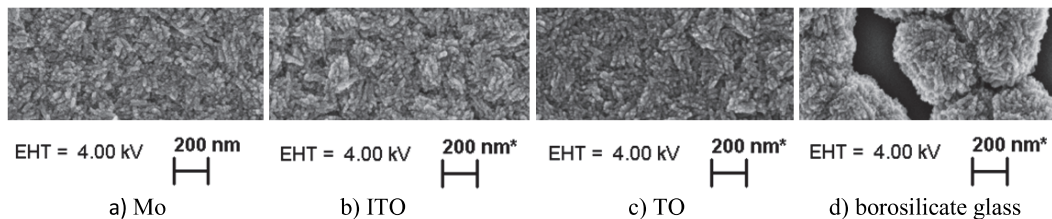


Fig.1 SEM images of the SnS thin films deposited at concentration of 0.03M .

Starting from solution concentration of 0.05 M and higher the formed films, except films deposited on TO, did not have good adhesion to the surface of substrate and peeled easily off. The coverage of substrate by formed films is complete and uniform on all substrates, except borosilicate glass. Films deposited on Mo, ITO and TO substrates have thicknesses of 215 nm , 220 nm and 250 nm , respectively. Analyse of the experimental process allows us to conclude that at these concentrations of constituents mechanism of formation of SnS changes from ion-by-ion mechanism to cluster deposition [5].

It is also well seen at concentration of 0.07M on the Fig. 2. Formation of big clusters on the surface with increasing of concentration was also reported by other researchers [6]. The changes in deposition mechanism result in the decrease of the thickness of formed SnS films (Fig.3) at concentrations higher than 0.05M . Pinhole-free, uniform and complete coverage of the Mo and ITO substrates was noticed (Fig. 2.). SnS films deposited on borosilicate glass still have incomplete coverage of the substrate surface. Thickness of the films decreased compared with thickness of films in use of smaller concentrations of film components in solution (Fig.3).

At the highest concentration of 0.09M films deposited on all substrates have complete and uniform coverage of the surface, but these films are easily peeling off from the surface. The films are visually inhomogeneous with spots of greenish or reddish colour. The reason might be that at higher concentrations of constituents in solution SnS forms already in the volume of solution and films growth occur by the rapid precipitation of already formed in solution SnS colloidal particles.

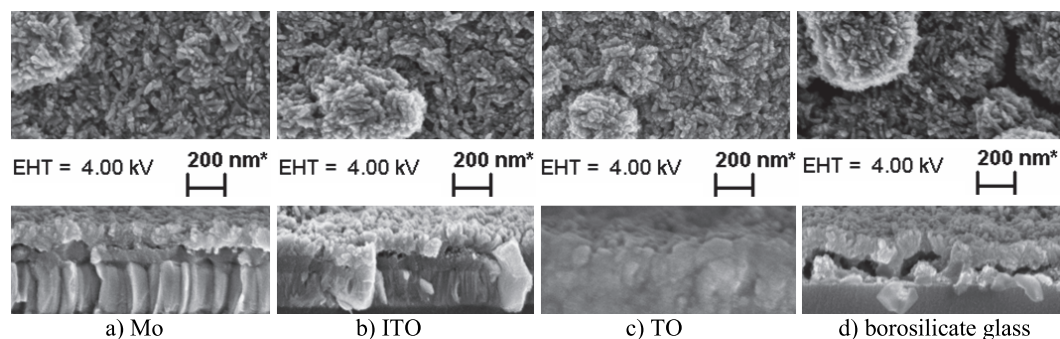


Fig.2 SEM pictures of the SnS thin films deposited at concentration of 0.07M.

The thickness of films diminishes comparing with films deposited from solutions with smaller concentration of tin and sulphur. SnS films deposited on TO substrates at concentration of 0.07M and 0.09M in contrast with other substrates were not peeling off, but visually the films are inhomogeneous and their surface was covered with spots of different colour.

EDX results showed that films are Sn-rich at all concentrations [7]. Sn-rich content of films could be explained by the formation and the existence of oxygen and tin containing separate phases in deposited SnS films.

Raman analysis was made to evaluate phase composition of the films. Fig.4 shows Raman graphs for SnS films deposited on ITO substrates. Graphs obtained for all concentrations are similar and have main peaks corresponding to SnS phase: 82 cm^{-1} [8], 95 cm^{-1} , 163 cm^{-1} , 188 cm^{-1} , 227 cm^{-1} , 288 cm^{-1} [9]. There are two peaks additionally: at 309 cm^{-1} at conc. 0.01 M which corresponds to Sn_2S_3 phase [10] and peak at 333 cm^{-1} at all concentrations which is not identified in the literature. Peak at 333 cm^{-1} is found on all films and does not depend on the nature of substrate that allows us to conclude that this peak belongs to SnS film or has the origin of formation of SnS.

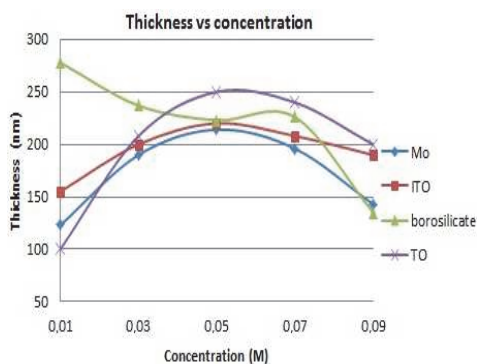


Fig 3. Thickness dependence on concentration.

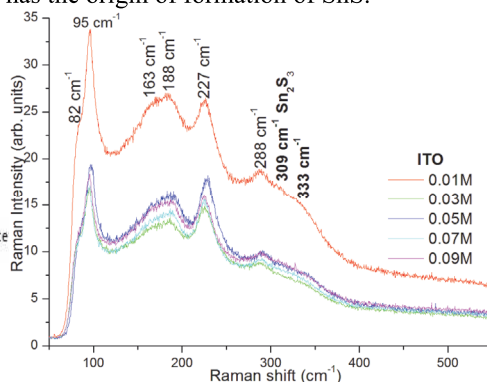


Fig. 4 Raman graphs of SnS films deposited on ITO at different conc.

Raman spectra of films deposited on Mo and TO substrates were similar. The only difference we could notice is the formation of additional Sn_2S_3 peak at 233 cm^{-1} [10] in films deposited on Mo at concentration of 0.01M.

Conclusions

At concentration of 0.01M all films have incomplete coverage of the substrates and have additional peaks of Sn_2S_3 phase. Deposited at 0.03M concentration films have nearly similar thickness on all substrates. At higher concentration of Sn and S in deposition solution thickness of films began to diminish. The SnS films were Sn-rich due to formation of oxygen and tin containing phases in.

Acknowledgements

Estonian Centre of Excellence in Research Project TK117T "High-technology Materials for Sustainable Development", Estonian Energy Technology program (project AR 10128), Estonian Ministry of Higher Education and Science (project T099) and Estonian Science Foundation (MJD213, G8147) are acknowledged for the financing of the research.

References

- [1] S.A. Bashkirov, V.F. Gremenok, V.A. Ivanov, V.V. Lazenka, K. Bente, Tin sulfide thin films and Mo/p-SnS/n-CdS/ZnO heterojunctions for photovoltaic applications, *Thin Sol. Films* 520 (2012) 5807-5810.
- [2] T.H. Patel, Influence of Deposition Time on Structural and Optical Properties of Chemically Deposited SnS Thin Films, *J. Open Surf. Sci.* 4 (2012) 6.
- [3] G. Sreedevi, K. T. R. Reddy, Properties of Tin Monosulphide Films Grown by Chemical Bath Deposition, *Conf. Papers in En.* 2013 (2013) 5 pages.
- [4] P.P. Hankare, A.V. Jadhav, P.A. Chate, K.C. Rathod, P.A. Chavan, S.A. Ingole, Synthesis and characterization of tin sulphide thin films grown by chemical bath deposition technique, *J. Alloys and Comp.* 463 (2008) 581-584.
- [5] G. Hodes, *Chemical solution deposition of semiconductor films*, Marcel Dekker Inc., New York, 2002.
- [6] Y. Jayasree, U. Chalapathi, P. Uday Bhaskar, V. Sundara Raja, Effect of precursor concentration and bath temperature on the growth of chemical bath deposited tin sulphide thin films, *Appl. Surface Sci.* 258 (2012) 2732-2740.
- [7] A.R. Garcia-Angelmo, M.T.S. Nair, P.K. Nair, Evolution of crystalline structure in SnS thin films prepared by chemical deposition, *J. Sol. State Sci.* 30 (2014) 26-35.
- [8] H.R. Chandrasekhar, R.G. Humphreys, U. Zwick, M. Cardona, Infrared and Raman spectra of the IV-VI compounds SnS and SnSe, *Phys. Rev. B* 15 (1977) 2177-2183.
- [9] P. Sinsermuksamul, J.Heo, W.Noh, A.S. Hock, R.G. Gordon, Atomic layer deposition of tin monosulfide thin films, *Adv. En. Mat.* 1 (2014) 1116-1125.
- [10] L. S. Price, I.P.Parkin, A.M.E. Hardy, R.J.H. Clark, Atmospheric Pressure Chemical Vapour Deposition of Tin Sulfides (SnS, Sn₂S₃, SnS₂) on glass, *Chem. Mater.* 11 (1999) 1792-1799.

Chemical Bath Deposition of SnS Thin Films from the Solutions with Different Concentrations of Tin and Sulphur

10.4028/www.scientific.net/AMR.1117.183

DOI References

- [1] S.A. Bashkirov, V.F. Gremenok, V.A. Ivanov, V.V. Lazenka, K. Bente, Tin sulfide thin films and Mo/p-SnS/n-CdS/ZnO heterojunctions for photovoltaic applications, *Thin Sol. Films* 520 (2012) 5807-5810.
<http://dx.doi.org/10.1016/j.tsf.2012.04.030>
- [2] T.H. Patel, Influence of Deposition Time on Structural and Optical Properties of Chemically Deposited SnS Thin Films, *J. Open Surf. Sci.* 4 (2012) 6.
<http://dx.doi.org/10.2174/1876531901204010006>
- [4] P.P. Hankare, A.V. Jadhav, P.A. Chate, K.C. Rathod, P.A. Chavan, S.A. Ingole, Synthesis and characterization of tin sulphide thin films grown by chemical bath deposition technique, *J. Alloys and Comp.* 463 (2008) 581-584.
<http://dx.doi.org/10.1016/j.jallcom.2007.11.065>
- [6] Y. Jayasree, U. Chalapathi, P. Uday Bhaskar, V. Sundara Raja, Effect of precursor concentration and bath temperature on the growth of chemical bath deposited tin sulphide thin films, *Appl. Surface Sci.* 258 (2012) 2732-2740.
<http://dx.doi.org/10.1016/j.apsusc.2011.10.124>
- [7] A.R. Garcia-Angelmo, M.T.S. Nair, P.K. Nair, Evolution of crystalline structure in SnS thin films prepared by chemical deposition, *J. Sol. State Sci.* 30 (2014) 26-35.
<http://dx.doi.org/10.1016/j.solidstatesciences.2014.02.002>
- [8] H.R. Chandrasekhar, R.G. Humphreys, U. Zwick, M. Cardona, Infrared and Raman spectra of the IV-VI compounds SnS and SnSe, *Phys. Rev. B* 15 (1977) 2177-2183.
<http://dx.doi.org/10.1103/PhysRevB.15.2177>
- [9] P. Sinsermsuksakul, J. Heo, W. Noh, A.S. Hock, R.G. Gordon, Atomic layer deposition of tin monosulfide thin films, *Adv. En. Mat.* 1 (2014) 1116-1125.
<http://dx.doi.org/10.1002/aenm.201100330>
- [10] L. S. Price, I.P. Parkin, A.M.E. Hardy, R.J.H. Clark, Atmospheric Pressure Chemical Vapour Deposition of Tin Sulfides (SnS, Sn₂S₃, SnS₂) on glass, *Chem. Mater.* 11 (1999) 1792-1799.
<http://dx.doi.org/10.1021/cm990005z>

APPENDIX A

Article III

M. Safonova, P.K. Nair, E. Mellikov, R. Aragon, K. Kerm, R. Naidu, V. Mikli, O. Volobujeva. Thermal annealing of sequentially chemically deposited SnS thin films, *Proceedings of the Estonian Academy of Sciences* 64 (4) (2015) 488-494.



Thermal annealing of sequentially deposited SnS thin films

Maria Safonova^{a*}, Padmanabhan Pankajakshy Karunakaran Nair^b, Enn Mellikov^a,
Rebeca Aragon^b, Karin Kerm^a, Revathi Naidu^a, Valdek Mikli^a, and Olga Volobujeva^a

^a Department of Materials Science, Tallinn Technical University, Ehitajate tee 5, 19086 Tallinn, Estonia

^b Department of Solar Energy Materials, Centro de Investigación en Energía, Universidad Nacional Autónoma de México, Temixco, Morelos 62580, Mexico

Received 16 June 2014, revised 23 April 2015, accepted 14 June 2015, available online 26 November 2015

Abstract. The influence of thermal treatment with the number of deposition cycles on the properties of SnS films on CdS and ZnS substrates was investigated. Annealing under an argon atmosphere made amorphous SnS films formed in one deposition cycle crystalline, but did not markedly change the crystallinity of SnS films formed after multiple deposition cycles. All annealed films were consistent with the orthorhombic phase of herzenbergite SnS, and no additional Sn-containing phases were identified. The CdS/SnS films maintained their initial stoichiometric composition of tin monosulphide after annealing. The films deposited on ZnS substrate films were rich in tin and poor in sulphur and their composition was unaffected by thermal annealing. Both the deposited and thermally annealed films possessed uniform pinhole-free surfaces. Only minor changes in the optical transmittance and reflectance spectra of the CdS/SnS films were observed after annealing, whereas the spectra of the ZnS/SnS films exhibited substantial changes after annealing. As the annealing temperature increased, the absorption edge of the ZnS/SnS films shifted to a longer wavelength. The optical bandgap of the CdS/SnS films was indirect and decreased from 1.28 eV for the three-deposition-cycle CdS/SnS film to 1.22 eV after annealing at 460 °C. The ZnS/SnS films showed a similar change: the bandgap of 1.39 eV for the unannealed films decreased to 1.23 eV after annealing. All deposited and annealed SnS films showed p-type conductivity and their photoconductivity increased with the increasing annealing temperature. Solar cells with reverse structures were fabricated; their performance decreased with the increasing annealing temperature of the SnS film.

Key words: SnS thin films, chemical-bath deposition, X-ray diffraction, optical spectroscopy, atomic force microscopy, scanning electron microscopy.

1. INTRODUCTION

Humankind today is in intensive search for sustainable energy sources. Renewable energy sources such as sun, wind, and water are being examined to increase their proportion in the energy market. Among these, solar radiation has the greatest potential because of its abundance. Materials such as CuInSe₂ [1], CuInS₂ [2], CdTe [3], and SnS [4] have been used as absorber layers in thin-film solar cells to convert solar radiation to electricity. For this SnS is very promising because of its high absorption coefficient (10^5), suitable bandgap for

solar cells, and abundance in nature [5]. SnS thin films have been deposited by techniques such as electrodeposition [6], spray pyrolysis [7], sputtering [8], vacuum evaporation [9], and chemical-bath deposition (CBD) [10–15]. Despite the relatively low cost and simplicity of CBD, research reported on the formation of SnS thin films by CBD is insufficient and the topic needs further investigation.

The focus in this paper is on the CBD of SnS thin films onto different substrates [16] and their subsequent annealing. The novelty of our results lies in the description of the effect of different annealing on the structure, chemical and phase composition, and properties of multiple-cycle deposited and annealed SnS

* Corresponding author, marija.safonova@gmail.com

films. Our results on the influence of substrate material on the chemical and phase compositions and properties of deposited and annealed thin SnS films add new, very valuable information for providing predata to the production of cheap thin-film solar cells used in chemically deposited SnS absorber layers.

2. EXPERIMENTAL

2.1. Deposition of ZnS films

The ZnS thin films were prepared by a CBD technique described elsewhere [17]. Corning glass substrates, which were first washed with a detergent, were placed vertically in a solution and held at room temperature for 24 h. The resulting films were washed, rinsed with deionized water, and then dried. Films were heated in air for 15 min at 270°C to promote good adherence of the consecutively deposited SnS film.

2.2. Deposition of CdS films

The CdS thin films were prepared by a CBD technique described elsewhere [18]. Corning glass substrates, which were first washed with a detergent and then in an ultrasonic bath with acetone, were placed vertically in a solution for 1.5 h at 80°C. The resulting films were washed, rinsed with deionized water, and then dried.

2.3. Deposition of SnS films

The SnS thin films were also prepared by the CBD technique. A few drops of hydrochloric acid were added to stannous chloride to dissolve it in order to obtain a molar concentration of 0.03 M of stannous chloride. Tartaric acid was then added to give a molar concentration of 0.44 M. Deionized water and then ammonium hydroxide were added until the pH of the solution was 7. Sodium thiosulphate was added with a molar concentration of 0.03 M. The total volume of the solution was 100 mL. Corning glass substrates with previously deposited CdS or ZnS thin films were placed vertically in this solution at room temperature for 24 h. The obtained films were rinsed with deionized water and then dried. Thicker films were obtained by consecutive deposition for two or three times.

2.4. Thermal annealing

The deposited films were heated under argon for 30 min at 300, 400, or 460°C in a vacuum oven. The samples were covered with aluminium foil, placed in a Petri dish, and covered again with aluminium foil. The covered samples were placed in the oven and then the chamber was evacuated to about 30 mTorr. Argon was

introduced into the chamber to give a pressure of 10 Torr, and the furnace was heated.

2.5. Characterization of films

The crystalline structure of the films was investigated by X-ray diffraction (XRD) analyses with a RigakuUltima IV X-ray diffractometer using Cu K α radiation with 2θ ranging from 10° to 70°. Raman spectral measurements were made at room temperature on a high-resolution micro-Raman spectrometer (Horiba JobinYvon HR800) equipped with a multichannel CCD detection system in backscattering configuration. An Nd-YAG laser ($\lambda = 532$ nm) with a spot size of 10 μ m was used for excitation.

Scanning electron microscope (SEM) (Hitachi SUI 510 and HR-SEM Zeiss ULTRA 55) images were recorded to obtain information about film surface morphology. The elemental composition of the films was determined by energy-dispersive X-ray spectroscopy (EDX; Oxford, x-act). An atomic force microscope (AFM; Bruker Multimode) with a Nanoscope V controller was used to determine the surface roughness of the films. A profilometer (XP Plus Stylus) was used to determine the thickness of the films. The optical transmittance and near-normal specular reflectance of the films were recorded using a scanning spectrophotometer (Shimadzu UV-VIS-NIK) in the wavelength range of 250–2500 nm. Electrical characteristics were measured using an electrometer (Keithley 619) with a programmable voltage source (Keithley 230).

Pairs of three different types of paint electrodes with a size of 5 mm \times 5 mm and separation of 5 mm were printed on the surface of the films for the photocurrent measurements. The photocurrent responses of the films were measured under a tungsten halogen lamp providing illumination of 850 W/m².

3. RESULTS

3.1. Film thickness

Both series of films (CdS/SnS and ZnS/SnS) decreased in thickness after thermal annealing, which indicates that annealing caused densification of the films. The effect of annealing was more pronounced for films formed by a single deposition cycle compared with those exposed to multiple deposition cycles. For example, the thickness of the one-deposition-cycle CdS/SnS film decreased from 215 to 164 nm upon annealing at 400°C under Ar for 30 min, whereas the thickness of the two-deposition-cycle CdS/SnS film decreased from 300 to 258 nm after annealing under the same conditions. The thickness of the three-deposition-cycle ZnS/SnS film decreased from 455 to 429 nm after

annealing at 460 °C under Ar for 30 min. This indirectly confirms our conclusion presented in the XRD measurement part that annealing improves the crystallinity of films and makes them denser.

3.2. Structural properties

Figure 1 shows the influence of heat treatment on the crystalline structure of the SnS films deposited on CdS and ZnS substrates. The absence of peaks consistent with the orthorhombic herzenbergite structure of SnS in the XRD patterns of the one-deposition-cycle films indicates that the deposited films are amorphous. The broad peak situated at a small diffraction angle is specific to the amorphous network. However, as the number of deposition cycles increases, the crystallinity of the films improves: the peaks related to SnS become narrower and more intense. The films formed after three deposition cycles exhibit intense, sharp peaks consistent with SnS. Thermal annealing improved the crystallinity of the one-deposition-cycle CBD films, but did not induce any noteworthy changes in the crystallinity of the SnS films formed using multiple deposition cycles. All annealed films clearly show peaks at 31.60°, 26.5°, 22.6°, 38.9°, and 45.3° corresponding to the (040), (120), (110), (131), and (150) planes of the orthorhombic phase of the herzenbergite SnS structure, respectively (see the standard database card 01-072-8499). The existence of CdS with peaks at 26.5°, 30.7°, 51.2°, 53.1°, and 64.1° (standard database cards 04-008-2190 and 04-008-2191) in the XRD patterns of the films containing a CdS underlayer could not be determined precisely because these peaks are very close to those of dominating SnS. No indication of other possible Sn-containing phases in the XRD patterns of the annealed films was found.

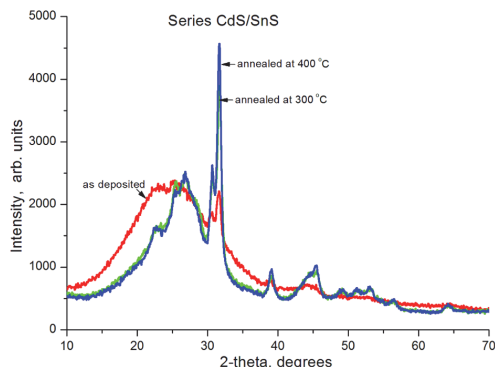


Fig. 1. XRD patterns of CdS/SnS thin films showing the influence of heat treatment on the crystallinity of the two-deposition-cycle SnS deposited films and films annealed at 300 and 400 °C.

The XRD patterns of one-, two-, and three-deposition-cycle SnS films deposited on CdS and ZnS and annealed at 460 °C are compared in Fig. 2. The CdS/SnS films annealed at 460 °C are more crystalline than those deposited on ZnS substrates. All the films exhibit a preferred (040) plane. The peak associated with this plane was used to calculate the crystallite size.

Crystallite size increased with annealing more in films deposited by one deposition cycle than by multiple depositions; for the series annealed at 460 °C from 130 to 163 Å for the one-deposition-cycle CdS/SnS films and from 130 to 143 Å for the three-deposition-cycle ZnS/SnS films.

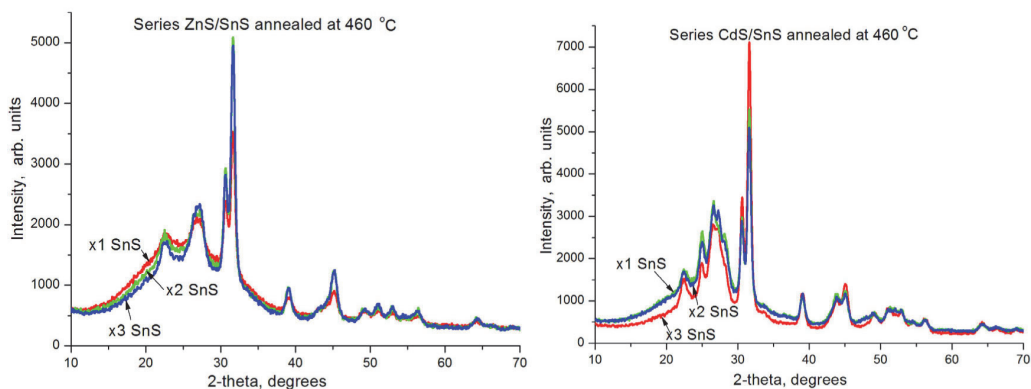


Fig. 2. XRD patterns of ZnS/SnS and CdS/SnS films annealed at 460 °C for 30 min.

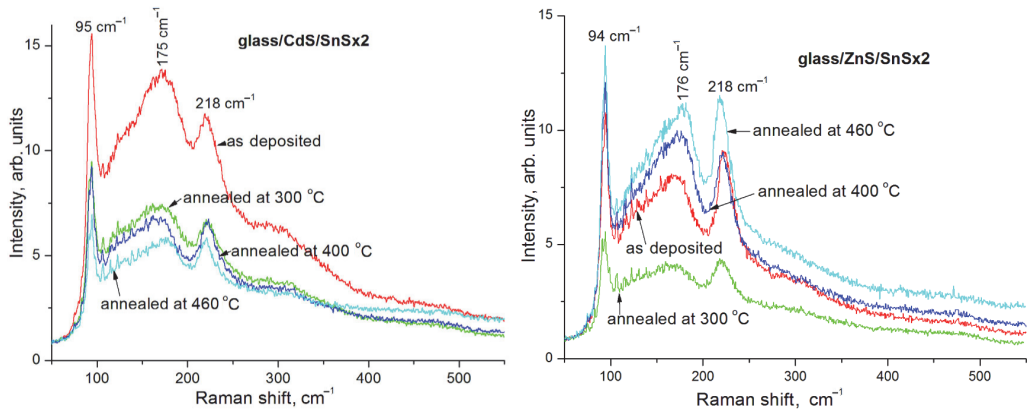


Fig. 3. Raman analyses of two-deposition-cycle films of CdS/SnS and ZnS/SnS annealed at various temperatures.

Results of Raman analyses of the films are presented in Fig. 3. The films show only peaks corresponding to the SnS phase. In the Raman spectrum of the one-deposition-cycle CdS/SnS film, a weak peak at 306 cm⁻¹ was detected, which was attributed to CdS (305 cm⁻¹) [19]. This peak could also be attributed to Sn₂S₃ (307 cm⁻¹) [20]; however, other analyses like XRD and EDX showed no presence of any additional SnS phases. This peak disappeared upon thermal annealing. The absence of this peak from the spectra of the ZnS/SnS films (Fig. 3) indirectly supports our assumption that this peak originates in the CdS substrate.

3.3. Elemental analyses and surface morphology

Table 1 shows the atomic ratios of Sn to S in deposited and thermally annealed CdS/SnS and ZnS/SnS films. EDX revealed ratios of Sn to S of almost 1:1 in the deposited and annealed films formed on CdS substrates. So annealing did not lead to large changes in the composition of the films; the annealed CdS/SnS films maintained their initial stoichiometric composition of tin monosulphide. Annealing at 460°C caused the tin composition of films to increase, probably because more

sulphur is lost during annealing at higher temperatures. The films deposited on ZnS substrates were rich in tin and poor in sulphur after deposition and their composition remained the same after thermal annealing.

Figures 4 and 5 show SEM images of the CdS/SnS and ZnS/SnS films. Uniform pinhole-free surfaces were observed for both the deposited and thermally annealed

Table 1. Atomic ratios of Sn and S in films of series CdS/SnS and ZnS/SnS

Deposition counts	Series ZnS/SnS		Series CdS/SnS	
	Sn : S Atomic %		Sn : S Atomic %	
Unannealed				
one	50.95	48.04	50.18	49.82
two	53.44	46.56	50.20	49.80
three	56.09	43.60	50.69	49.31
460°C 30 min				
one	55.46	44.54	51.34	48.66
two	53.02	46.98	51.44	48.56
three	55.17	44.83	52.69	47.31

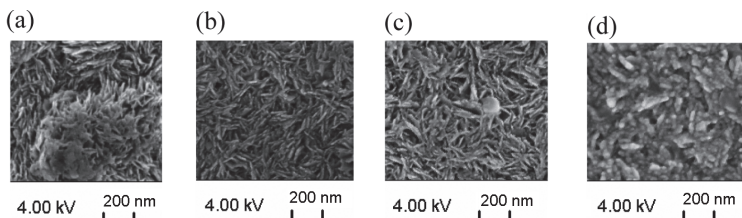


Fig. 4. SEM images of CdS/SnS films formed after two deposition cycles: (a) as deposited, (b) annealed at 300°C, (c) annealed at 400°C, and (d) annealed at 460°C.

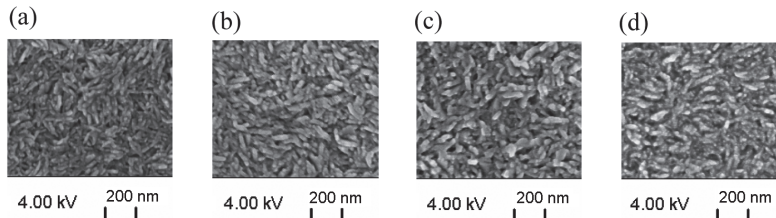


Fig. 5. SEM images of ZnS/SnS films formed after two deposition cycles: (a) as deposited, (b) annealed at 300 °C, (c) annealed at 400 °C, and (d) annealed at 460 °C.

films. Particle size remained nearly the same regardless of the annealing temperature. Films deposited on ZnS substrates have rod-shaped particles, whereas CdS/SnS films contain flake-shaped particles. Annealing at 460 °C changed the surface structure of the films and resulted in films with rod-shaped particles.

3.4. Optical and electrical properties

The optical transmittance (%T) and reflectance (%R) spectra of the CdS/SnS and ZnS/SnS thin films show that the CdS/SnS films exhibit only minor changes in optical transmittance and reflectance after annealing, whereas those of the ZnS/SnS films change markedly. The absorption edge of the ZnS/SnS films shifts to longer wavelengths with increasing annealing temperature. After annealing at 460 °C, the transmittance spectra show bending in the region of 750–900 nm. This could be the reason why the bandgap of these films changed more than that of the CdS/SnS films. However, XRD and Raman data showed no additional SnS phases, so we attribute this bending to defects appearing at the higher annealing temperature. In the present films, the transition was indirect. The energy bandgap (E_g) of the

films was determined from the plots of $(\alpha h\nu)^{1/2}$ against photon energy ($h\nu$). The calculated optical bandgaps for the CdS/SnS thin films varied from 1.28 eV for the film formed after three deposition cycles to 1.22 eV after annealing at 460 °C for 30 min under an inert atmosphere. For the ZnS/SnS films, the bandgap of the three-deposition-cycle film was 1.39 eV and decreased to 1.23 eV as the annealing temperature was increased to 460 °C.

The hot-probe method was used to determine the type of conductivity of the films. All deposited and annealed SnS films showed p-type conductivity. All of the films were photosensitive, and their photosensitivity increased with the annealing temperature.

Solar cells were made by depositing a CdS buffer layer onto transparent electrically conductive (TEC) glass substrates and consecutive deposition of SnS films. Different types of electrodes were painted onto the structures to produce solar cells. The best results were obtained using electrodes made of carbon mixed with Se/ZnS powder. Figure 6 presents voltage versus current density curves of solar cells containing SnS deposited on CdS. The performance of the solar cells decreased with the increasing annealing temperature. The best performance was obtained for the unannealed

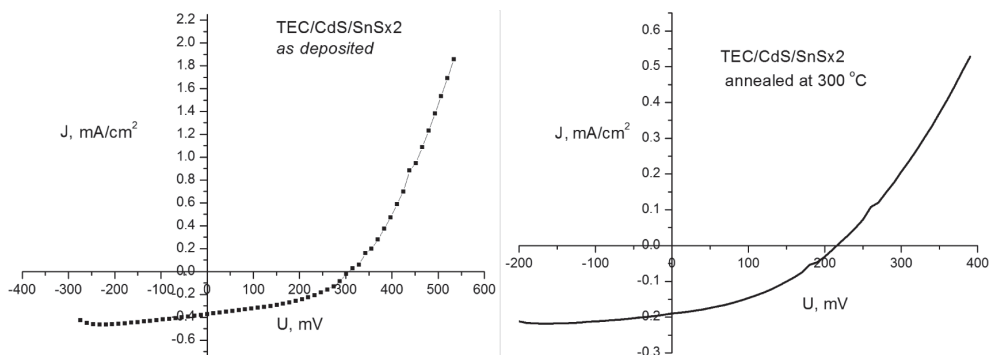


Fig. 6. Voltage–current density curve of a solar cell containing an unannealed SnS film formed after two deposition cycles and annealed at 300 °C.

SnS film formed after two deposition cycles with an open-circuit voltage (V_{oc}) of 0.3 V, short-circuit current density (J_{sc}) of 0.373 mA/cm², fill factor of 31.7%, and efficiency of 0.04%.

4. CONCLUSIONS

Our results confirm that after the first deposition cycle, the SnS films are amorphous. As the annealing temperature increases, the films exhibit crystalline structure with preferential orientation. A CdS substrate promotes formation of films with higher crystallinity than a ZnS substrate. The deposited CdS/SnS films had stoichiometric SnS composition, although this was influenced by thermal annealing. A ZnS substrate led to the formation of Sn-rich SnS films with compositions unaltered after thermal annealing. Solar cells containing the films were fabricated; the best results were $V_{oc} = 0.3$ V and $J_{sc} = 0.373$ mA/cm².

ACKNOWLEDGEMENTS

The authors thank Ana Rosa Garcia for help with experiments, Patricia Altuzar for XRD measurements, Jose Campos for SEM-compositional analyses and photoconductivity response measurements, and Oscar Gomez Daza for optical measurements. All these researchers are based at the Instituto de Energias Renovables – UNAM.

The Estonian Centre of Excellence in Research Project TK117T ‘High-technology Materials for Sustainable Development’, Estonian Energy Technology Program (project AR 10128), Estonian Ministry of Education and Research (targeted project T099), and Estonian Science Foundation (MJD213, G8147) are acknowledged for financial support.

REFERENCES

- Jeong, S., Lee, B.-S., Ahn, S. J., Yoon, K. H., Seo, Y. H., and Choi, Y. An 8.2% efficient solution-processed CuInSe₂ solar cell based on multiphase CuInSe₂ nanoparticles. *Energy Environ. Sci.*, 2012, **5**, 7539–7542.
- Hussain, K. M. A., Podder, J., Saha, D. K., and Ichimura, M. Structural, electrical and optical characterization of CuInS₂ thin films deposited by spray pyrolysis. *Indian J. Pure Appl. Phys.*, 2012, **50**, 117–122.
- Mohammed, W. F., Daoud, O., and Al-Tikriti, M. Power conversion enhancement of CdS/CdTe solar cell interconnected with tunnel diode. *Circuits and Systems*, 2012, **3**, 230–237.
- Schneikart, A., Schimper, H.-J., Klein, A., and Jaegermann, W. Efficiency limitations of thermally evaporated thin-film SnS solar cells. *J. Phys. D: Appl. Phys.*, 2013, **46**, 305109.
- Andersson, B. A. Materials availability for large-scale thin-film photovoltaics. *Prog. Photovolt. Res. Appl.*, 2000, **8**, 61–76.
- Mariappan, R., Ragavendar, M., and Ponnuswamy, V. Structural and optical characterization of SnS thin films by electrodeposition technique. *Opt. Appl.*, 2011, **XLI**, 988–997.
- Reddy, K. T. R., Reddy, P. P., Miles, R. W., and Datta, P. K. Investigations on SnS films deposited by spray pyrolysis. *Opt. Mater.*, 2001, **17**(1–2), 295–298.
- Hartman, K., Johnson, J. L., Bertoni, M. I., Recht, D., Aziz, M. J., and Scarpulla, M. A. SnS thin-films by RF sputtering at room temperature. *Thin Solid Films*, 2011, **519**, 7421–7424.
- Ghosh, B., Das, M., Banerjee, P., and Das, S. Fabrication of vacuum-evaporated SnS/CdS heterojunction for PV applications. *Sol. Energ. Mat. Sol. C.*, 2008, **92**, 1099–1104.
- Sreedevi, G. and Reddy, K. T. R. Properties of tin monosulphide films grown by chemical bath deposition. *Conference Papers in Energy*, 2013, **2013**, Article ID 528724.
- Ming Du, Xuesong Yin, and Hao Gong. Effects of triethanolamine on the morphology and phase of chemically deposited tin sulfide. *Mater. Lett.*, 2015, **152**, 40–44.
- Sreedevi Gedi, Vasudeva Reddy Minnam Reddy, Chinho Park, Jeon Chan-Wook, and Ramakrishna Reddy, K. T. Comprehensive optical studies on SnS layers synthesized by chemical bath deposition. *Opt. Mater.*, 2015, **42**, 468–475.
- Patel, T. H. Influence of deposition time on structural and optical properties of chemically deposited SnS thin films. *The Open Surface Science Journal*, 2012, **4**, 6–13.
- Ragina, A. J., Preetha, K. C., Murali, K. V., Deepa, K., and Remadevi, T. L. Wet chemical synthesis and characterization of tin sulphide thin films from different host solutions. *Advances in Applied Science Research*, 2011, **2**(3), 438–444.
- Chao Gao, Honglie Shen, and Lei Sun. Preparation and properties of zinc blende and orthorhombic SnS films by chemical bath deposition. *Appl. Surf. Sci.*, 2011, **257**, 6750–6755.
- Safonova, M., Nair, P., Mellikov, E., Garcia, A., Kerm, K., Revathi, N., Romann, T., Mikli, V., and Volobujeva, O. Chemical bath deposition of SnS thin films on ZnS and CdS substrates. *J. Mater. Sci.–Mater. El.*, 2014, **25**, 3160.
- Arenas, O. L., Nair, M. T. S., and Nair, P. K. Chemical bath deposition of ZnS thin films and modification by air annealing. *Semicond. Sci. Tech.*, 1997, **12**, 1323.
- Nair, P. K., Daza, O. G., Readigos, A. A.-C., Campos, J., and Nair, M. T. S. Formation of conductive CdO layer on CdS thin films during air heating. *Semicond. Sci. Tech.*, 2001, **16**, 651–656.

19. Leite, R. C. C. and Porto, S. P. S. Enhancement of Raman cross section in CdS due to resonant absorption. *Phys. Rev. Lett.*, 1966, **17**, 10.
20. Price, L. S., Parkin, I. P., Hardy, A. M. E., Clark, R. J. H., Hibbert, T. G., and Molloy, K. C. Atmospheric pressure chemical vapor deposition of tin sulfides (SnS, Sn₂S₃, SnS₂) on glass. *Chem. Mater.*, 1999, **11**, 1792–1799.

SnS kilede keemiline sadestamine ZnS ja CdS alusele ning nende järgnev termiline töötlemine

Maria Safonova, Padmanabhan Pankajakshy Karunakaran Nair, Enn Mellikov, Rebeca Aragon, Karin Kerm, Revathi Naidu, Valdek Mikli ja Olga Volobujeva

On uuritud erinevate kasutatavate aluspindade ja Ar atmosfääris läbiviidud termiliste käsitluste mõju keemiliselt sadestatud SnS kilede keemilisele ning faasikoostisele, nende kristallstruktuurile ja optilistele omadustele. On näidatud, et ühekordselt keemiliselt sadestatud SnS kiled on amorfed. Mitmekordne keemiline sadestus viib ortorombilise kristallstruktuuriga SnS kilede moodustumisele, sõltumata sadestamisel kasutatavast aluspinnast. CdS alusele sadestatud kiled on stöhhiomeetrilise koostisega, mis on muudetav nende kilede järgnevate termiliste käsitlustega. ZnS aluse kasutamine viib Sn-rikaste kilede moodustumisele. Kilede mitteotsese keelutsooni laius E_g on muudetav nende järgnevate termiliste töötlustega. Kolmekordselt sadestatud CdS/SnS kilede keelutsooni laius muutus termilisel käsitlusel temperatuuril 460 °C 1,28 eV-lt kuni 1,22 eV-ni. Analoogselt ZnS/SnS kiledele muutus keelutsooni laius kilede termilistel käsitlustel 1,39 eV-lt kuni 1,23 eV-ni. Keemiliselt sadestatud SnS kilede alusel valmistatud päikesepatarei struktuurid CdS-SnS olid parameetritega $V_{oc} = 0,3$ V ja $J_{sc} = 0,373$ mA/cm².

APPENDIX B

Curriculum Vitae

1. Isikuandmed

Ees- ja perekonnainimi	Maria Safonova
Sünniaeg ja -koht	29 august 1986, Narva
Kodakondsus	EST
E-posti aadress	marija.safonova@gmail.com

2. Haridus

2011- ... Tallinna Tehnikaülikool, doktorantuur, keemia- ja materjalitehnoloogia.

2008-20010 Tallinna Tehnikaülikool, magister, polümeeride tehnoloogia.

2005-2008 Tallinna Tehnikaülikool, bakalaureus, polümeeride tehnoloogia.

1992-2005 Sillamäe Kannuka Kool, keskkharidus.

3. Keelteoskus

vene (emakeel)

eesti (kesktase)

inglise (kesktase)

hispaania (kesktase)

4. Täiendusõpe

September – November 2013 Universidad Nacional Autonoma de Mexico, Instituto de energias renovables, Temixco, Mexico

5. Teenistuskäik

2010 - ... Tallinna Tehnikaülikool, Keemia ja Materjaliteaduse instituut, insener.

6. Tunnustused

2013 Archimedes DoRa stipendium.

Curriculum Vitae

1. Personal data

First name and surname Maria Safonova
Date and place of birth 29 august 1986, Narva
Citizenship EST
E-mail marija.safonova@gmail.com

2. Education

2011- ... Tallinn University of Technology,
doctoral studies

2008-2010 Tallinn University of Technology,
Master of Science, Department of Polymer
Materials.

2005-2008 Tallinn University of Technology,
Bachelor of Science, Department of Polymer
Materials.

1992-2005 Sillamäe Kannuka gymnasium,
secondary education

3. Keelteoskus

Russian (native)

Estonian (fluent)

English (fluent)

Spanish (fluent)

4. Täiendusõpe

September – November 2013 Universidad
Nacional Autonoma de Mexico, Instituto de
energias renovables, Temixco, Mexico

5. Employment

2010 - ... Tallinn University of Technology,
Department of Materials Science, engineer.

6. Recognitions

2013 Archimedes DoRa scholarship.

List of publications

1. M. Safonova, P.K. Nair, E. Mellikov, R. Aragon, K. Kerm, R. Naidu, V. Mikli, O. Volobujeva. Thermal annealing of sequentially chemically deposited SnS thin films, *Proceedings of the Estonian Academy of Sciences* 64 (4) (2015) 488-494.
2. Revathi, N.; Bereznev, S.; Lehner, J.; Traksmaa, R.; Safonova, M.; Mellikov, E.; Volobujeva, O., Thin Tin Monosulfide films deposited with the HVE method for photovoltaic applications, *Materials and technology* 49(1) (2015) 149 - 152.
3. Safonova, M.; Mellikov, E.; Mikli, V.; Kerm, K.; Revathi, N.; Volobujeva, O., Chemical bath deposition of SnS thin films from the solutions with different concentrations of tin and sulphur. *Advanced Materials Research. Trans Tech Publications Ltd* (2015) 183 - 186.
4. Safonova, M.; Nair, P; Mellikov, E.; Garcia, A; Kerm, K.; Revathi, N.; Romann, T; Mikli, V.; Volobujeva, O., Chemical bath deposition of SnS thin films on ZnS and CdS substrates. *Journal of Material Science : Materials in Electronics* 25(7) (2014) 3160 - 3165.
5. Revathi, N.; Bereznev, S.; Iljina, J.; Safonova, M.; Mellikov, E.; Volobujeva, O. PVD grown SnS thin films onto different substrate surfaces. *Journal of Materials Science: Materials in electronics* (2013)1- 6.

**DISSERTATIONS DEFENDED AT
TALLINN UNIVERSITY OF TECHNOLOGY ON
NATURAL AND EXACT SCIENCES**

1. **Olav Kongas**. Nonlinear Dynamics in Modeling Cardiac Arrhythmias. 1998.
2. **Kalju Vanatalu**. Optimization of Processes of Microbial Biosynthesis of Isotopically Labeled Biomolecules and Their Complexes. 1999.
3. **Ahto Buldas**. An Algebraic Approach to the Structure of Graphs. 1999.
4. **Monika Drews**. A Metabolic Study of Insect Cells in Batch and Continuous Culture: Application of Chemostat and Turbidostat to the Production of Recombinant Proteins. 1999.
5. **Eola Valdre**. Endothelial-Specific Regulation of Vessel Formation: Role of Receptor Tyrosine Kinases. 2000.
6. **Kalju Lott**. Doping and Defect Thermodynamic Equilibrium in ZnS. 2000.
7. **Reet Koljak**. Novel Fatty Acid Dioxygenases from the Corals *Plexaura homomalla* and *Gersemia fruticosa*. 2001.
8. **Anne Paju**. Asymmetric oxidation of Prochiral and Racemic Ketones by Using Sharpless Catalyt. 2001.
9. **Marko Vendelin**. Cardiac Mechanoenergetics *in silico*. 2001.
10. **Pearu Peterson**. Multi-Soliton Interactions and the Inverse Problem of Wave Crest. 2001.
11. **Anne Menert**. Microcalorimetry of Anaerobic Digestion. 2001.
12. **Toomas Tiivel**. The Role of the Mitochondrial Outer Membrane in *in vivo* Regulation of Respiration in Normal Heart and Skeletal Muscle Cell. 2002.
13. **Olle Hints**. Ordovician Scolecodonts of Estonia and Neighbouring Areas: Taxonomy, Distribution, Palaeoecology, and Application. 2002.
14. **Jaak Nõlvak**. Chitinozoan Biostratigraphy in the Ordovician of Baltoscandia. 2002.
15. **Liivi Kluge**. On Algebraic Structure of Pre-Operad. 2002.
16. **Jaanus Lass**. Biosignal Interpretation: Study of Cardiac Arrhythmias and Electromagnetic Field Effects on Human Nervous System. 2002.
17. **Janek Peterson**. Synthesis, Structural Characterization and Modification of PAMAM Dendrimers. 2002.
18. **Merike Vaher**. Room Temperature Ionic Liquids as Background Electrolyte Additives in Capillary Electrophoresis. 2002.
19. **Valdek Mikli**. Electron Microscopy and Image Analysis Study of Powdered Hardmetal Materials and Optoelectronic Thin Films. 2003.
20. **Mart Viljus**. The Microstructure and Properties of Fine-Grained Cermets. 2003.
21. **Signe Kask**. Identification and Characterization of Dairy-Related *Lactobacillus*. 2003
22. **Tiiu-Mai Laht**. Influence of Microstructure of the Curd on Enzymatic and Microbiological Processes in Swiss-Type Cheese. 2003.
23. **Anne Kuusksalu**. 2–5A Synthetase in the Marine Sponge *Geodia cydonium*. 2003.
24. **Sergei Bereznev**. Solar Cells Based on Polycrystalline Copper-Indium Chalcogenides and Conductive Polymers. 2003.

25. **Kadri Kriis.** Asymmetric Synthesis of C₂-Symmetric Bimorpholines and Their Application as Chiral Ligands in the Transfer Hydrogenation of Aromatic Ketones. 2004.
26. **Jekaterina Reut.** Polypyrrole Coatings on Conducting and Insulating Substrates. 2004.
27. **Sven Nõmm.** Realization and Identification of Discrete-Time Nonlinear Systems. 2004.
28. **Olga Kijatkina.** Deposition of Copper Indium Disulphide Films by Chemical Spray Pyrolysis. 2004.
29. **Gert Tamberg.** On Sampling Operators Defined by Rogosinski, Hann and Blackman Windows. 2004.
30. **Monika Übner.** Interaction of Humic Substances with Metal Cations. 2004.
31. **Kaarel Adamberg.** Growth Characteristics of Non-Starter Lactic Acid Bacteria from Cheese. 2004.
32. **Imre Vallikivi.** Lipase-Catalysed Reactions of Prostaglandins. 2004.
33. **Merike Peld.** Substituted Apatites as Sorbents for Heavy Metals. 2005.
34. **Vitali Syritski.** Study of Synthesis and Redox Switching of Polypyrrole and Poly(3,4-ethylenedioxythiophene) by Using *in-situ* Techniques. 2004.
35. **Lee Põllumaa.** Evaluation of Ecotoxicological Effects Related to Oil Shale Industry. 2004.
36. **Riina Aav.** Synthesis of 9,11-Secosterols Intermediates. 2005.
37. **Andres Braunbrück.** Wave Interaction in Weakly Inhomogeneous Materials. 2005.
38. **Robert Kitt.** Generalised Scale-Invariance in Financial Time Series. 2005.
39. **Juss Pavelson.** Mesoscale Physical Processes and the Related Impact on the Summer Nutrient Fields and Phytoplankton Blooms in the Western Gulf of Finland. 2005.
40. **Olari Ilison.** Solitons and Solitary Waves in Media with Higher Order Dispersive and Nonlinear Effects. 2005.
41. **Maksim Säkki.** Intermittency and Long-Range Structurization of Heart Rate. 2005.
42. **Enli Kiipli.** Modelling Seawater Chemistry of the East Baltic Basin in the Late Ordovician–Early Silurian. 2005.
43. **Igor Golovtsov.** Modification of Conductive Properties and Processability of Polyparaphenylene, Polypyrrole and polyaniline. 2005.
44. **Katrin Laos.** Interaction Between Furcellaran and the Globular Proteins (Bovine Serum Albumin β -Lactoglobulin). 2005.
45. **Arvo Mere.** Structural and Electrical Properties of Spray Deposited Copper Indium Disulphide Films for Solar Cells. 2006.
46. **Sille Ehala.** Development and Application of Various On- and Off-Line Analytical Methods for the Analysis of Bioactive Compounds. 2006.
47. **Maria Kulp.** Capillary Electrophoretic Monitoring of Biochemical Reaction Kinetics. 2006.
48. **Anu Aaspõllu.** Proteinases from *Vipera lebetina* Snake Venom Affecting Hemostasis. 2006.

49. **Lyudmila Chekulayeva.** Photosensitized Inactivation of Tumor Cells by Porphyrins and Chlorins. 2006.
50. **Merle Uudsemaa.** Quantum-Chemical Modeling of Solvated First Row Transition Metal Ions. 2006.
51. **Tagli Pitsi.** Nutrition Situation of Pre-School Children in Estonia from 1995 to 2004. 2006.
52. **Angela Ivask.** Luminescent Recombinant Sensor Bacteria for the Analysis of Bioavailable Heavy Metals. 2006.
53. **Tiina Lõugas.** Study on Physico-Chemical Properties and Some Bioactive Compounds of Sea Buckthorn (*Hippophae rhamnoides* L.). 2006.
54. **Kaja Kasemets.** Effect of Changing Environmental Conditions on the Fermentative Growth of *Saccharomyces cerevisiae* S288C: Auxo-accelerostat Study. 2006.
55. **Ildar Nisamedtinov.** Application of ^{13}C and Fluorescence Labeling in Metabolic Studies of *Saccharomyces* spp. 2006.
56. **Alar Leibak.** On Additive Generalisation of Voronoï's Theory of Perfect Forms over Algebraic Number Fields. 2006.
57. **Andri Jagomägi.** Photoluminescence of Chalcopyrite Tellurides. 2006.
58. **Tõnu Martma.** Application of Carbon Isotopes to the Study of the Ordovician and Silurian of the Baltic. 2006.
59. **Marit Kauk.** Chemical Composition of CuInSe₂ Monograin Powders for Solar Cell Application. 2006.
60. **Julia Kois.** Electrochemical Deposition of CuInSe₂ Thin Films for Photovoltaic Applications. 2006.
61. **Iiona Oja Açıık.** Sol-Gel Deposition of Titanium Dioxide Films. 2007.
62. **Tiia Anmann.** Integrated and Organized Cellular Bioenergetic Systems in Heart and Brain. 2007.
63. **Katrin Trummal.** Purification, Characterization and Specificity Studies of Metalloproteinases from *Vipera lebetina* Snake Venom. 2007.
64. **Gennadi Lessin.** Biochemical Definition of Coastal Zone Using Numerical Modeling and Measurement Data. 2007.
65. **Enno Pais.** Inverse problems to determine non-homogeneous degenerate memory kernels in heat flow. 2007.
66. **Maria Borissova.** Capillary Electrophoresis on Alkylimidazolium Salts. 2007.
67. **Karin Valmsen.** Prostaglandin Synthesis in the Coral *Plexaura homomalla*: Control of Prostaglandin Stereochemistry at Carbon 15 by Cyclooxygenases. 2007.
68. **Kristjan Piirimäe.** Long-Term Changes of Nutrient Fluxes in the Drainage Basin of the Gulf of Finland – Application of the PolFlow Model. 2007.
69. **Tatjana Dedova.** Chemical Spray Pyrolysis Deposition of Zinc Sulfide Thin Films and Zinc Oxide Nanostructured Layers. 2007.
70. **Katrin Tomson.** Production of Labelled Recombinant Proteins in Fed-Batch Systems in *Escherichia coli*. 2007.
71. **Cecilia Sarmiento.** Suppressors of RNA Silencing in Plants. 2008.
72. **Vilja Mardla.** Inhibition of Platelet Aggregation with Combination of Antiplatelet Agents. 2008.

73. **Maie Bachmann.** Effect of Modulated Microwave Radiation on Human Resting Electroencephalographic Signal. 2008.
74. **Dan Huvonen.** Terahertz Spectroscopy of Low-Dimensional Spin Systems. 2008.
75. **Ly Villo.** Stereoselective Chemoenzymatic Synthesis of Deoxy Sugar Esters Involving *Candida antarctica* Lipase B. 2008.
76. **Johan Anton.** Technology of Integrated Photoelasticity for Residual Stress Measurement in Glass Articles of Axisymmetric Shape. 2008.
77. **Olga Volobujeva.** SEM Study of Selenization of Different Thin Metallic Films. 2008.
78. **Artur Jogi.** Synthesis of 4'-Substituted 2,3'-dideoxynucleoside Analogues. 2008.
79. **Mario Kadastik.** Doubly Charged Higgs Boson Decays and Implications on Neutrino Physics. 2008.
80. **Fernando Perez-Caballero.** Carbon Aerogels from 5-Methylresorcinol-Formaldehyde Gels. 2008.
81. **Sirje Vaask.** The Comparability, Reproducibility and Validity of Estonian Food Consumption Surveys. 2008.
82. **Anna Menaker.** Electrosynthesized Conducting Polymers, Polypyrrole and Poly(3,4-ethylenedioxythiophene), for Molecular Imprinting. 2009.
83. **Lauri Ilison.** Solitons and Solitary Waves in Hierarchical Korteweg-de Vries Type Systems. 2009.
84. **Kaia Ernits.** Study of In₂S₃ and ZnS Thin Films Deposited by Ultrasonic Spray Pyrolysis and Chemical Deposition. 2009.
85. **Veljo Sinivee.** Portable Spectrometer for Ionizing Radiation "Gammamapper". 2009.
86. **Juri Virkepu.** On Lagrange Formalism for Lie Theory and Operadic Harmonic Oscillator in Low Dimensions. 2009.
87. **Marko Piirsoo.** Deciphering Molecular Basis of Schwann Cell Development. 2009.
88. **Kati Helmja.** Determination of Phenolic Compounds and Their Antioxidative Capability in Plant Extracts. 2010.
89. **Merike Sõmera.** Sobemoviruses: Genomic Organization, Potential for Recombination and Necessity of P1 in Systemic Infection. 2010.
90. **Kristjan Laes.** Preparation and Impedance Spectroscopy of Hybrid Structures Based on CuIn₃Se₅ Photoabsorber. 2010.
91. **Kristin Lippur.** Asymmetric Synthesis of 2,2'-Bimorpholine and its 5,5'-Substituted Derivatives. 2010.
92. **Merike Luman.** Dialysis Dose and Nutrition Assessment by an Optical Method. 2010.
93. **Mihhail Berezovski.** Numerical Simulation of Wave Propagation in Heterogeneous and Microstructured Materials. 2010.
94. **Tamara Aid-Pavlidis.** Structure and Regulation of BDNF Gene. 2010.
95. **Olga Bragina.** The Role of Sonic Hedgehog Pathway in Neuro- and Tumorigenesis. 2010.

96. **Merle Randrüüt.** Wave Propagation in Microstructured Solids: Solitary and Periodic Waves. 2010.
97. **Marju Laars.** Asymmetric Organocatalytic Michael and Aldol Reactions Mediated by Cyclic Amines. 2010.
98. **Maarja Grossberg.** Optical Properties of Multinary Semiconductor Compounds for Photovoltaic Applications. 2010.
99. **Alla Maloverjan.** Vertebrate Homologues of Drosophila Fused Kinase and Their Role in Sonic Hedgehog Signalling Pathway. 2010.
100. **Priit Pruunsild.** Neuronal Activity-Dependent Transcription Factors and Regulation of Human *BDNF* Gene. 2010.
101. **Tatjana Knjazeva.** New Approaches in Capillary Electrophoresis for Separation and Study of Proteins. 2011.
102. **Atanas Katerski.** Chemical Composition of Sprayed Copper Indium Disulfide Films for Nanostructured Solar Cells. 2011.
103. **Kristi Timmo.** Formation of Properties of CuInSe_2 and $\text{Cu}_2\text{ZnSn}(\text{S},\text{Se})_4$ Monograin Powders Synthesized in Molten KI. 2011.
104. **Kert Tamm.** Wave Propagation and Interaction in Mindlin-Type Microstructured Solids: Numerical Simulation. 2011.
105. **Adrian Popp.** Ordovician Proetid Trilobites in Baltoscandia and Germany. 2011.
106. **Ove Pärn.** Sea Ice Deformation Events in the Gulf of Finland and This Impact on Shipping. 2011.
107. **Germo Väli.** Numerical Experiments on Matter Transport in the Baltic Sea. 2011.
108. **Andrus Seiman.** Point-of-Care Analyser Based on Capillary Electrophoresis. 2011.
109. **Olga Katargina.** Tick-Borne Pathogens Circulating in Estonia (Tick-Borne Encephalitis Virus, *Anaplasma phagocytophilum*, *Babesia* Species): Their Prevalence and Genetic Characterization. 2011.
110. **Ingrid Sumeri.** The Study of Probiotic Bacteria in Human Gastrointestinal Tract Simulator. 2011.
111. **Kairit Zovo.** Functional Characterization of Cellular Copper Proteome. 2011.
112. **Natalja Makarytsheva.** Analysis of Organic Species in Sediments and Soil by High Performance Separation Methods. 2011.
113. **Monika Mortimer.** Evaluation of the Biological Effects of Engineered Nanoparticles on Unicellular Pro- and Eukaryotic Organisms. 2011.
114. **Kersti Tepp.** Molecular System Bioenergetics of Cardiac Cells: Quantitative Analysis of Structure-Function Relationship. 2011.
115. **Anna-Liisa Peikolainen.** Organic Aerogels Based on 5-Methylresorcinol. 2011.
116. **Leeli Amon.** Palaeoecological Reconstruction of Late-Glacial Vegetation Dynamics in Eastern Baltic Area: A View Based on Plant Macrofossil Analysis. 2011.
117. **Tanel Peets.** Dispersion Analysis of Wave Motion in Microstructured Solids. 2011.

118. **Liina Kaupmees**. Selenization of Molybdenum as Contact Material in Solar Cells. 2011.
119. **Allan Olsper**. Properties of VPg and Coat Protein of Sobemoviruses. 2011.
120. **Kadri Koppel**. Food Category Appraisal Using Sensory Methods. 2011.
121. **Jelena Gorbatšova**. Development of Methods for CE Analysis of Plant Phenolics and Vitamins. 2011.
122. **Karin Viipsi**. Impact of EDTA and Humic Substances on the Removal of Cd and Zn from Aqueous Solutions by Apatite. 2012.
123. **David Schryer**. Metabolic Flux Analysis of Compartmentalized Systems Using Dynamic Isotopologue Modeling. 2012.
124. **Ardo Illaste**. Analysis of Molecular Movements in Cardiac Myocytes. 2012.
125. **Indrek Reile**. 3-Alkylcyclopentane-1,2-Diones in Asymmetric Oxidation and Alkylation Reactions. 2012.
126. **Tatjana Tamberg**. Some Classes of Finite 2-Groups and Their Endomorphism Semigroups. 2012.
127. **Taavi Liblik**. Variability of Thermohaline Structure in the Gulf of Finland in Summer. 2012.
128. **Priidik Lagemaa**. Operational Forecasting in Estonian Marine Waters. 2012.
129. **Andrei Errapart**. Photoelastic Tomography in Linear and Non-linear Approximation. 2012.
130. **Külliki Krabbi**. Biochemical Diagnosis of Classical Galactosemia and Mucopolysaccharidoses in Estonia. 2012.
131. **Kristel Kaseleht**. Identification of Aroma Compounds in Food using SPME-GC/MS and GC-Olfactometry. 2012.
132. **Kristel Kodar**. Immunoglobulin G Glycosylation Profiling in Patients with Gastric Cancer. 2012.
133. **Kai Rosin**. Solar Radiation and Wind as Agents of the Formation of the Radiation Regime in Water Bodies. 2012.
134. **Ann Tiiman**. Interactions of Alzheimer's Amyloid-Beta Peptides with Zn(II) and Cu(II) Ions. 2012.
135. **Olga Gavrilova**. Application and Elaboration of Accounting Approaches for Sustainable Development. 2012.
136. **Olesja Bondarenko**. Development of Bacterial Biosensors and Human Stem Cell-Based *In Vitro* Assays for the Toxicological Profiling of Synthetic Nanoparticles. 2012.
137. **Katri Muska**. Study of Composition and Thermal Treatments of Quaternary Compounds for Monograin Layer Solar Cells. 2012.
138. **Ranno Nahku**. Validation of Critical Factors for the Quantitative Characterization of Bacterial Physiology in Accelerostat Cultures. 2012.
139. **Petri-Jaan Lahtvee**. Quantitative Omics-level Analysis of Growth Rate Dependent Energy Metabolism in *Lactococcus lactis*. 2012.
140. **Kerti Orumets**. Molecular Mechanisms Controlling Intracellular Glutathione Levels in Baker's Yeast *Saccharomyces cerevisiae* and its Random Mutagenized Glutathione Over-Accumulating Isolate. 2012.
141. **Loreida Timberg**. Spice-Cured Sprats Ripening, Sensory Parameters Development, and Quality Indicators. 2012.

142. **Anna Mihhalevski.** Rye Sourdough Fermentation and Bread Stability. 2012.
143. **Liisa Arike.** Quantitative Proteomics of *Escherichia coli*: From Relative to Absolute Scale. 2012.
144. **Kairi Otto.** Deposition of In₂S₃ Thin Films by Chemical Spray Pyrolysis. 2012.
145. **Mari Sepp.** Functions of the Basic Helix-Loop-Helix Transcription Factor TCF4 in Health and Disease. 2012.
146. **Anna Suhhova.** Detection of the Effect of Weak Stressors on Human Resting Electroencephalographic Signal. 2012.
147. **Aram Kazarjan.** Development and Production of Extruded Food and Feed Products Containing Probiotic Microorganisms. 2012.
148. **Rivo Uiboupin.** Application of Remote Sensing Methods for the Investigation of Spatio-Temporal Variability of Sea Surface Temperature and Chlorophyll Fields in the Gulf of Finland. 2013.
149. **Tiina Kriščiunaite.** A Study of Milk Coagulability. 2013.
150. **Tuuli Levandi.** Comparative Study of Cereal Varieties by Analytical Separation Methods and Chemometrics. 2013.
151. **Natalja Kabanova.** Development of a Microcalorimetric Method for the Study of Fermentation Processes. 2013.
152. **Himani Khanduri.** Magnetic Properties of Functional Oxides. 2013.
153. **Julia Smirnova.** Investigation of Properties and Reaction Mechanisms of Redox-Active Proteins by ESI MS. 2013.
154. **Mervi Sepp.** Estimation of Diffusion Restrictions in Cardiomyocytes Using Kinetic Measurements. 2013.
155. **Kersti Jääger.** Differentiation and Heterogeneity of Mesenchymal Stem Cells. 2013.
156. **Victor Alari.** Multi-Scale Wind Wave Modeling in the Baltic Sea. 2013.
157. **Taavi Päll.** Studies of CD44 Hyaluronan Binding Domain as Novel Angiogenesis Inhibitor. 2013.
158. **Allan Niidu.** Synthesis of Cyclopentane and Tetrahydrofuran Derivatives. 2013.
159. **Julia Geller.** Detection and Genetic Characterization of *Borrelia* Species Circulating in Tick Population in Estonia. 2013.
160. **Irina Stulova.** The Effects of Milk Composition and Treatment on the Growth of Lactic Acid Bacteria. 2013.
161. **Jana Holmar.** Optical Method for Uric Acid Removal Assessment During Dialysis. 2013.
162. **Kerti Ausmees.** Synthesis of Heterobicyclo[3.2.0]heptane Derivatives *via* Multicomponent Cascade Reaction. 2013.
163. **Minna Varikmaa.** Structural and Functional Studies of Mitochondrial Respiration Regulation in Muscle Cells. 2013.
164. **Indrek Koppel.** Transcriptional Mechanisms of BDNF Gene Regulation. 2014.
165. **Kristjan Pilt.** Optical Pulse Wave Signal Analysis for Determination of Early Arterial Ageing in Diabetic Patients. 2014.
166. **Andres Anier.** Estimation of the Complexity of the Electroencephalogram for Brain Monitoring in Intensive Care. 2014.

167. **Toivo Kallaste**. Pyroclastic Sanidine in the Lower Palaeozoic Bentonites – A Tool for Regional Geological Correlations. 2014.
168. **Erki Kärber**. Properties of ZnO-nanorod/In₂S₃/CuInS₂ Solar Cell and the Constituent Layers Deposited by Chemical Spray Method. 2014.
169. **Julia Lehner**. Formation of Cu₂ZnSnS₄ and Cu₂ZnSnSe₄ by Chalcogenisation of Electrochemically Deposited Precursor Layers. 2014.
170. **Peep Pitk**. Protein- and Lipid-rich Solid Slaughterhouse Waste Anaerobic Co-digestion: Resource Analysis and Process Optimization. 2014.
171. **Kaspar Valgepea**. Absolute Quantitative Multi-omics Characterization of Specific Growth Rate-dependent Metabolism of *Escherichia coli*. 2014.
172. **Artur Noole**. Asymmetric Organocatalytic Synthesis of 3,3'-Disubstituted Oxindoles. 2014.
173. **Robert Tsanev**. Identification and Structure-Functional Characterisation of the Gene Transcriptional Repressor Domain of Human Gli Proteins. 2014.
174. **Dmitri Kartofelev**. Nonlinear Sound Generation Mechanisms in Musical Acoustic. 2014.
175. **Sigrid Hade**. GIS Applications in the Studies of the Palaeozoic Graptolite Argillite and Landscape Change. 2014.
176. **Agne Velthut-Meikas**. Ovarian Follicle as the Environment of Oocyte Maturation: The Role of Granulosa Cells and Follicular Fluid at Pre-Ovulatory Development. 2014.
177. **Kristel Hälvin**. Determination of B-group Vitamins in Food Using an LC-MS Stable Isotope Dilution Assay. 2014.
178. **Mailis Päre**. Characterization of the Oligoadenylate Synthetase Subgroup from Phylum Porifera. 2014.
179. **Jekaterina Kazantseva**. Alternative Splicing of *TAF4*: A Dynamic Switch between Distinct Cell Functions. 2014.
180. **Jaanus Suurväli**. Regulator of G Protein Signalling 16 (RGS16): Functions in Immunity and Genomic Location in an Ancient MHC-Related Evolutionarily Conserved Synteny Group. 2014.
181. **Ene Viiard**. Diversity and Stability of Lactic Acid Bacteria During Rye Sourdough Propagation. 2014.
182. **Kristella Hansen**. Prostaglandin Synthesis in Marine Arthropods and Red Algae. 2014.
183. **Helike Lõhelaid**. Allene Oxide Synthase-lipoxygenase Pathway in Coral Stress Response. 2015.
184. **Normunds Stivriņš**. Postglacial Environmental Conditions, Vegetation Succession and Human Impact in Latvia. 2015.
185. **Mary-Liis Kütt**. Identification and Characterization of Bioactive Peptides with Antimicrobial and Immunoregulating Properties Derived from Bovine Colostrum and Milk. 2015.
186. **Kazbulat Šogenov**. Petrophysical Models of the CO₂ Plume at Prospective Storage Sites in the Baltic Basin. 2015.
187. **Taavi Raadik**. Application of Modulation Spectroscopy Methods in Photovoltaic Materials Research. 2015.

188. **Reio Põder**. Study of Oxygen Vacancy Dynamics in Sc-doped Ceria with NMR Techniques. 2015.
189. **Sven Siir**. Internal Geochemical Stratification of Bentonites (Altered Volcanic Ash Beds) and its Interpretation. 2015.
190. **Kaur Jaanson**. Novel Transgenic Models Based on Bacterial Artificial Chromosomes for Studying BDNF Gene Regulation. 2015.
191. **Niina Karro**. Analysis of ADP Compartmentation in Cardiomyocytes and Its Role in Protection Against Mitochondrial Permeability Transition Pore Opening. 2015.
192. **Piret Laht**. B-plexins Regulate the Maturation of Neurons Through Microtubule Dynamics. 2015.
193. **Sergei Žari**. Organocatalytic Asymmetric Addition to Unsaturated 1,4-Dicarbonyl Compounds. 2015.
194. **Natalja Buhhalke**. Processes Influencing the Spatio-temporal Dynamics of Nutrients and Phytoplankton in Summer in the Gulf of Finland, Baltic Sea. 2015.
195. **Natalia Maticiuc**. Mechanism of Changes in the Properties of Chemically Deposited CdS Thin Films Induced by Thermal Annealing. 2015.
196. **Mario Öeren**. Computational Study of Cyclohexylhemicucurbiturils. 2015.
197. **Mari Kalda**. Mechanoenergetics of a Single Cardiomyocyte. 2015.
198. **Ieva Grudzinska**. Diatom Stratigraphy and Relative Sea Level Changes of the Eastern Baltic Sea over the Holocene. 2015.
199. **Anna Kazantseva**. Alternative Splicing in Health and Disease. 2015.
200. **Jana Kazarjan**. Investigation of Endogenous Antioxidants and Their Synthetic Analogues by Capillary Electrophoresis. 2015.